

https://dspace.org/

Consolidation and compressibility properties of non-plastic tailings

Nchabeleng, Mokgadi Mahlatse

2021
https://hdl.handle.net/10539/31915

Downloaded from a DSpace repository. https://dspace.org/

CONSOLIDATION AND COMPRESSIBILITY PROPERTIES OF NON-PLASTIC TAILINGS.

Mokgadi Mahlatse Nchabeleng

A dissertation submitted to the Faculty of Engineering and the Built Environment, University of the Witwatersrand, Johannesburg, in fulfilment of the requirements for the degree of Master of Science in Engineering.

Johannesburg 2021

Declaration

I declare that this dissertation is my own unaided work. It is being submitted for the Degree of Master of Science in Engineering to the University of the Witwatersrand, Johannesburg. It has not been submitted before for any degree or examination to any other university.

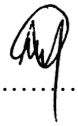

……..

(Signature of the Candidate)

……26……..day of ……April…… year ……2021……

Abstract

The safe operation of tailings dams requires a thorough understanding of the mechanical behaviour of tailings. These mechanical properties can consist of consolidation and compressibility, which vary with particle size distribution, density, mineralogy and mining technology. Both these properties have a direct effect on the shear strength, by way of influencing the in-situ densities and pore pressures existing in tailings dams.

This study aimed to characterize the compressibility and consolidation properties of non-plastic platinum tailings by testing two gradations of remoulded specimens in a 100 mm diameter Rowe-Barden consolidation cell. Laboratory reconstituting methods included moist tamping and slurry deposition upon which the effect of fabric was analysed. Stepped loading and constant rate of loading methods of testing were conducted on specimens at different densities from which the effect of loading was investigated. The study also explored the goodness of fit of five models recently proposed for modelling compression curves.

The results confirmed that the compressibility was in the same range as documented tailings showing a direct correlation with the D_{50}. However, the consolidation behaviour showed little dependence on the particle size distribution. It was also found that high density specimens were less compressible and their compressive behaviour independent of the loading method. The highest discrepancy was observed when comparing low density stepped loading and constant rate of loading tests compression curves. The five models captured the compression curves of the experimental and documented tailings fairly well in comparison with conventional models and offer an alternative to modelling the compressive behaviour of tailings.

To the geotechnical engineering community.

Acknowledgements

Yet you, Lord, are our Father.
We are the clay, you are the potter;
we are all the work of your hand.

Isaiah 64:8

Several individuals and institutions are hereby acknowledged:

- My supervisor Dr Luis Alberto Torres Cruz, for his patience, support and guidance throughout my studies. For encouraging and exposing me to the geotechnical engineering community.
- Dr Thushan Ekneligoda for insightful feedback and guidance.
- The Geoffrey Blight Geotechnical laboratory technical staff, Tumelo Sithole and Samuel Mabote for their support during the experimental stage of my studies.
- Fellow Postgraduate students within the School of Civil and Environmental Engineering.
- The National Research Foundation for financial assistance.
- The Department of Science and Technology and TATA International for awarding me a scholarship.
- Finally, my friends and family for providing exceptional support and encouragement.

Table of Contents

List of Figures viii

List of Tables xii

List of Symbols xiii

1 Introduction 1

1.1 Topic overview 1

1.2 Objective 2

1.3 Thesis Outline 2

2 Literature review 3

2.1 Introduction 3

2.2 Compressibility 3

2.2.1 Stress-strain relationships 3

2.2.2 Four-parameter compressibility models 4

2.2.3 Compressibility behaviour of tailings 6

2.2.4 Effect of fabric on compressibility 7

2.3 Consolidation 7

2.3.1 Theory of consolidation 7

2.3.2 Effect of fabric on consolidation 8

2.4 Summary 8

3 Materials and Methods 19

3.1 Introduction 19

3.2 Tested material 19
3.3 Testing equipment 20
3.4 Specimen preparation 20
3.5 Testing procedure 21
3.6 Calculations of stress and void ratio 23
3.7 Summary 24
4 Results and analysis 31
4.1 Introduction 31
4.2 Method of analysis 31
4.3 Compression results 31
4.3.1 Effect of loading method 32
4.3.2 Effect of fabric 33
4.3.3 Coefficient of volume compressibility 33
4.4 Consolidation results 34
4.4.1 Coefficient of consolidation 34
4.4.2 Effect of fabric 35
4.5 Summary 35
5 Model fitting 47
5.1 Introduction 47
5.2 Non-plastic tailings 47
5.3 Published compression curves 48

5.4 Summary 49

6 Conclusion 65

7 Recommendations 66

8 References 67

Appendix A Tangent Modulus equations of the four-parameter models. 72

Appendix B Calculation of the forces acting on the spindle 73

Appendix C Void ratio calculations 75

List of Figures

Figure 2-1: Void ratio (e) vs vertical effective stress (σ'_v) relationship of Oil Sand Tailings. Source: Ito and Azam (2013). 13

Figure 2-2: Coefficient of volume compressibility for some tailings listed in Table 2-1. 14

Figure 2-3: Schematic of the four-parameter on a compression curve. Note: β and σ'_c define the curvature of the compression curve. 14

Figure 2-4: Remoulded clay-Sodium Montmorillonite fitted with four-parameter models, a) semi-log scale and b) linear scale Source: Chong and Santamarina (2016a). 15

Figure 2-5: Particle size distribution of tailings reported in Table 2-1. 15

Figure 2-6: A correlation between the compression index and the plasticity index. Source: Sridharan and Nagaraj (2011). 16

Figure 2-7: Compression index vs plasticity index relationship of tailings reported in Table 2-1. 16

Figure 2-8: Correlation between D_{50} and compression index of tailings reported in Table 2-1. 17

Figure 2-9: Effect of the initial void ratio on the compressibility of Gold and Iron tailings. Source: Reid and Fourie (2015). 17

Figure 2-10: The coefficient of consolidation for reported tailings in Table 2-2. 18

Figure 2-11: Particle size distribution versus the coefficient of consolidation relationship for tailings in Table 2-2. 18

Figure 3-1: Scanning electron microscope images of a) coarse (250x) and b) fine particles (800x). Source Torres-Cruz and Santamarina (2020) 27

Figure 3-2: XRF results of oxide concentration. Note that Fine = < 75 μm , medium = > 75μm but < 150 μm, and coarse = > 150 but < 600 μm grain sizes. 27

Figure 3-3: Grain size distribution comparison from laser diffractometer and sieve analysis a) 64/61 b) 98/68. 28

Figure 3-4: Rowe-Barden consolidation cell setup. 29

Figure 3-5: Cross-section of Rowe-Barden consolidation cell. Source: Kianfar (2013). 29

Figure 3-6: Apparatus used for moist tamping method. 30

Figure 4-1: Compression curves of the 64/61 mix a) Stepped loading test b) Constant rate of loading test. 36

Figure 4-2: Compression curves of the 98/68 mix a) Stepped loading test b) Constant rate of loading test. 36

Figure 4-3: Compression index relationship with effective stress a) 64/61 mix and b) 98/68 mix. 37

Figure 4-4: Compression indices of the 64/61 and 98/68 mixes. Note: grey markers are compression indices of tailings reported in Table 2-1 and Table 2-2..... 38

Figure 4-5: Correlation of the recompression indices with the initial void ratio. 38

Figure 4-6: 64/61 stepped loading and constant rate of loading test comparison a) compression curves b, c and d) tangent constrained modulus. Note that CRL=constant rate of loading and SL=stepped loading... 39

Figure 4-7: 98/68 stepped loading and constant rate of loading test comparison a) compression curves b, c and d) tangent constrained modulus. Note that CRL=constant rate of loading and SL=stepped loading... 40

Figure 4-8: Effect of fabric from stepped loading test a) compression curves and b) tangent constrained modulus..... 41

Figure 4-9: Effect of fabric from the constant rate of loading test a) compression curves and b) tangent constrained modulus. 42

Figure 4-10: Coefficient of volume compressibility for the 64/61 loose, medium and dense specimens a) stepped loading test b) constant rate of loading test. 43

Figure 4-11: Coefficient of volume compressibility for the 98/68 loose, medium and dense specimens a) stepped loading test b) constant rate of loading test 43

Figure 4-12: Coefficient of volume compressibility of the 64/61 and 98/68 mixes. Note: grey plots are m_v values of tailings reported in Table 2-1 and Table 2-2. 44

Figure 4-13: Pore pressure dissipation curve. 44

Figure 4-14: Coefficient of consolidation plots of the 64/61 and 98/68 mix. Grey lines are plots from previous studies presented in Table 2-1 and Table 2-2. 45

Figure 4-15: Coefficient of consolidation plot of a) 64/61 and b) 98/68. 46

Figure 4-16: Effect of fabric on the coefficient of consolidation. 46

Figure 5-1: 64/61 Stepped loaded compression curves (a and c) and tangent modulus of (b and d) of the loose and medium density specimen. 51

Figure 5-2: 64/61 Stepped loaded compression curves (a and c) and tangent modulus (b and d) of the dense and slurry specimen. 52

Figure 5-3: 98/68 Stepped loaded compression curves (a and c) and tangent modulus (b and d) of the loose and medium density specimen. 53

Figure 5-4: 98/68 Stepped loaded compression curves (a and b) and tangent modulus (c and d) of the dense and slurry specimen. 54

Figure 5-5: 64/61 CRL compression curves (a and c) and tangent modulus (b and d) of the loose and medium density specimen. 55

Figure 5-6: 64/61 CRL compression curves (a and c) and tangent modulus (b and d) of the dense and slurry specimen. 56

Figure 5-7: 98/68 CRL compression curves (a and c) and tangent modulus (b and d) of the loose and medium density specimen. 57

Figure 5-8: 98/68 CRL compression curves (a and c) and tangent modulus (b and d) of the dense and slurry specimen. 58

Figure 5-9: Power model correlation of the void ratio range with the initial void ratio of the 64/61 and 98/68 mix (where e_L is the limiting void ratio at low stress, e_H is the limiting void ratio at high stress and e_0 is the void ratio at 10 kPa). 59

Figure 5-10: Compression curves (a) and tangent modulus (b and c) of Oil sand tailings fitted with the power model 59

Figure 5-11: Compression curves (a) and tangent modulus (b) of Aluminium Bauxite fitted with the arctangent model. 60

Figure 5-12: Compression curves (a) and tangent modulus (b and c) of Iron tailings fitted with the hyperbolic model. 60

Figure 5-13: Compression curves (a) and tangent modulus (b and c) of Gold tailings fitted with the modified Terzaghi model. 61

Figure 5-14: Compression curves (a) and tangent modulus (b and c) for tailings fitted with the exponential model. 62

Figure 5-15: Compression curves (a) and tangent modulus (b and c) for tailings reported by (Mittal and Morgenstern, 1976) fitted with the arctangent model. 63

Figure 5-16: Residual plot of each model 64

List of Tables

Table 2-1: Summary of physical properties of tailings. 9

Table 2-2: Compression index and consolidation properties of tailings reported in Table 2-1. 11

Table 2-3: Fitting parameters for remoulded soil-sodium Montmorillonite. Modified from (Chong and Santamarina, 2016b) 13

Table 3-1:Summary of index properties of non-plastic platinum tailings. Source: Torres Cruz (2016). ... 25

Table 3-2: Summary of the testing programme. 26

Table 3-3: Methods of tracking the void ratio throughout the test. 26

Table 5-1: R^2 values of the 64/61 mix 50

Table 5-2: R^2 values of the 98/68 mix. 50

List of Symbols

AP	Axial pressure	$\log \sigma'$	The logarithm of vertical stress
BP	Back pressure	LVDT	Linear variable displacement transducer
β	Parameter defining the central trend of a compression curve	M	Tangent stiffness
C_c	Compression index	max σ	Maximum stress
CO_2	Carbon dioxide	m_{dry}	Dry mass of solids
C_r	Recompression index	ML	Non-plastic silt
CRL	Constant rate of loading	MT	Moist tamping
C_u	Coefficient of uniformity	m_v	Coefficient of volume compressibility
c_v	Coefficient of consolidation	m_{water}	Mass of water
D	Tangent constrained modulus	m_{wet}	Wet mass of solids and water
D_{10}	Particle size in mm where 10% of the material passes	PI	Plasticity index
D_{30}	Particle size in mm where 30% of the material passes	ρ_s	Particle density
D_{50}	Particle size in mm where 50% of the material passes	RD	Relative density
D_{60}	Particle size in mm where 60% of the material passes	R^2	Root mean square error
e	Void ratio	SL	Stepped loading
e_0	Initial void ratio	SLU	Slurry
e_{100}	Void ratio at 100 kPa	t	Time
Δe	Void ratio change	t_{50}	Time at 50% dissipation
e_c	Void ratio defining the central trend of compression curves	u	Pore pressure
e_{EOT}	Void ratio at the end of the test	μ	viscosity
e_{int}	Intermediate void ratio	ΔV	Volume changes
e_H	Asymptotic void ratio at high stress	ΔV_H	Height changes in terms of volume
Δe_H	Void ratio changes calculated from height changes	V_{max}	Total volume of the specimen at maximum stress
e_L	Asymptotic void ratio at low stress	V_s	Volume of solids
e_{max}	Maximum void ratio	V_v	Volume of voids

e_{min}	Minimum void ratio	$w_{\%}$	Water content
Δe_v	Void ratio changes calculated from volume changes	γ_w	Unit weight of water
$e_{(\Delta H_EOT)}$	Void ratio calculated from the end of test void ratio while tracking height changes	z	Thickness
$e_{(\Delta H_max)}$	Void ratio calculated from maximum stress void ratio while tracking height changes	σ	Total stress
$e_{(\Delta v_EOT)}$	Void ratio calculated from the end of test void ratio while tracking volume changes	σ'	Effective stress
$e_{(\Delta v_max)}$	Void ratio calculated from maximum stress void ratio while tracking volume changes	Δσ	Total stress change
EOT	End of test	σ'^{β}	Term for exponential models
F_{AP}	Axial force	σ'_c	Effective stress defining the central trend of compression curves
F_{BP}	Back force	σ'_H	Effective stress corresponding to e_H
FC	Fines content	σ'_L	Effective stress corresponding to e_L
G_s	Specific gravity	σ'_{max}	Maximum stress
ΔH	Height change	σ_v	Total vertical stress
H_{max}	Height of the specimen at maximum stress	σ'_v	Vertical effective stress
k	Hydraulic conductivity		
LL	Liquid limit	e_{max}	Void ratio at maximum stress

1 Introduction

1.1 Topic overview

The mining industry has been experiencing an increase in tailings dam failures. Most recently, the Brumadinho tailings dam in Brazil collapsed, causing a massive mudslide that killed at least 232 people. The failure occurred several years after the Mount Polley and Samarco dam failures which also resulted in disastrous social, environmental and economic losses (Oberie et al., 2020). Forensic analysis of some of the tailings dam failures has revealed several procedures which could prevent the occurrence of failures. Among them are the improvement of material characterization, effective engineering and management of dams (Santamarina et al., 2019).

Material characterization is required prior to the construction of tailing dams of which consolidation and compressibility properties of tailings are some of the properties to be investigated (Blight, 2010). Consolidation is a time-dependent process of pore water pressure dissipation. It affects the position of the phreatic line in the dam which affects the effective stresses, and thus the mechanical stability of the impoundment during and after the mining operation. Consolidation is dependent on compressibility (Ahmed and Siddiqua, 2014) which has a significant effect on the final in-situ void ratio and consequently on the shear strength of the tailings (Vick, 1990).

Studies on the consolidation and compressibility properties of tailings have shown that their behaviour is unique for tailings and that their properties are related to the grain size distribution, mining technology, mineralogical composition and deposition methods (Blight, 1979; Hu et al., 2017; Qiu and Sego, 2001). Therefore, in order to understand the behaviour of the tailings, a site-specific study is required.

Conventionally, the one-dimensional oedometer was used to investigate consolidation and compressibility properties of tailings but more advanced apparatus have been developed. The Rowe-Barden consolidation cell is a one-dimensional testing apparatus that allows different loading conditions to be applied, control of drainage, back pressure application and measurement of pore pressure (Head, 1994). The apparatus has not been popularly used in the study of tailing dams and this thesis aims to contribute to filling this gap. The current study is an investigation of the compressibility and consolidation behaviour of non-plastic tailings and the effect that their physical properties have on tailings behaviour.

1.2 Objective

The main objective of this study is to characterize the compressibility and consolidation properties of non-plastic platinum tailings using the Rowe-Barden consolidation cell.

The specific objectives are:

- Conducting stepped loading tests (SL) on two gradations of non-plastic platinum tailings at different densities, from which compressibility and consolidation behaviour can be evaluated.
- Conducting continuous loading tests (CRL) on similar specimens to the ones used for the stepped loading testing.
- Comparing the compressibility and consolidation behaviour of non-plastic platinum tailings to documented tailings.
- Comparing laser diffractometer particle size distribution to the conventional sieve analysis and hydrometer particle size distribution curves.
- Exploring the effect of loading methods on the compressibility behaviour.
- Investigating the effect of fabric on the compressibility and consolidation behaviours of the tailings.
- Exploring new models to capture the compression curves.

1.3 Thesis Outline

The thesis has been organised as follows: Chapter 2 discusses the conventional methods of reporting stress-strain relationships and introduces relatively novel models proposed by Chong and Santamarina (2016a) to model the relationship between void ratio (e) and effective stress (σ′). The chapter also describes the compressibility and consolidation behaviour of tailings reported in the literature. Chapter 3 describes the apparatus and methods used to test non-plastic platinum tailings and also discusses in detail the different methods used to calculate the void ratio. Chapter 4 presents the results of the tests conducted and compares them with the results reported in the literature. Chapter 5 explores the fitting of the models proposed by Chong and Santamarina (2016a) on the compression curves obtained from the test conducted. Compression curves derived from literature are also fitted. Chapter 6 presents a summary of the findings.

2 Literature review

2.1 Introduction

The objective of this chapter is to present the available literature on the consolidation and compressibility behaviour of tailings, as well as the models used to characterise this behaviour. The stress-strain relationships that are commonly used to model soil behaviour and updated models to account for a wide stress range are discussed. The compressibility and consolidation properties of tailings from documented literature are also presented. Furthermore, the compressibility and consolidation properties of documented tailings are discussed by considering the effect of particle size distribution, plasticity and density.

2.2 Compressibility

Compressibility is the property through which the particles of soil are brought closer to each other by pressure, as a result, volume change occurs. It is an important property in the study of tailings behaviour because conventional, tailings are transported continuously as highly saturated material that undergoes large volume changes (Blight and Bentel, 1983). Stresses in the dam accumulate due to the increasing height of the tailings resulting from continuous deposition of residual material. The accumulation of stress results in volume changes which can be quantified by studying the compression behaviour of the tailings. In the current study, a dataset from well documented studies of the consolidation and compressibility behaviour of tailings was compiled (Table 2-1 and Table 2-2). Table 2-1 reports on the physical properties and Table 2-2 shows a summary of the compressibility and consolidation parameters and the method that was used to conduct the test. The information will be used herein to assess the compressibility behaviour of tailings.

2.2.1 Stress-strain relationships

To understand the process of compressibility, the stress-strain relationship existing within the tailings mass and the effect that gradation has on this relationship needs to be studied. That can be achieved by conducting a laterally confined compression test or an isotropic test in the triaxial apparatus (Lambe and Whitman, 1969). The present study will consider the stress-strain relationship in a Rowe-Barden cell which imposes confined compression conditions. Three parameters are used to define the stress-strain relationship in confined compression testing, the compression index (C_c), the coefficient of volume compressibility (m_v) and the tangent constrained modulus (D).

The compression index (C_c) is the slope of the void ratio (e) versus the logarithm of vertical effective stress (σ'_v) for the linear part of the one-dimensional curve. This type of plot is commonly used to illustrate the stress-strain behaviour over a wide range of stresses. For most clays, the void ratio (e) versus the logarithm

of vertical effective stress (σ'_v) is essentially a straight line beyond the pre-consolidation pressure and therefore the compression index (C_c) is reported as a constant, independent of the stress level (Knappett and Craig, 2012; Lambe and Whitman, 1969). However, in some soils, like Oil Sand tailings shown in Figure 2-1, the void ratio (e) versus the logarithm of vertical effective stress (σ'_v) plot is not straight but can be concave upward or downward depending on the characteristics of the soils (Butterfield, 1979; Sridharan and Gurtug, 2005).

The coefficient of volume compressibility (m_v) is an alternative stress-strain relationship defined as the slope of the volumetric strain (ϵ_v) vs the vertical effective stress (σ'_v) curve (Lambe and Whitman, 1969). Its value for a particular soil is not constant but it depends on the stress range or void ratio over which it is calculated. Figure 2-2 illustrates this by showing the relationship between the coefficient of volume compressibility (m_v) and void ratio (e) for several tailings listed in Table 2-1. Finally, the tangent constrained modulus (D) is the reciprocal of the coefficient of volume compressibility (m_v) and it defines the stiffness behaviour of soils (Craig, 2004).

2.2.2 Four-parameter compressibility models

The conventional way of describing the stress-strain relationship using the compression index (C_c) is not always sufficient. Studies have shown that in more compressible soil which undergoes relatively large strains, the slope of the void ratio (e) versus the logarithm of vertical effective stress is not straight but could be slightly concave upward or downward (Sridharan and Nagaraj, 2011). This has led to several compressibility models being proposed to improve the modelling of compressive behaviour of soils (Butterfield, 1979; Gregory et al., 2006; Juarez-Badillo, 1981 and Pestana and Whittle, 1995). Among the models proposed are five models, each of which contains four fitting parameters (Chong and Santamarina, 2016a). The models were modified from previously suggested models and other functions to satisfy asymptotic void ratio at high stresses (e_H) and void ratio at low stresses (e_L). The models are named: power, hyperbolic, modified Terzaghi, exponential and arctangent. They describe the compressibility curve over wide stress ranges by defining the physical asymptotic values and the curvature of the compression curves. Figure 2-3 shows a schematic of the features of the compression curve controlled by the four-parameters. The models were fitted to remoulded and natural plastic soils and were found to accurately model the compression curves (Figure 2-4 and Table 2-3) (Chong and Santamarina, 2016a).

The five models fall into two broad categories: 1) semi-logarithmic (e-log σ') stress and 2) exponential (e-σ'^{β}). The modified Terzaghi model (Equation 1a) is the only one that falls in the semi-logarithmic category. It was modified from Terzaghi's classic linear semi-logarithmic model to satisfy the void ratios e_L and e_H

to which soils asymptotically tend at low and high stresses, respectively. In this model, C_c and e_c define the central trend.

$$e = e_c - C_c \log\left(\frac{1\ \text{kPa}}{\sigma' + \sigma'_L} + \frac{1\ \text{kPa}}{\sigma'_H}\right)^{-1} \quad \text{Equation 1a}$$

σ'_L and σ'_H are computed in kPa as shown in Equations 1b and 1c:

$$\sigma'_H = 10^{(e_c - e_H)/C_c} \quad \text{Equation 1b}$$

$$\sigma'_L = \frac{\sigma'_H}{10^{(e_L - e_H)/C_c} - 1} \quad \text{Equation 1c}$$

Models in terms of e-σ'^{β} include the power (Equation 2), exponential (Equation 3), hyperbolic (Equation 4) and the arctangent model (Equation 5) were β and σ'_c are parameters defining the central trend of the curves.

$$e = e_H + (e_L - e_H)\left(\frac{\sigma' + \sigma'_c}{\sigma'_c}\right)^{-\beta} \quad \text{Equation 2}$$

$$e = e_H + (e_L - e_H)\exp^{-\left(\frac{\sigma'}{\sigma'_c}\right)^{\beta}} \quad \text{Equation 3}$$

$$e = e_L - (e_L - e_H)\frac{1}{1 + \left(\frac{\sigma'_c}{\sigma'}\right)^{\beta}} \quad \text{Equation 4}$$

$$e = e_L + \frac{2}{\pi}(e_L - e_H)\arctan\left[-\left(\frac{\sigma'}{\sigma'_c}\right)^{\beta}\right] \qquad \text{Equation 5}$$

The four e-σ'^{β} models were found to be more flexible to capture the compression behaviour of structured natural soils while the remoulded soils were adequately fitted by all five models. Tangent stiffness equations for each model were derived by Chong and Santamarina (2016a). The resulting expressions, presented in Appendix A, are fundamentally different from the small strain stiffness in that they reveal the instantaneous rate of fabric change during large strain tests (Chong and Santamarina, 2016a).

2.2.3 Compressibility behaviour of tailings

The magnitude of deformation that will take place in an impoundment depends on the state and physical properties of the tailings. This includes the plasticity, particle size distribution, and the initial void ratio. Their influence on compressive behaviour is discussed below using as a basis the tailings whose properties are summarised in Table 2-1, and whose particle size distributions are shown in Figure 2-5.

Sridharan and Nagaraj (2011) found a correlation between the compression index (C_c) and the plasticity index (PI) of natural soils. In their findings, the compression index (C_c) increases with plasticity index (Figure 2-6). Figure 2-7 presents a plot of the relationship between the compression index and plasticity index for reported tailings in Table 2-1. No clear correlation is observed, however, the compressibility of tailings from the same impoundment shows highly plastic tailings to be more compressible in comparison to low plastic tailings. From Table 2-1 and Table 2-2, the compression index of Iron_30 (ID 6) with a plasticity index of 9 is higher than Iron_120 (ID 5) with non-plastic behaviour.

The particle size distribution influences the packing efficiency of a material, and hence compressibility (Blight, 1979). Figure 2-8 plots the compression index (C_c) versus D_{50}. An inverse correlation is observed as the compression index (C_c) decreases with increasing D_{50}. The slope of the trend is much higher below a D_{50} of 0.1 mm while above a D_{50} of 0.1 mm, the compression index does not show much dependence on D_{50}. Generally, a coarser particle size distribution will exhibit lower compressibility (Hu et al., 2017). Particle size distribution also affects the void ratios that soil material can attain and therefore, compressibility. The effect of the initial void ratio was studied by Reid and Fourie (2015) on Gold and Iron tailings. They found that high initial void ratio specimens although more compressible tend to have a much lower in-situ void ratio at a stress of 1000 kPa (Figure 2-9). Similarly, Li (2017) showed that the compression curves of tailings tested at different densities tend to converge at high stresses of above 7 MPa.

2.2.4 Effect of fabric on compressibility

The difficulty in attaining undisturbed samples of tailings has resulted in multiple methods adopted to prepare a specimen for laboratory testing. These methods result in different fabrics. The effect of fabric from sample preparation on the compression behaviour of tailings has not been extensively studied. Mainly because specimens have to be tested at the same void ratio such that any changes observed in the behaviour of the tailings can be attributed to differences in fabric. A study on the effect of fabric by Chang (2009) found slurry deposition to produce a fabric similar to the undisturbed Gold tailings while moist tamping produced a flocked fabric. Minor fabric effects were observed on the compression behaviour of fine pond tailings. However, slurry specimens were more compressible than moist tamping specimens of the coarse-grained Gold tailings (Chang, 2009).

2.3 Consolidation

2.3.1 Theory of consolidation

The rate at which conventional tailings deposition can safely take place depends on the rate at which pore water pressure dissipates within a saturated mass. In this dissipation process, the stresses, strain and time bear certain definite relationships to each other (Taylor, 1948). The gradual process which simultaneously involves an escape of water and gradual compression is called consolidation. It can be classified as primary or secondary consolidation. Primary consolidation involves the drainage and compression of a saturated soil as excess pore pressure dissipates. Secondary consolidation is attributed to the realignment of particles and grain to grain slippage with time under constant stress condition. Secondary consolidation is reported to be small and relatively insignificant in tailings compared to primary consolidation (Vick, 1990).

Primary consolidation is further described by Terzaghi's one-dimensional theory of consolidation which assumes full saturation, incompressibility of water and particles, constant coefficient of permeability (k), Darcy's law is valid, and the time lag of consolidation is due to the low permeability of the soil (Terzaghi, 1943). The governing equation is

$$\left[\frac{k}{m_v \gamma_w}\right] \times \frac{\partial^2 u}{\partial z^2} = \frac{\partial u}{\partial t} \qquad \text{Equation 6}$$

where k is the hydraulic conductivity, m_v is the coefficient of volume compressibility, u is the excess hydrostatic pressure, t is time, z is the depth and γ_w is the unit weight of water. The fraction in the square brackets of Equation 6 is defined as the coefficient of consolidation (c_v):

$$c_v = \frac{k}{m_v \times \gamma_w}$$ Equation 7

From Equation 7, it is clear that consolidation (c_v) is dependent on the compressibility (m_v) and the permeability (k) characteristics of soils. The consolidation characteristics can be dominated by permeability or by compressibility (Hu et al., 2017; Vick, 1990). The variability of the consolidation behaviour is evident when considering the studies of tailings by different authors in Figure 2-10. For instance, Mittal and Morgenstern (1976) showed an increase in the coefficient of consolidation (c_v) with decreasing void ratio (ID 19), however, the opposite of behaviour was shown by Adajar & Cutora (2018) who observed a decrease in c_v with decreasing void ratio on Gold tailings (ID 38). Furthermore, data presented by Shamsai et al. (2007) on Copper tailings indicated a constant c_v with decreasing void ratio (ID 27). This highlights the complexity of tailings behaviour. Permeability characteristics may dominate at some void ratios and compressibility characteristics at others (Vick, 1990).

A relationship between the coefficient of consolidation and particle size was assessed by plotting the coefficient of consolidation (c_v) vs D_{50} for the tailings in Table 2-1. As seen in Figure 2-11 no correlation exists. The coefficient of consolidation (c_v) ranges between 0.0003 to 4 cm^2/s and can range within two orders of magnitude for a particular soil depending on its void ratio.

2.3.2 Effect of fabric on consolidation

The effect of fabric from sample preparation on the coefficient of consolidation was studied by Chang (2009) on Gold tailings. He found the coefficient of consolidation for the moist tamping specimens to be 2 to 3 times higher than that of the slurry specimens. Both moist tamped and slurry specimens displayed a higher coefficient of consolidation (c_v) value than the undisturbed specimens.

2.4 Summary

The stress-strain relationships, compressibility and consolidation behaviour of documented tailings have been presented. It is recognized that the particle size distribution has a greater effect on the compressive behaviour of tailings with D_{50} below 0.1 mm. Highly plastic tailings and those prepared at a high initial void ratio also exhibit high compressibility.

The consolidation behaviour of tailings greatly varies and is not uniquely correlated to the particle size D_{50}. The coefficient of consolidation can increase, decrease or remain constant with decreasing void ratio. Fabric effect on both compressibility and consolidation properties have been reported for Gold tailings.

Table 2-1: Summary of physical properties of tailings.

Tailings name	ID	G_s	PSD			Atterberg limits		Reference
			FC (%)	D_{50} (mm)	C_u	LL (%)	PI (%)	
Copper_ 120	1	2.75	31.3	0.12	9.43	-	-	(Qiu and Sego, 2001)
Gold_44	2	3.17	81.3	0.044	10.8	-	-	
Coal_29	3	1.94	66.4	0.0292	45.8	40	16	
Oil sand_182	4	2.6	21.2	0.182	75.5	-	-	
Iron_120	5	3.23	14.9	0.12	3.11	-	-	(Hu et al., 2017)
Iron_30	6	3.08	78.4	0.03	8.82	28	9	
Copper_120	7	2.77	14.24	0.12	2.15	-	-	
Copper_60	8	2.76	61.12	0.06	14.8	28	15	
Copper_74	9	2.72	65-27	0.074	67	18	-	(Volpe, 1979)
Copper_9	10	2.72	100-65	0.009	30	40	13	
SI_28	11	-	70	0.028	-	17.5	17.5	(Aubertin et al., 1996)
BE_32	12	-	77	0.032	-	17.5	17.5	
Sef_43	13	-	68	0.043	-	17.5	17.5	
SEC_75	14	-	53	0.075	-	17.5	17.5	
Copper_40	15	2.98	73	0.04	9	-	-	(Mittal and Morgenstern, 1976)
Copper_12	16	2.72	87	0.012	25	30.3	10.3	
Copper-Molybdenum_40	17	2.76	70	0.04	17	28.2	9	
Copper-Molybdenum_100	18	2.74	44	0.1	20	19.8	-	
Copper_100	19	2.96	44	0.1	28	23.3	-	
Iron_12	20	3.75	93	0.012	-	26	13	(de Oliveira Filho and Menezes, 2012)
Aluminium Bauxite_2.5	21	3.65	100	0.0025	4	48	17	
Gold	22	-	67	-	-	-	-	(Reid and Fourie, 2015)
Iron	23	-	69	-	-	27	8	
Gold_80	24	2.72	40	0.08	-	24	0	(Adajar and Zarco, 2013)
Gold	25	-	-	-	-	-	-	(Stone et al., 1994)
Copper_30	26	2.79	70	0.03	-	-	-	(Shamsai et al., 2007)

Tailings name	ID	G_s	PSD			Atterberg limits		Reference
			FC (%)	D_{50} (mm)	C_u	LL (%)	PI (%)	
Copper_10	27	2.79	100	0.01	-	29	8.00	
Copper_150	28	2.82	-	0.15	-	32	6	(Adajar and Cutora, 2018)
Oil sand_1.5	29	_	98	0.0015	-	59	36	(Suthaker and Scott, 1994)
Oil sand_8	30	_	86	0.008	6	-	-	(Wong et al., 2008)
Lead-Zinc_20	31	2.95	-	0.02	13	27	1	(Williams, 1977)
Flourite_20	32	2.72	10	0.02	-	27.4	9.4	(Carrere et al., 2011)
Oil sand_3	33	2.28	89	0.003	-	50	29	(Jeeravipoolvarn et al., 2009)
Coal	34	_	-	-	-	-	-	(Morris et al., 2000)
Gold_11	35	2.89	98	0.011	7.3	-	-	(Li et al., 2018)
Iron_220	36	3.365	20	0.22	10.4	-	-	(Li and Coop, 2018)
Gold_60	37	-	70	0.06	35	-	-	(Blight and Steffen, 1979)
Gold _10	38	-	98	0.01	9.5	-	-	

Note: Tailings names represent commodity_D_{50}(μm), G_s = specific gravity, FC = fines content, C_u = coefficient of uniformity, LL = liquid limit, PI = plasticity index and – shows that values were not reported by the scholar.

Table 2-2: Compression index and consolidation properties of tailings reported in Table 2-1.

ID	e_{100}	C_c	c_v (m^2/year)	k (cm/s) (10^{-6})	$\sigma'_{min} - \sigma'_{max}$ (kPa)	c_v -Calculation method	Experimental apparatus used	Type of tests
1	0.7	0.06-0.09	22.3-104.2	45-98	0.5-100	Curve fitting	Large strain consolidometer	One-dimensional test
2	0.7	0.08-0.16	13.5-80.1	27-67				
3	0.69	0.37-0.40	1.5-17.2	0.4-11				
4	0.5	0.27-0.32	0.3-8.5	0.22-0.63				
5	0.65	0.05	-	-	12.5-1600	-	Oedometer	One-dimensional test
6	0.89	0.26	-	0.2-2				
7	0.8	0.03	-	-				
8	0.87	0.09	-	5.1-30				
9	-	0.09	1166.8	500-8000	-	Curve fitting	Triaxial	Isotropic test
10	-	0.28	473	0.9-200				
11	0.7-0.48	0.05-0.08	15.8-1513.7	10-170	8-1100	Measured k and m_v and used equation 1	Oedometer	One-dimensional test
12	0.73-0.59	0.07-0.10	46.7-1715.6	20-200				
13	0.69-0.53	0.07-0.10	124.6-2188.6	25-200				
14	0.71-0.525	0.09-0.13	63.4-8893.2	50-400				
15	0.95	0.14	189.2-12164.4	10-50	2-3000	Measured k and m_v and used equation 1	Oedometer	One-dimensional test
16	0.91	0.32	3.15-315	0.4-3				
17	0.54	0.27	9.46-946.1	2-30				
18	0.54	0.17	-	50-200				
19	0.24	0.25	9.46-315	5.1-20				
20	1.45-1.4	0.74	-	0.1-20	0.001-100	-	Hydraulic consolidation test	One-dimensional test
21	1.87	4.05	-	0.1-100				
22	0.9	0.14	-	-	10-710	-	Slurry consolidometer	-
23	1.01	0.28	-	-				
24	-	0.08	12.6-31.5	5-2000	5-160	Curve fitting	Oedometer	One-dimensional test

ID	e_{100}	C_c	c_v (m^2/year)	k (cm/s) (10^{-6})	σ'_{min} – σ'_{max} (kPa)	c_v -Calculation method	Experimental apparatus used	Type of tests
25	1.3	0.39	6.1-26	0.12-0.38	5-600	Curve fitting	Rowe cell	-
26	-	-	15.8-63.1	0.03-40	10-1200	Curve fitting	Oedometer	One-dimensional test
27	-	-	31.5	-				
28	-	0.3416	12.44-49.77	-	5-200	Curve fitting	Oedometer	One-dimensional test
29	1.21	0.94	-	0.0006-2	0.2-700	-	-	-
30	1.12	1	1-1000	0.2-7	0.2-400	-	Slurry consolidometer	-
31	1.14	1.08	-	-	-	-	-	One-dimensional test
32	0.97	0.17	-	-	-	-	Oedometer	One-dimensional test
33	0.81	1.33	-	0.001-46.3	0.01-700	-	10 m standpipe tests	-
34	0.67	0.14	-	-	10-1650	-	-	-
35	1.09	0.23	-	-	17-20000	-	Oedometer	One-dimensional test
36	0.92	0.15	-	-	10-7000	-	Oedometer	One-dimensional test
37	-	-	309-385	-	200-850	-	Triaxial	Isotropic test
38	-	-	21-154	-				

Note: e_{100}= void ratio at 100 kPa, C_c = compression index, c_v = coefficient of consolidation, k = hydraulic conductivity, σ'_{min}=mimimum stress, σ'_{max}= maximum stress and – shows that values were not reported by the scholar.

Table 2-3: Fitting parameters for remoulded soil-sodium Montmorillonite. Modified from (Chong and Santamarina, 2016a)

Model	Parameter	Montmorillonite
Modified Terzaghi	e_L	36.5
	e_H	0.20
	e_c	52
	C_c	21.5
Power	e_L	35.1
	e_H	0.40
	β	1.0
	σ'_c (kPa)	48
Exponential	e_L	38.5
	e_H	1.40
	β	0.55
	σ'_c (kPa)	70
Hyperbolic	e_L	36.0
	e_H	0.40
	β	0.9
	σ'_c (kPa)	43
Arctangent	e_L	36.5
	e_H	0.30
	β	0.7
	σ'_c (kPa)	42

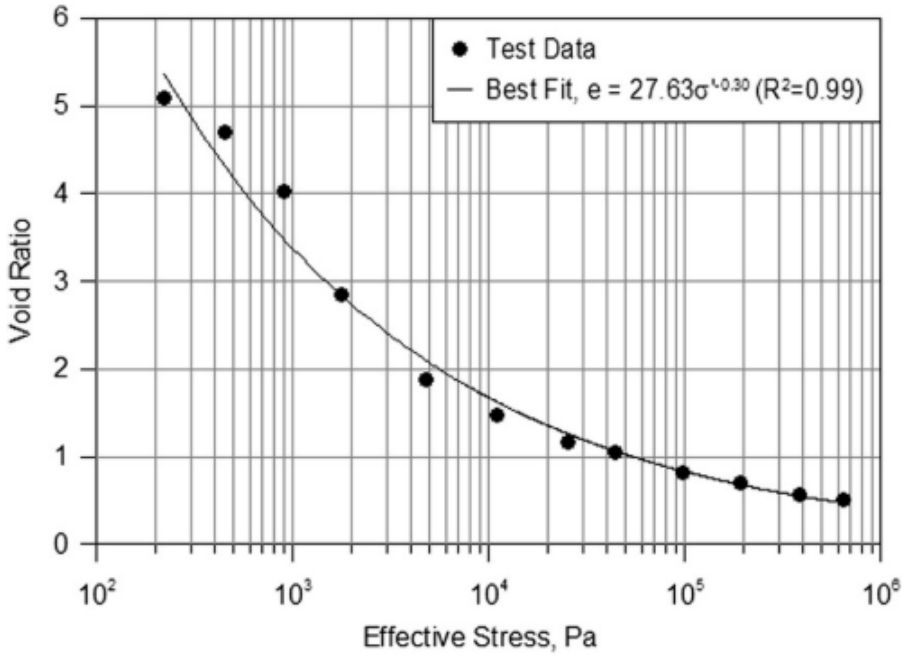

Figure 2-1: Void ratio (e) vs vertical effective stress (σ'_v) relationship of Oil Sand Tailings. Source: Ito and Azam (2013).

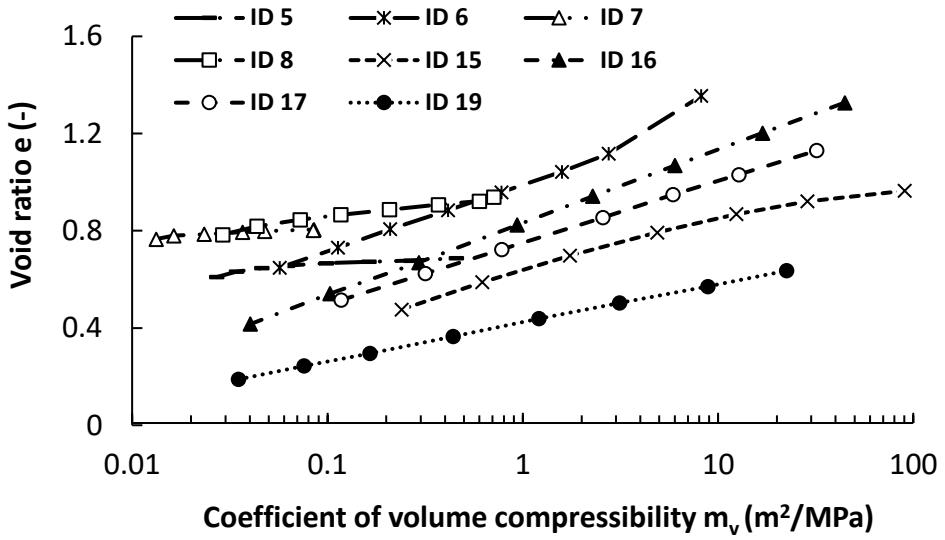

Figure 2-2: Coefficient of volume compressibility for some tailings listed in Table 2-1.

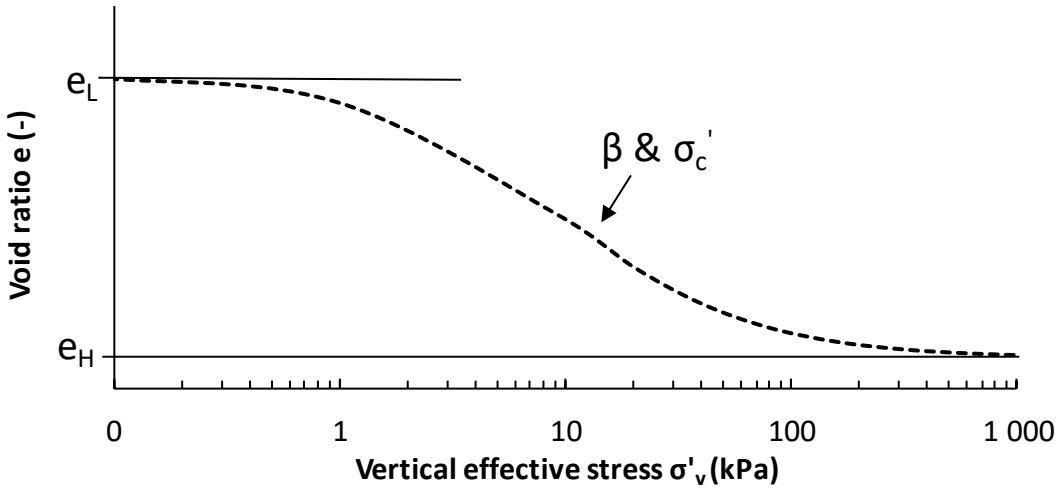

Figure 2-3: Schematic of the four-parameter on a compression curve. Note: β and σ'_c define the curvature of the compression curve.

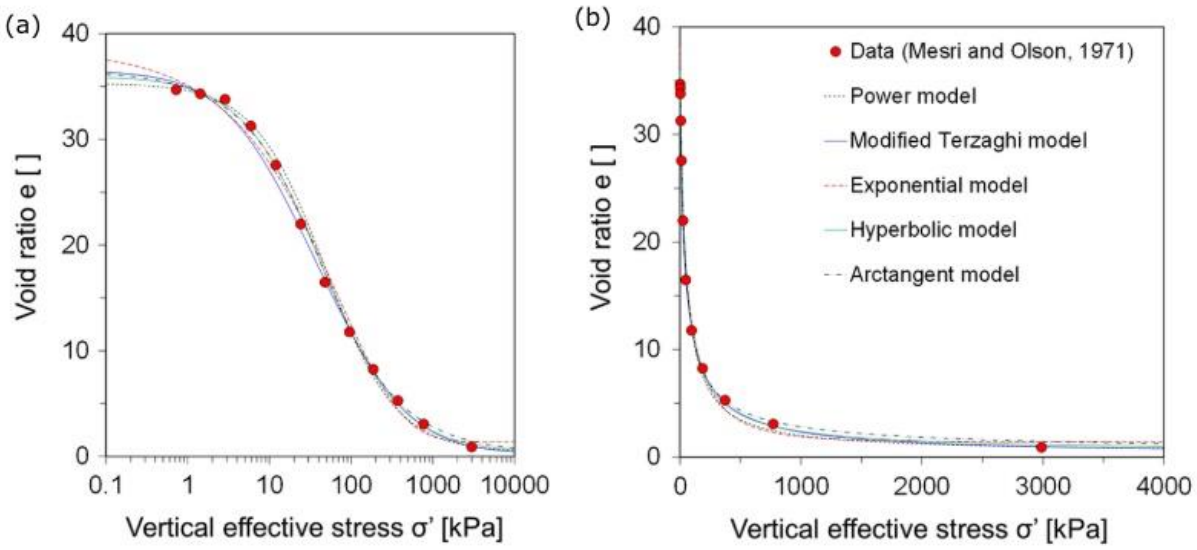

Figure 2-4: Remoulded clay-Sodium Montmorillonite fitted with four-parameter models, a) semi-log scale and b) linear scale Source: Chong and Santamarina (2016a).

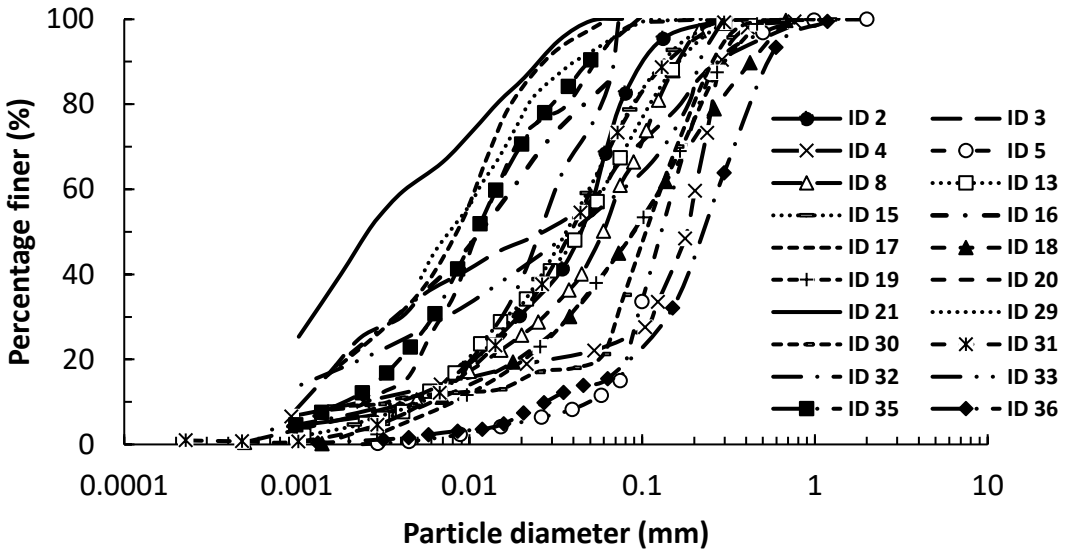

Figure 2-5: Particle size distribution of tailings reported in Table 2-1.

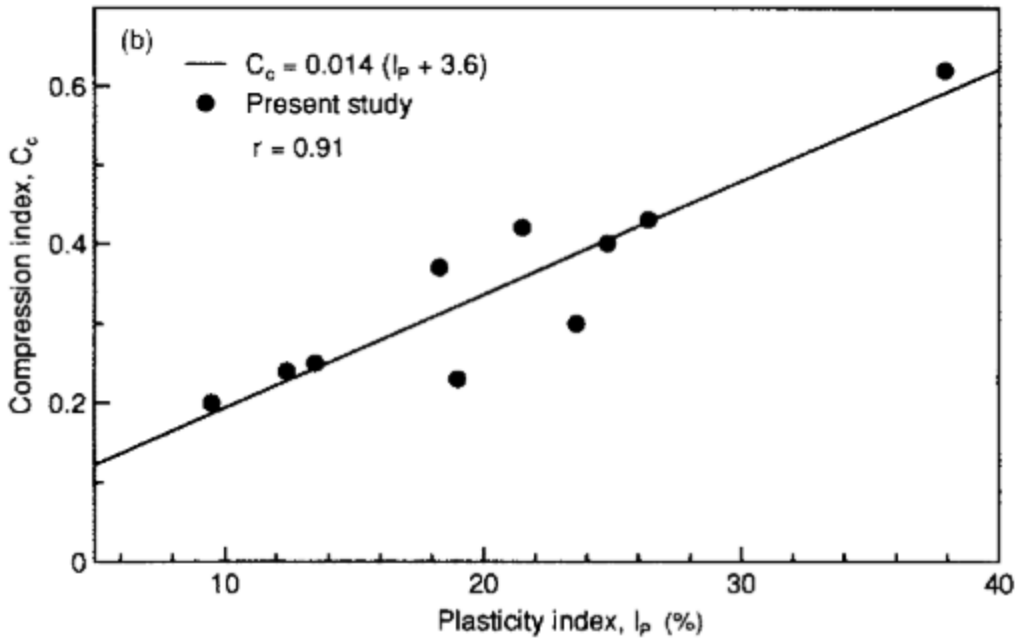

Figure 2-6: A correlation between the compression index and the plasticity index. Source: Sridharan and Nagaraj (2011).

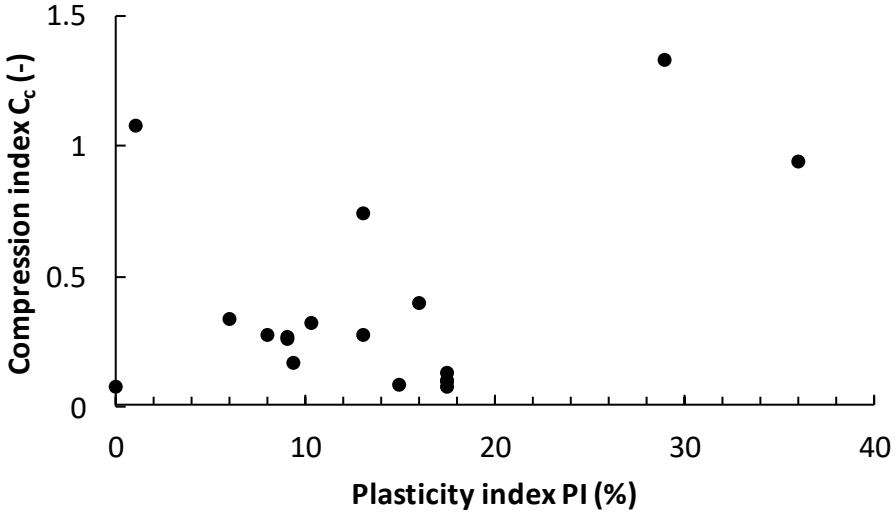

Figure 2-7: Compression index vs plasticity index relationship of tailings reported in Table 2-1.

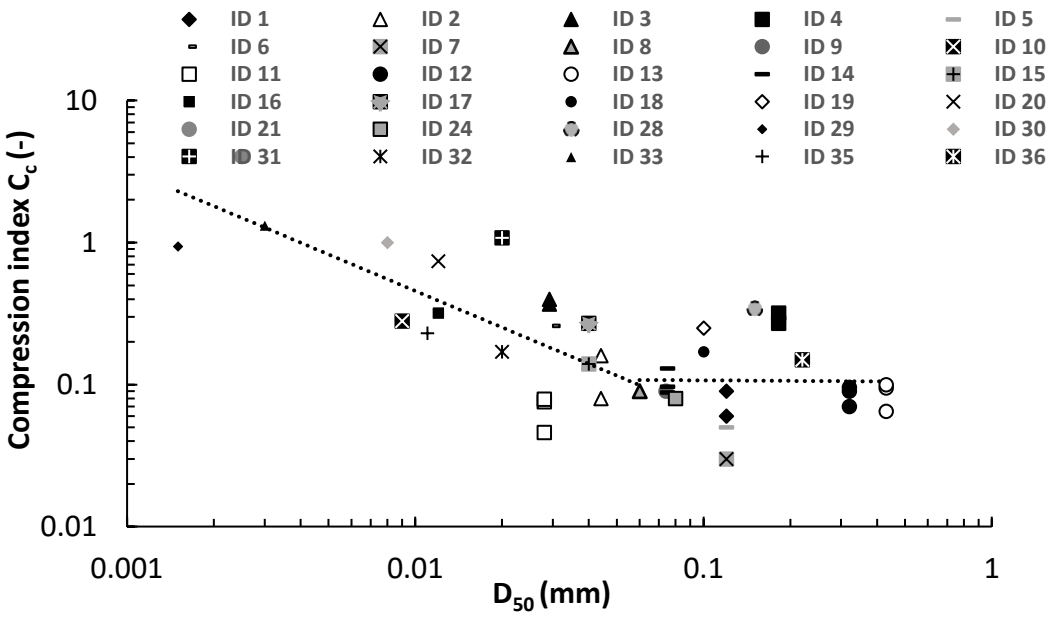

Figure 2-8: Correlation between D_{50} and compression index of tailings reported in Table 2-1.

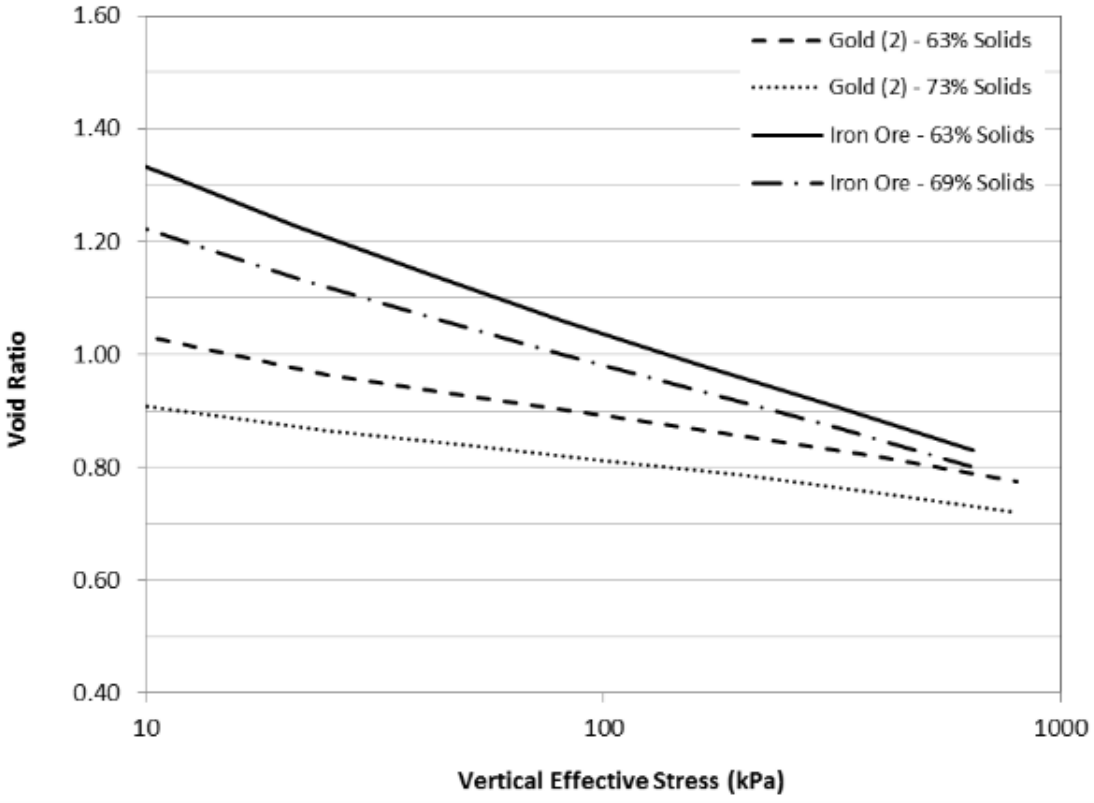

Figure 2-9: Effect of the initial void ratio on the compressibility of Gold and Iron tailings. Source: Reid and Fourie (2015).

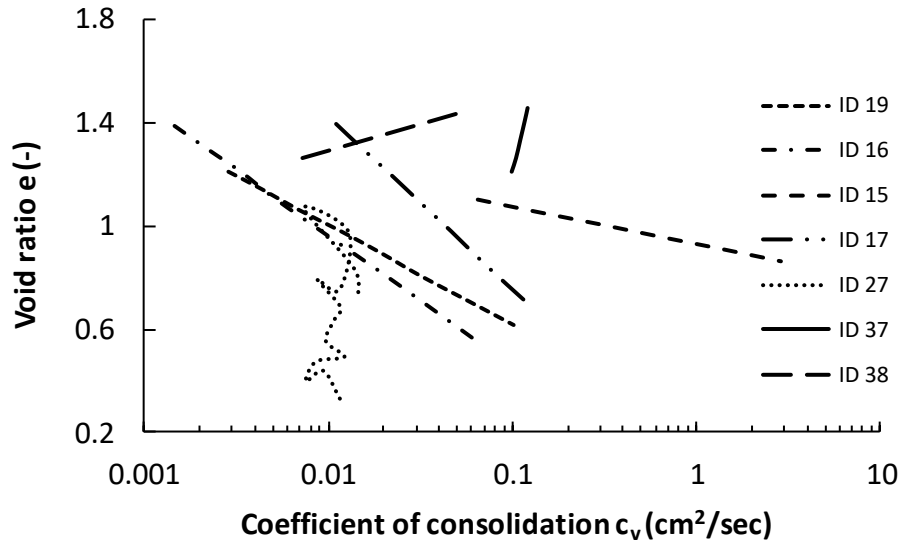

Figure 2-10: The coefficient of consolidation for reported tailings in Table 2-2.

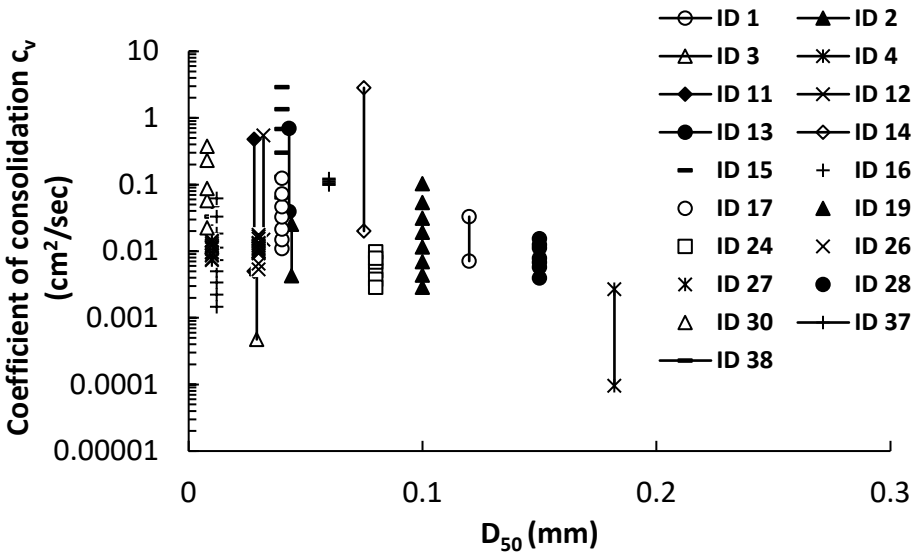

Figure 2-11: Particle size distribution versus the coefficient of consolidation relationship for tailings in Table 2-2.

3 Materials and Methods

3.1 Introduction

Chapter 3 describes the properties of the tailings tested and presents in detail the experimental work conducted. This includes the description of the experimental methods as well as the equipment used in the testing. The sample preparation method and the methods of calculating void ratio are also discussed.

3.2 Tested material

Platinum tailings were collected from an upstream platinum tailings dam located in the North West Province of South Africa. The tailings come from the same samples collected by Torres-Cruz (2016) to investigate their critical state line. The tailings are non-plastic and exhibit a predominantly angular shape for all particle sizes (Figure 3-1). Four major minerals make up the mineralogical concentration of the platinum tailings, Orthopyroxene (~ 35), plagioclase (~ 26), chromite (~19) and hornblende (~8%). Clinopyroxene and biotite are present at lower concentrations of less than 4 % (Dacosta, 2017). The elemental composition of the tailings was investigated in this study using an X-ray fluorescence technique. Figure 3-2 reports the dominant oxides.

To explore the effect of grain size distribution, the tailings were sieved and recombined into two mixes, 64/61 and 98/68. The mixes were assigned a code with the format $FC/e_{min}\cdot 100$, where FC is the fines content in % and e_{min} is the minimum void ratio. Both mixes classify as non-plastic silts (ML) in the Unified Soil Classification System and their physical properties are summarized in Table 3-1.

Torres-Cruz (2016) determined the particle size distribution of the mixes by using dry sieving and sedimentation (i.e., hydrometer analysis). As a verification, the current study used a laser diffractometer to measure the particle size distribution of the tailings. Figure 3-3 shows that the particle size distribution obtained with the laser diffractometer underestimates the amount of fines and presents a much coarser distribution than the curves obtained from sieving and sedimentation procedures. Similar results were reported by others and they attributed the observed differences to the non-spherical form of the particles (Beuselinck et al., 1998; Blott and Pye, 2006; and Konert and Vandenberghe, 1997). For consistency, the index properties reported in Table 3-1 and the codes for the mixes were based on the particle size distribution reported by Torres-Cruz (2016).

3.3 Testing equipment

The mechanical properties of the tailings were investigated using the Rowe-Barden consolidation cell in which vertical stress was applied under zero lateral strain conditions (Rowe and Barden, 1966). This apparatus offers several advantages over the conventional oedometer cell such as reduced vibrations during loading, control and measurement of drainage during consolidation, pore pressure measurement, redundancy in volume change measurements and back pressure application (Head, 1986 & Rowe and Barden, 1966).

The Rowe-Barden cell used has a 100 mm diameter and a 32 mm height. The cell is connected to two pressure controllers, an LVDT and a pore pressure transducer (Figure 3-4). The Rowe-Barden cell applies vertical total stress by means of water pressure acting on a flexible diaphragm. A standard pressure controller (3 MPa capacity) connects to the flexible diaphragm through the axial pressure valve and controls the water pressure. The resulting deformation of the specimen is measured by a displacement transducer that connects to a spindle attached to the flexible diaphragm. Back pressure is applied by a second pressure controller (3 MPa capacity) through the spindle onto the top of the specimen. Drainage during consolidation is permitted by a bronze porous stone through the back pressure line and it is recorded by the back pressure controller. Pore pressure is measured at the base of the specimen (Figure 3-5).

3.4 Specimen preparation

Two specimen preparation methods were used: slurry deposition and moist tamping. For the slurry deposition method, four specimens were created. Two 98/68 mix specimens (SLU_ 98) and two 64/61 mix specimens (SLU_64). The specimens were prepared by mixing them with deaired water until the consistency of the mixture resembled that of a slurry. Care was taken to reduce bleeding in the mixture. The specimen was enclosed to reduce excessive evaporation and allowed to cure overnight. A similar preparation method was used in previous testing programmes investigating the mechanical behaviour of tailings (e.g. Li, 2017). Following curing, the slurry was spooned into the Rowe-Barden cell and a filter paper and bronze porous disc were placed on top of the specimens. The cover was secured and bolted.

For the moist tamping method, 16 specimens were created to encompass the maximum void ratio (MT_L), intermediate (MT_M), minimum (MT_D) void ratios and the slurry deposition void ratio (MT_SLU). The specimens were tamped in three layers of equal mass and height. The soil mass required for each layer was calculated as a function of the target formation void ratio of the specimen. Each layer was initially prepared in a container to a water content of approximately 10 % and allowed to cure overnight. Following curing, each layer was deposited in the cell and tamped down to one third of the cell height (i.e., 32/3 mm). To

ensure that all layers had the desired height, the tamper had an adjustable crossbar which could be moved to specific heights along the stem of the bar that were marked by grooves (Figure 3-6). When sliding the cross bar along the stem, a spring and ball mechanism indicated when the cross bar was aligned with the groove. The crossbar was then secured into position by tightening a cap screw. Throughout tamping, an extension ring was placed over the consolidation cell, thus enabling the tamping of the uppermost layer (Figure 3-6). After tamping all layers, the extension ring was removed, and filter paper and a porous stone were placed on the specimen.

Both specimen formation methods have advantages and disadvantages. The high water contents used in the preparation of slurry deposited specimens may be conducive to a fabric of hydraulically deposited tailings (Chang, 2009 & Li, 2017). However, slurry deposition has the disadvantage of not allowing any control over the formation void ratio. Conversely, moist tamping provides good control over the formation void ratio, but specimens are formed at a relatively low water content that is not representative of hydraulically deposited tailings.

3.5 Testing procedure

In moist tamped specimens, CO_2 flushing was performed prior to flushing with deaired water to promote saturation. This was done by flushing CO_2 through the specimen from the bottom valve and vented from the top back pressure valve into a beaker of water open to the atmosphere (Chaney et al., 1979). After 30 minutes of CO_2 flushing, an axial pressure of 25 kPa was applied on the specimen prior to flushing with water to ensure positive effective stress in the specimen. Water at a pressure of 17 kPa was allowed to flow from the bottom valve and vent upward to the back pressure valve. 500 ml of deaired water was collected before back pressure could be applied to the sample. Saturation was achieved by applying increments of back pressure of 200 kPa, alternating with increments of vertical stress of 210 kPa. The procedure enabled the water to absorb into solution all the air in the voids. Saturation was deemed acceptable when the Skempton B value was at least 0.97. Because the slurry specimen was already prepared at a high water content, only deaired water was used to facilitate saturation.

Two types of loading methods were used, the conventional stepped loading (SL) test and the constant rate of loading (CRL) tests. During stepped loading, the vertical pressure was applied by increasing the ratio of the load increment to the existing load ($\Delta\sigma/\sigma$) by 1. The vertical effective stress was increased from 10 kPa to 20, 40, 80, 160, 320, 640, 1280 and 2560 kPa and excess pore water pressure was permitted to increase under undrained conditions for each loading stage. Once equilibrium was attained, drainage was permitted until excess pore pressure had fully dissipated. (BS 1377-6, 1990).

During the unloading stages, vertical effective stress decreased from 2560 kPa to 640, 320, 160, 80 and 40 kPa. To ensure that the pore water pressure never dropped below the backpressure value at saturation, unloading steps involved changing the back pressure and the total vertical stress (σ_v) to achieve the desired effective stress.

During the unloading phase of preliminary stepped loading (SL) tests, the spindle connected to the flexible membrane would suddenly shoot up and the pressures from the axial stress and backpressure controllers would tend to equalize. After opening the cell for inspection, it was found that the lower end of the spindle had disconnected from the flexible membrane. This suggested that the back pressure (BP) had pushed the spindle upwards, something that at first seemed counterintuitive because the downward acting axial pressure (AP) was greater than the upward acting back pressure (BP) at all times. Adequate checks ruled out malfunction of the pressure controllers. Closer analysis of the pressures made it clear that to avoid a net upward push on the spindle, the ratio of the back pressure (BP) to the axial pressure (AP) had to be smaller than 0.89. Accordingly, this condition was respected in all tests. The derivation of the condition $BP/AP \leq 0.89$ is presented in Appendix B.

For the constant rate of loading (CRL) tests, the vertical stress (σ_v) was increased from 10 kPa to 2560 kPa at a fixed rate of 21 kPa/min. The strain rate was just that it induced zero excess pore pressure. Unloading from 2560 kPa to 40 kPa was done at the same rate. The constant rate of loading test has the advantage of allowing a continuous reading of soil properties. However, in non-plastic soils, it is often not possible to apply loading rates that are high enough to induce significant excess pore water pressure. Indeed, for all tests, the maximum excess pore pressure was of 2 kPa. Accordingly, the test results can be used to infer compressibility parameters but not consolidation ones.

As the specimen height was reduced by the action of the effective vertical stress (σ'_v), there was also a reduction in the length of the spindle that remains outside of the cell. That is, the spindle was brought into the cell because its lower end is connected to the flexible membrane that pushes down on the specimen. Accordingly, the height of the specimen at any stage of the test can be inferred from the length of the spindle that remains outside of the Rowe-Barden cell. This approach was used in all tests to determine the height, and associated void ratio (e), of the specimens when the effective vertical stress (σ'_v) reached its maximum value of 2560 kPa. The external length of the spindle was measured with a Vernier calliper to a precision of ± 0.025 mm. The measurement was done when the specimen was subjected to the maximum effective vertical stress (σ'_v) to minimise the possibility of disturbing the specimen while placing the calliper against the spindle.

After unloading, the back pressure and subsequently the axial pressure were decreased to zero while keeping track of the volume changes of the specimen. The cell was then opened, and the water content of the specimen was determined by oven drying the bulk of the specimen which could be easily removed from the cell. Small portions of the specimen that remained attached to the cell and filter paper were removed with water. These small portions were then oven dried to determine their dry mass. Adding the dry mass of the bulk portion used to determine the water content and the dry mass of the small portions that were removed with water yields the total mass of solids. The water content and mass of solids was used to calculate the void ratio at the end of the test as per Verdugo and Ishihara (1996).

Table 3-2 summarises the testing programme. 10 tests were conducted for each mix, giving a total of 20 tests. Moist tamped specimens were tested at densities approaching the maximum void ratio (e_{max}), the minimum void ratio (e_{min}), an intermediate void ratio (e_{int}), and a void ratio that was similar to that attained by the slurry specimens. Four slurry deposited specimens were tested under nearly identical conditions to assess the repeatability of the procedure.

3.6 Calculations of stress and void ratio

The total vertical stress σ_v was calculated as

$$\sigma_v = AP\left(\frac{flexible\ piston\ area - spindle\ area}{flexible\ piston\ area}\right) \qquad \text{Equation 8}$$

Where AP is the axial pressure recorded by the transducer.

The effective vertical stress σ'_v was calculated as

$$\sigma_v = \sigma_v^{'} - u \qquad \text{Equation 9}$$

Tracking of the void ratio requires knowledge of: 1) how the void ratio changes throughout the test and 2) the actual void ratio at a specific point during the test. Both of these information could be measured in two ways. Void ratio changes were inferred from the volume changes (ΔV) recorded by the back pressure controller, and from the specimen height changes (ΔH) measured by the displacement transducer. The void ratio (e) was inferred at two stages. First when the height of the specimen was measured at the end of the loading process (max σ). And again, when the water content of the specimen was determined at the end of

the test (EOT). Table 3-3 shows how this redundancy of measurements yields four possible methods of tracking the void ratio (e) throughout the test. The detailed equations for each of these methods are provided in Appendix C. Chapter 4 discusses which of the four void ratio calculation methods was deemed the most reliable.

3.7 Summary

An experimental programme was designed to investigate the compressibility and consolidation properties of non-plastic platinum tailings. The programme included testing of two gradations of reconstituted platinum tailings tested at different densities. Two sample preparation methods and two loading methods were utilized.

Table 3-1:Summary of index properties of non-plastic platinum tailings. Source: Torres-Cruz (2016).

Properties	**64/61**	**98/68**
Particle density, ρ_s (g/cm^3)	3.538	3.607
FC (%)	64	98
D_{10} (mm)	0.024	0.020
D_{30} (mm)	0.043	0.034
D_{50} (mm)	0.062	0.045
D_{60} (mm)	0.071	0.052
Coefficient of uniformity	2.9	2.6
Coefficient of curvature	1.1	1.1
e_{min}	0.61	0.68
e_{max}	0.93	1.18

Table 3-2: Summary of the testing programme.

Specimen Preparation method	Code	Stepped loading test		Constant rate of loading test	
		e at σ'_v = 10 kPa	RD at σ'_v = 10 kPa	e at σ'_v = 10 kPa	RD at σ'_v = 10 kPa
Moist Tamping	MT_64_L	0.96	-9	0.96	-9
	MT_64_SLU	0.87	19	0.97	-13
	MT_64_M	0.82	35	0.83	31
	MT_64_D	0.70	72	0.69	75
	MT_98_L	1.16	4	1.18	0
	MT_98_SLU	1.17	2	1.03	30
	MT_98_M	0.98	40	0.91	54
	MT_98_D	0.81	74	0.78	80
Slurry deposition	SLU_64	0.84	28	0.88	16
	SLU_98	1.03	30	0.93	50

Note: Code name MT_64_M represents MT-Moist tamping, 64- the percentage of fines and M- Medium density. L -loose, D- dense, SL- Slurry and RD = Relative density.

Table 3-3: Methods of tracking the void ratio throughout the test.

		Method to measure void ratio changes	
		Volume changes (ΔV)	Height changes (ΔH)
Stage of void ratio measurement	At maximum stress (max σ)	e-(ΔV-max σ)	e-(ΔH-max σ)
	At end of test (EOT)	e-(ΔV-EOT)	e-(ΔH-EOT)

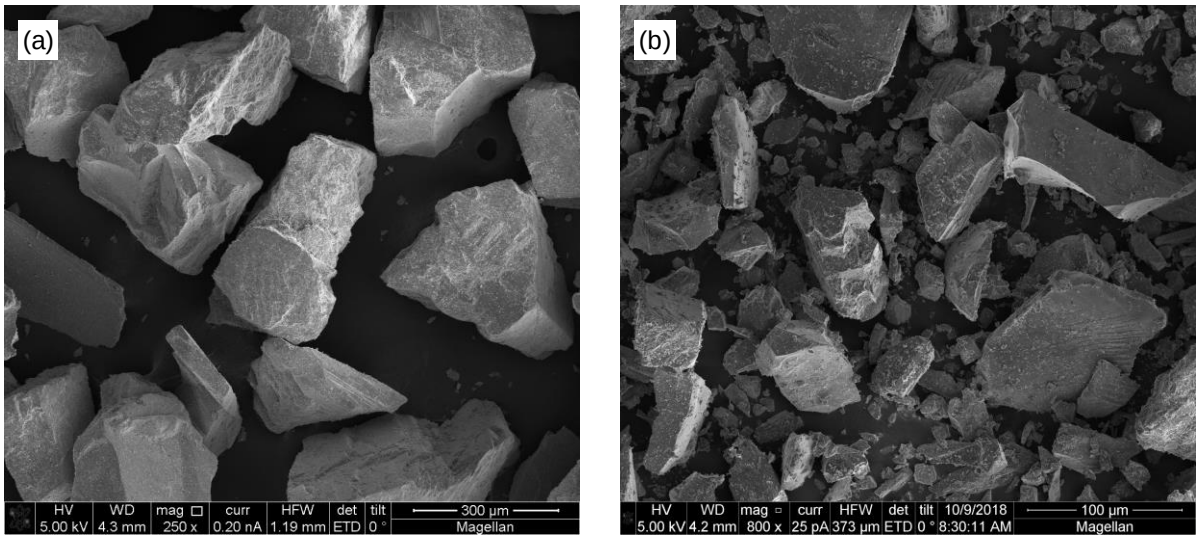

Figure 3-1: Scanning electron microscope images of a) coarse (250x) and b) fine particles (800x). Source Torres-Cruz and Santamarina (2020)

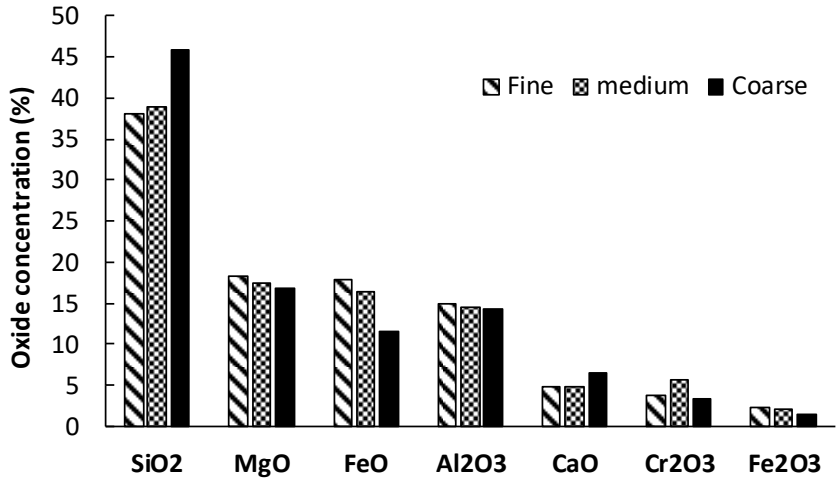

Figure 3-2: XRF results of oxide concentration. Note that Fine = < 75 µm , medium = > 75µm but < 150 µm, and coarse = > 150 but < 600 µm grain sizes.

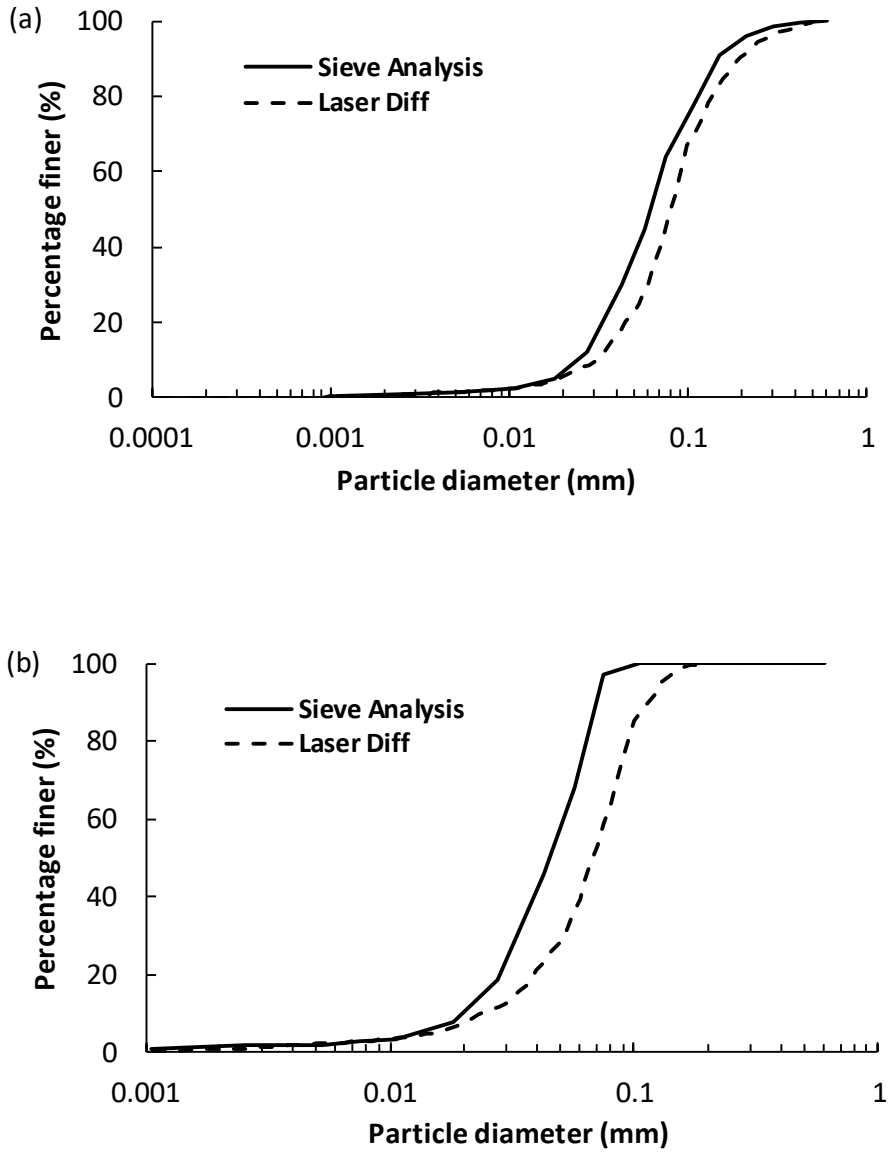

Figure 3-3: Grain size distribution comparison from laser diffractometer and sieve analysis a) 64/61 b) 98/68.

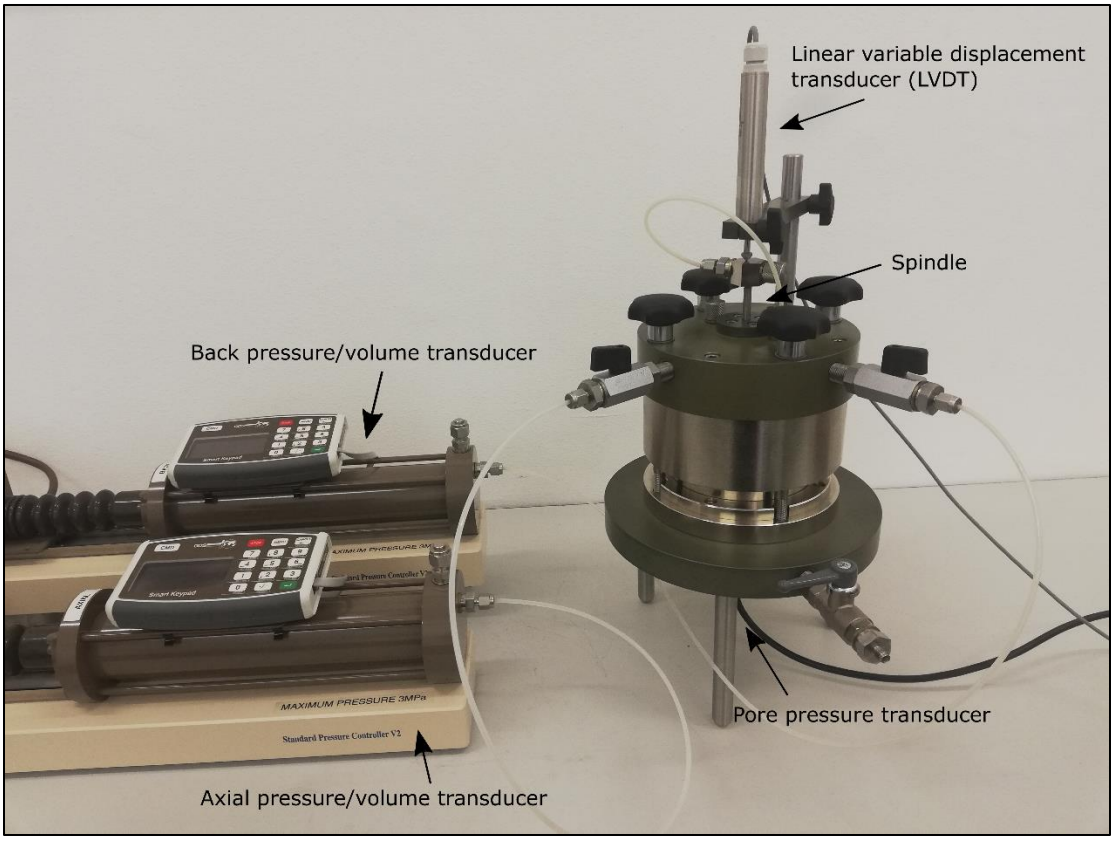

Figure 3-4: Rowe-Barden consolidation cell setup.

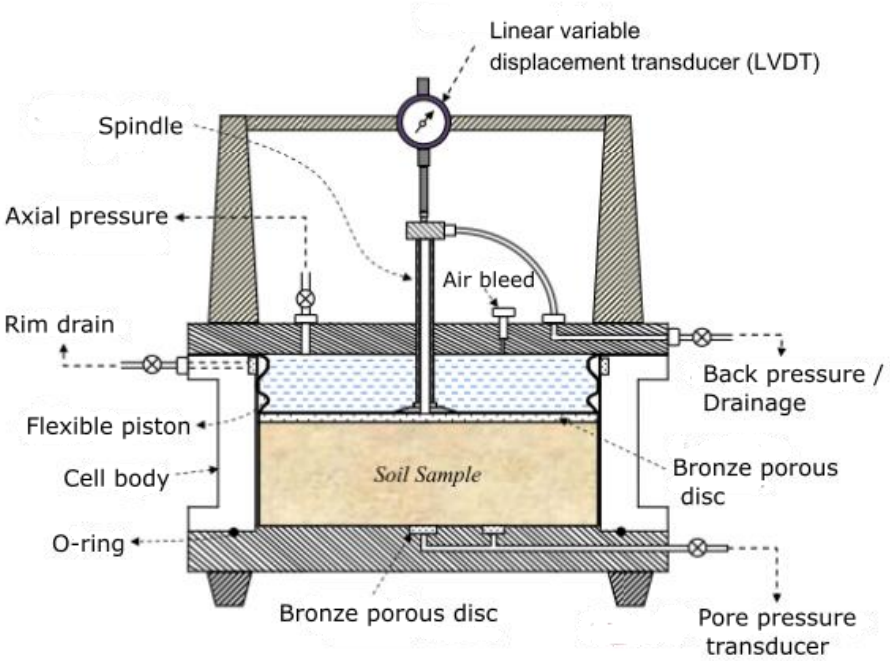

Figure 3-5: Cross-section of Rowe-Barden consolidation cell. Source: Kianfar (2013).

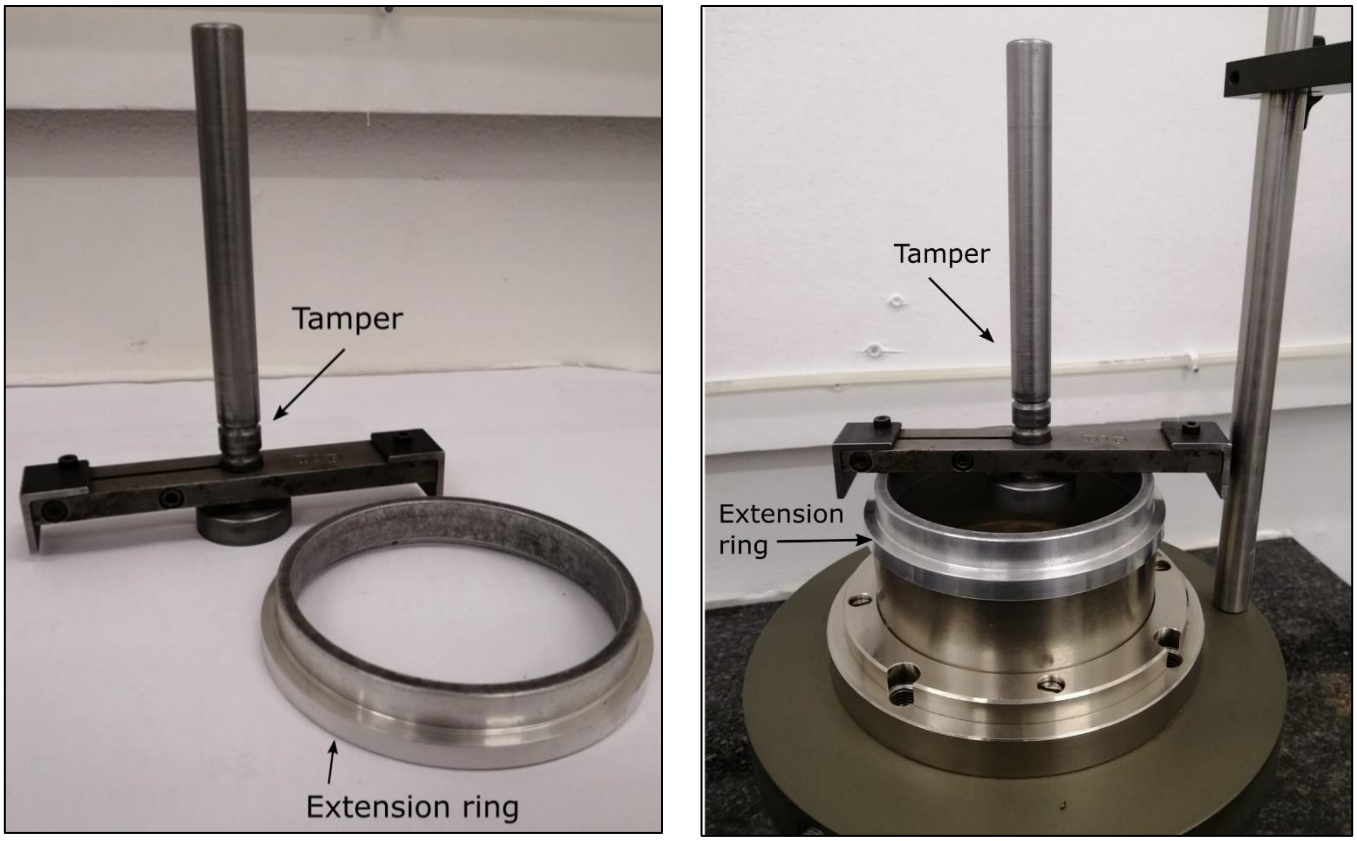

Figure 3-6: Apparatus used for moist tamping method.

4 Results and analysis

4.1 Introduction

Chapter 4 presents and discusses the experimental results.

The mechanical behaviour of soil material is controlled by the state of the material and the properties of the particles. Therefore, the consolidation and compressibility behaviour of the non-plastic tailings are discussed looking at the effect of the initial void ratio, particle size distribution and loading method. The experimental results are presented against the literature reviewed in Chapter 2 and the effect of fabric on the mechanical behaviour of non-plastic platinum tailings is also discussed.

4.2 Method of analysis

The changes in the void ratio during testing were measured by the pressure transducer, which measured volumetric changes and the displacement transducer which measured height changes. Of the two methods, the volumetric changes measured by the pressure controller was preferred. This is because the void ratio is a volumetric phase relationship, and the pressure controller offered the volumetric changes. The void ratio at the end of the test attained by measuring the water content was used as a point of reference void ratio. Similar practices have been adopted in triaxial testing and have produced reliable results. Therefore, further analysis of the mechanical behaviour of the tailings was based on the e-(ΔV-EOT) method of calculation discussed in Chapter 3 (Table 3-3).

4.3 Compression results

The compression and recompression curves of the loose, medium and dense moist tamped specimens of the 64/61 and 98/68 mixes are shown in Figure 4-1 and Figure 4-2 respectively. The figures show curves obtained from the stepped loading and constant rate of loading tests. The compression curves presented cannot be defined as a straight line on a semi-log scale and therefore no single value of the compression index could be calculated. Instead, the compression index (C_c) at every stage during the test was calculated for the stepped loading test results (Figure 4-3). This was achieved by calculating the gradient between two stages of the compression curve. Figure 4-3 shows that the compression index first decreases with increasing stress and then starts to increase at a vertical effective stress of approximately 200 kPa for both gradations. The values range from 0.12-0.02 and 0.3-0.02 for the 64/61 and 98/68 specimens respectively. As expected, both gradations tend to become less compressible as the initial void ratio decreases. There is good agreement with compression indices reported in the literature (Figure 4-4) as the compression indices

of the two gradations of platinum tailings tested herein follow the same trend in C_c-D_{50} space as the tailings reported by (Aubertin et al., 1996; Qiu and Sego, 2001).

The 98/68 specimens have higher compression indices than 64/68 specimens. This is because uniformly graded soils, in this instance being the 98/68 specimens attain much higher void ratios due to poor packing. This yields specimen with higher compressibility than well-graded soil (Mitchell and Soga, 2005). The recompression behaviour is linear for the specimens tested and the recompression indices are directly correlated to the initial void ratio of the specimens (Figure 4-5).

4.3.1 Effect of loading method

The effect of the loading method on the compression curves was evaluated by conducting stepped loading and constant rate of loading tests at the same initial void ratio. From the tests conducted, 6 comparisons were made from the moist tamped and slurry specimens. Figure 4-6a shows the compression curves of the 64/61 specimens with the corresponding tangent constrained moduli displayed in Figure 4-6b-d. The compression curves of the medium and dense specimens show excellent agreement in both the e-σ'_v and in the D- σ'_v space. However, there is a significant discrepancy between the compression curves of the loose specimens. In Figure 4-7a, the 98/68 specimens show greater discrepancy for the loose and dense specimens in the e-σ'_v space. The medium specimen shows excellent agreement. There is an excellent agreement in the tangent constrained moduli for all three comparisons (Figure 4-7b-d). In general, Figure 4-6 and Figure 4-7 support the idea that the behaviour of the specimens is independent of the mode of loading. This is particularly true for the tangent constrained moduli. Furthermore, it is not clear whether the observed difference between compressibility curves may be due to limitations in the test repeatability.

von Fay and Cotton (1986) found no difference in the compression behaviour of soils tested using the different methods. However, several authors have found that the amount of deformation depends on the rate of loading (Sengupta, 2018; Shokouhi and Williams, 2015; Soumaya and Kempfert, 2010). Soils that have been loaded at a fast rate show a high stiffness and slow loading rates allow for time-dependent deformation and tend to be more compressible. Denser specimens have less pronounced differences in their compressive behaviour and their stiffness behaviour are similar. This is similar to the finding made by Mitchell and Soga (2005) who found that the difference in the compression curves tends to be reduced as density increases.

4.3.2 Effect of fabric

The evaluation of the effect of the fabric caused by specimen preparation required the specimens to be tested at the same initial void ratio. This is to eliminate potential differences in behaviour caused by the density of the specimen. The 64/61 slurry and moist tamped specimens tested at a similar initial void ratio were analysed and the results are shown in Figure 4-8a and Figure 4-9a. Regardless of the loading method (SL or CRL), there are discrepancies in the compression curves yielded by the two specimen preparation techniques (Figure 4-8a and Figure 4-9a). Indeed, the compression curves of the moist tamped specimens (MT_64_SLU) are steeper than those of the slurry specimens. This behaviour is attributed to small discrepancies in the initial void ratio; however, it is noted that they could also be due to limitations in the repeatability.

This behaviour is contrary to the behaviour that has been reported for Gold tailings in which moist tamped specimens have exhibited lower compressibility than slurry specimens (Chang, 2009). Regarding the behaviour of the tangent constrained modulus, Figure 4-8b and Figure 4-9b shows that there is good agreement between the specimen preparation methods. The 98/68 specimens offered no comparison as specimens tested at the same initial void ratio were not attained.

4.3.3 Coefficient of volume compressibility

Figure 4-10 and Figure 4-11 shows how the coefficient of volume compressibility (m_v) correlates to the void ratio of the specimens. As seen in the figures, the coefficient of volume compressibility (m_v) is dependent on the initial void ratio. Specimens prepared at an initially high void ratio have higher m_v values. The values of the coefficient of volume compressibility (m_v) range from 1.5 – 0.005 m^2/MN in the 64/61 and 3.3-0.005 m^2/MN in the 98/68 mix. Similar values have been reported for fine and coarse tailings reported by Aubertin et al. (1996) and Hu et al. (2017) (Figure 4-12).

Figure 4-10 and Figure 4-11 shows that the correlation between e and m_v is approximately linear in semi-logarithmic space (e-ln(m_v)). The slope of the correlation is directly correlated to the initial void ratio of the specimens. The figures also show good agreement of the slope of the regression line for specimens tested using different loading methods at the same initial void ratio. For instance, the medium and dense 64/61 mix specimens, show a slope of 0.02 and 0.01 respectively. These values are independent of the loading method.

4.4 Consolidation results

4.4.1 Coefficient of consolidation

The coefficient of consolidation (c_v) was determined from pore pressure dissipation curves measured during the stepped loading tests (Figure 4-13). From the dissipation curve, the time at which 50 % (t_{50}) pore pressure dissipation had taken place was extracted and Equation 6 was used to derive the coefficient of consolidation. The values of c_v for the tailings in this study range within three orders of magnitude and are showed minimal dependence on the particle size distribution. The current tailings have a coefficient of consolidation (c_v) higher than the slimes reported by Blight and Steffen (1979) but have a much similar coefficient of consolidation (c_v) to sand copper tailings studied by Mittal and Morgenstern (1975) (Figure 4-14).

Figure 4-15 shows that the coefficient of consolidation (c_v) is dependent on the initial void ratio and it increases with decreasing void ratio. The opposite trend was reported for Platinum tailings reported by Blight (2010). They measured a decrease in the coefficient of consolidation (c_v) with decreasing void ratio. The behaviour observed for tailings under this study occurs because of the influence of the rate of change of the coefficient of volume compressibility (m_v) with respect to the hydraulic conductivity (k). The value of the coefficient of consolidation (c_v) increases during consolidation when the coefficient of volume compressibility (m_v) decreases at a rate higher than the hydraulic conductivity (k) (Hu et al., 2017; Shukla et al., 2009; Vick, 1990). An estimate of the hydraulic conductivity was calculated by the Modified Kozeny-Carmen equation proposed by Aubertin et al. (1996) as:

$$k = c \times \frac{\gamma_w}{\mu} \times D_{10}^2 \times C_U^{1/3} \times \frac{e^{3+x}}{(1+e)} \qquad \text{Equation 10}$$

Where k is the hydraulic conductivity, γ_w is the unit weight of water, μ is the water viscosity, D_{10} is the diameter corresponding to 10 % cumulative on a particle size distribution, C_u is the coefficient of uniformity, e is the void ratio and x and c are material constants. The hydraulic conductivity (k) ranged from 2.6×10^{-6}-2.25×10^{-5} cm/s for 98/68 mix and 1.6×10^{-6} – 1.44×10^{-5} cm/s for 64/61 mix.

4.4.2 Effect of fabric

The fabric effect was also evaluated on consolidation results by plotting the coefficient of consolidation for the slurry and moist tamped specimens (Figure 4-16). Comparisons were only made between specimens previously used when assessing fabric effect on the compression behaviour. The results in Figure 4-16 suggest that the coefficient of consolidation is largely independent of the specimen preparation technique.

4.5 Summary

This chapter presented compressibility curves and consolidation curves as part of the experimental programme. The compression curves could not be defined by a single constant in the void ratio versus the logarithm of effective stress space but rather the compression indices varied with increasing stress. Loose specimens were more compressible and showed the highest discrepancy when comparing the stepped loading and constant rate of loading tests compression curves.

The coefficient of consolidation displayed a dependence on the initial void ratio. The value of c_v increased with decreasing void ratio and its values were similar to sand Copper tailings. Minimal effect of gradation was observed. The fabric had a minor effect on the compressibility and consolidation behaviour of the tailings.

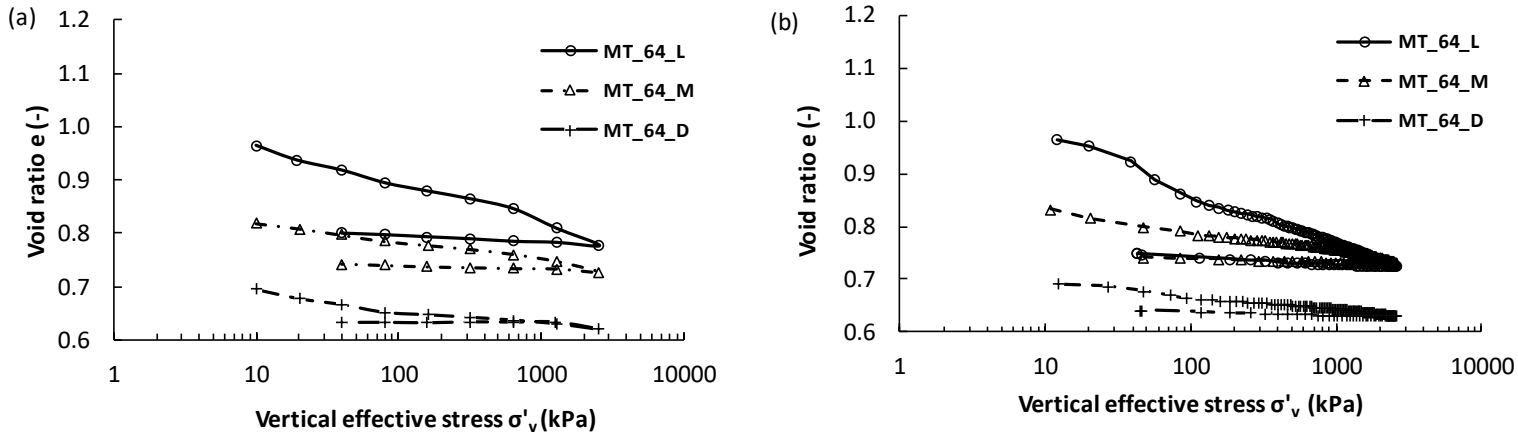

Figure 4-1: Compression curves of the 64/61 mix a) Stepped loading test b) Constant rate of loading test.

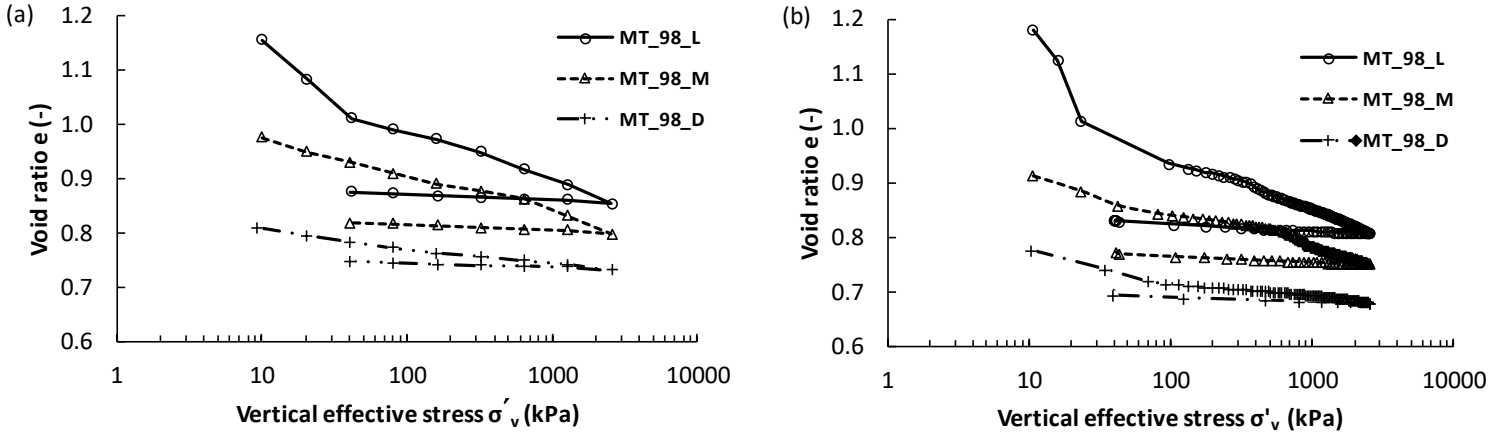

Figure 4-2: Compression curves of the 98/68 mix a) Stepped loading test b) Constant rate of loading test.

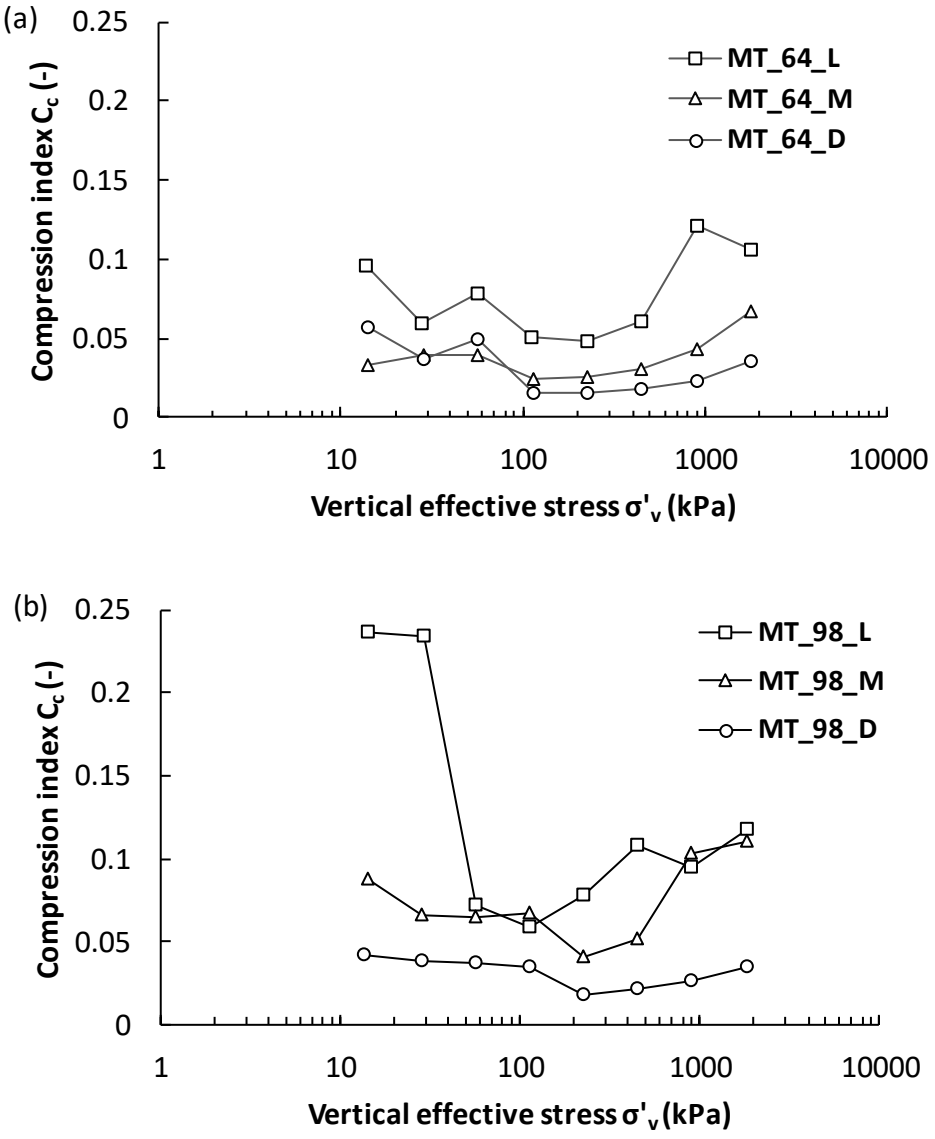

Figure 4-3: Compression index relationship with effective stress a) 64/61 mix and b) 98/68 mix.

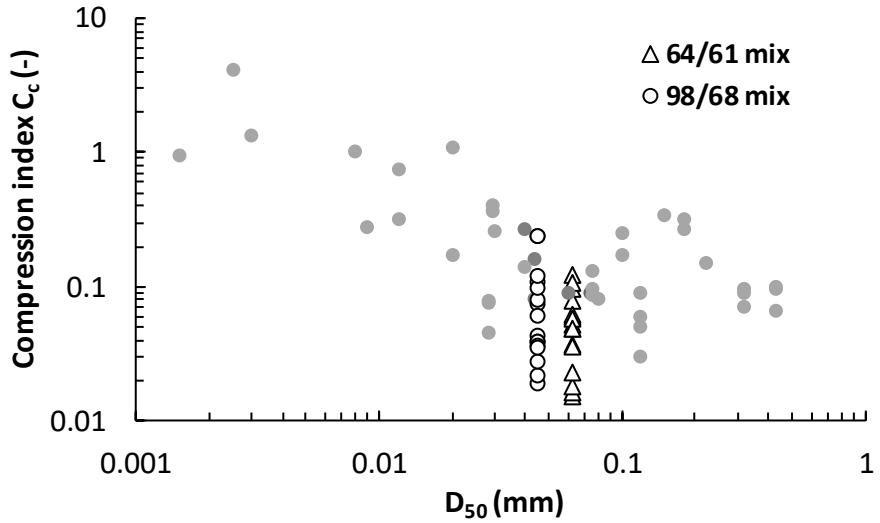

Figure 4-4: Compression indices of the 64/61 and 98/68 mixes. Note: grey markers are compression indices of tailings reported in Table 2-1 and Table 2-2.

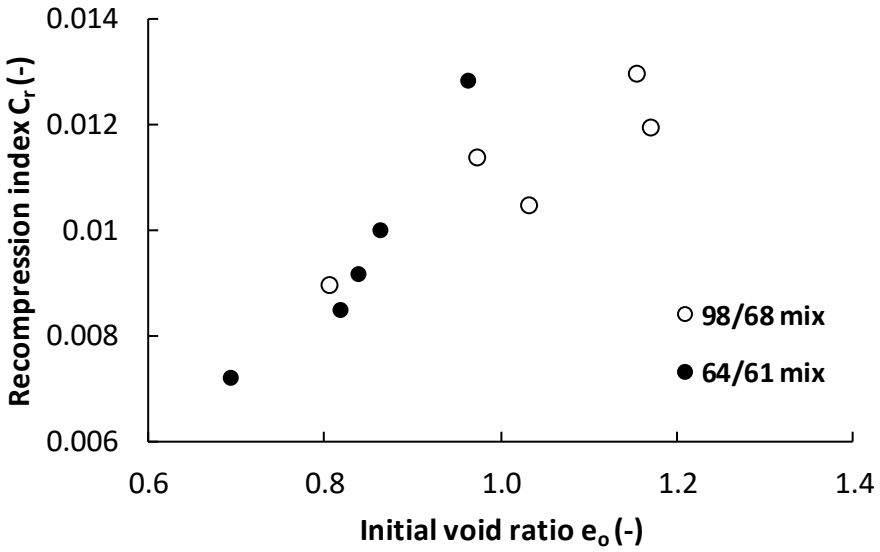

Figure 4-5: Correlation of the recompression indices with the initial void ratio.

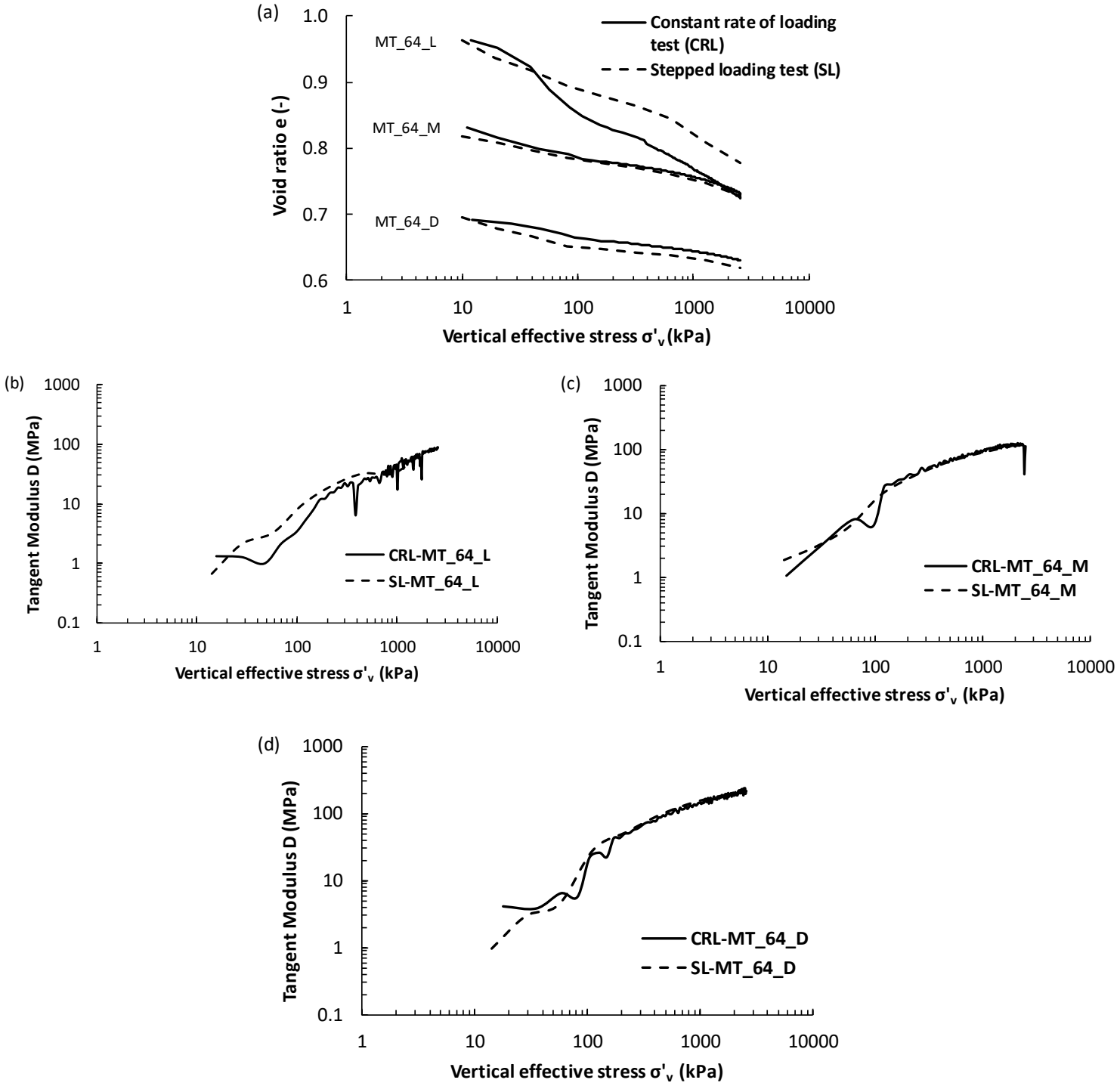

Figure 4-6: 64/61 stepped loading and constant rate of loading test comparison a) compression curves b, c and d) tangent constrained modulus. Note that CRL=constant rate of loading and SL=stepped loading.

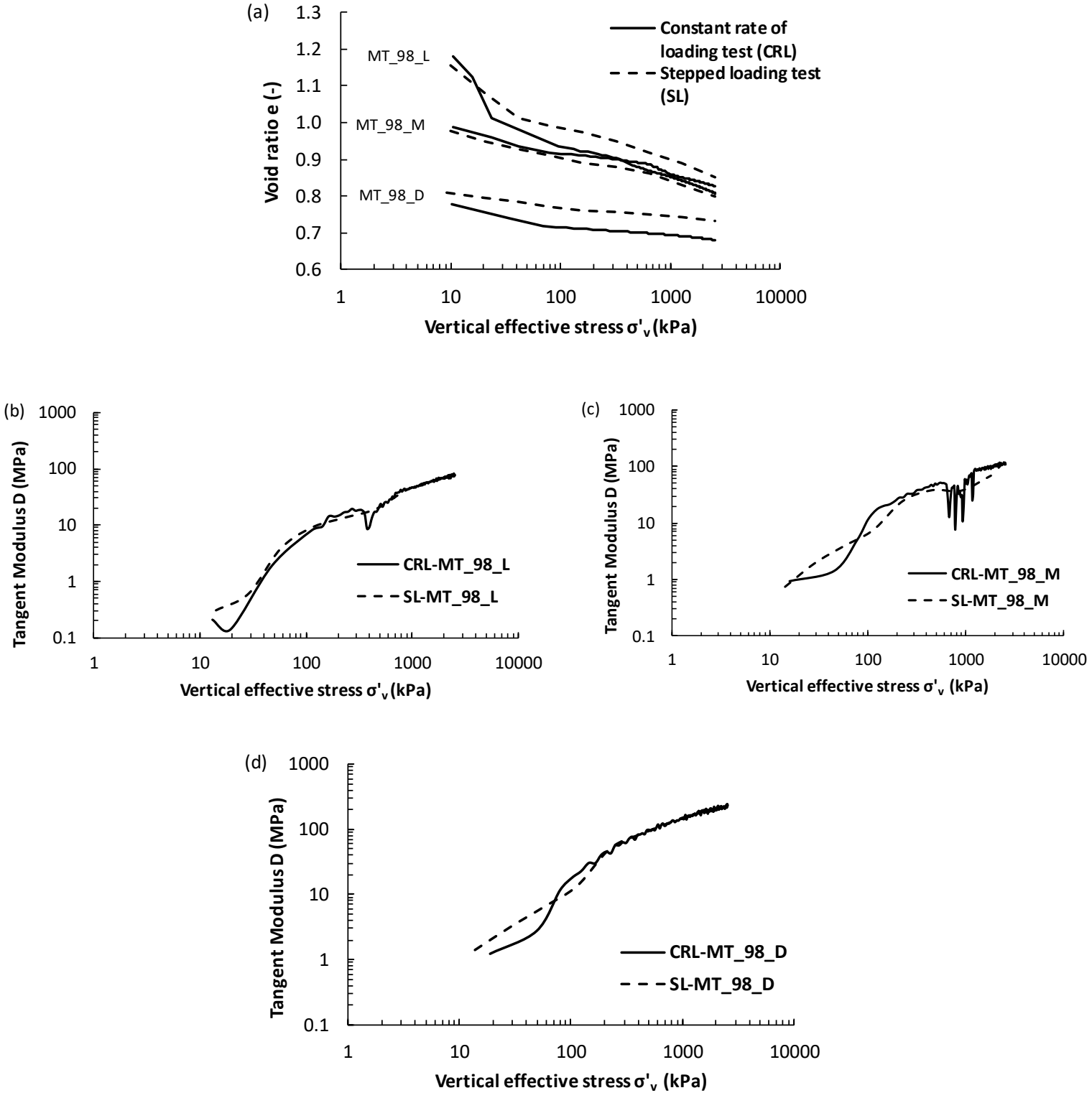

Figure 4-7: 98/68 stepped loading and constant rate of loading test comparison a) compression curves b, c and d) tangent constrained modulus. Note that CRL=constant rate of loading and SL=stepped loading.

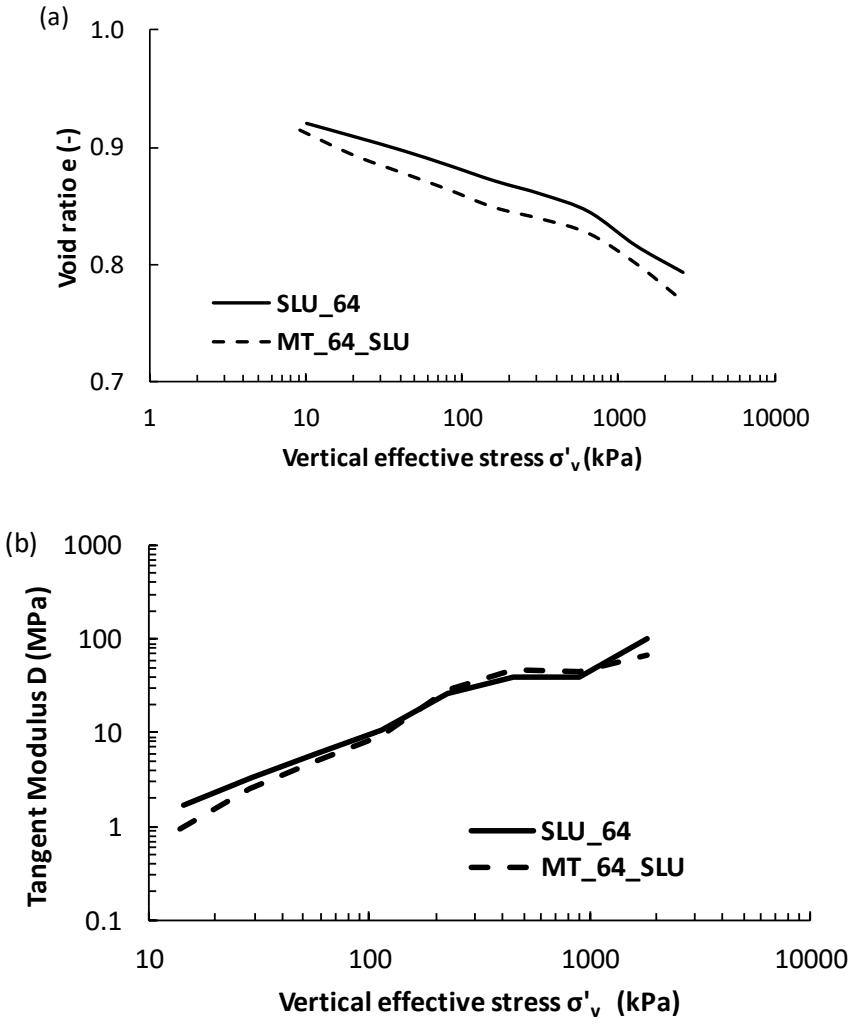

Figure 4-8: Effect of fabric from stepped loading test a) compression curves and b) tangent constrained modulus.

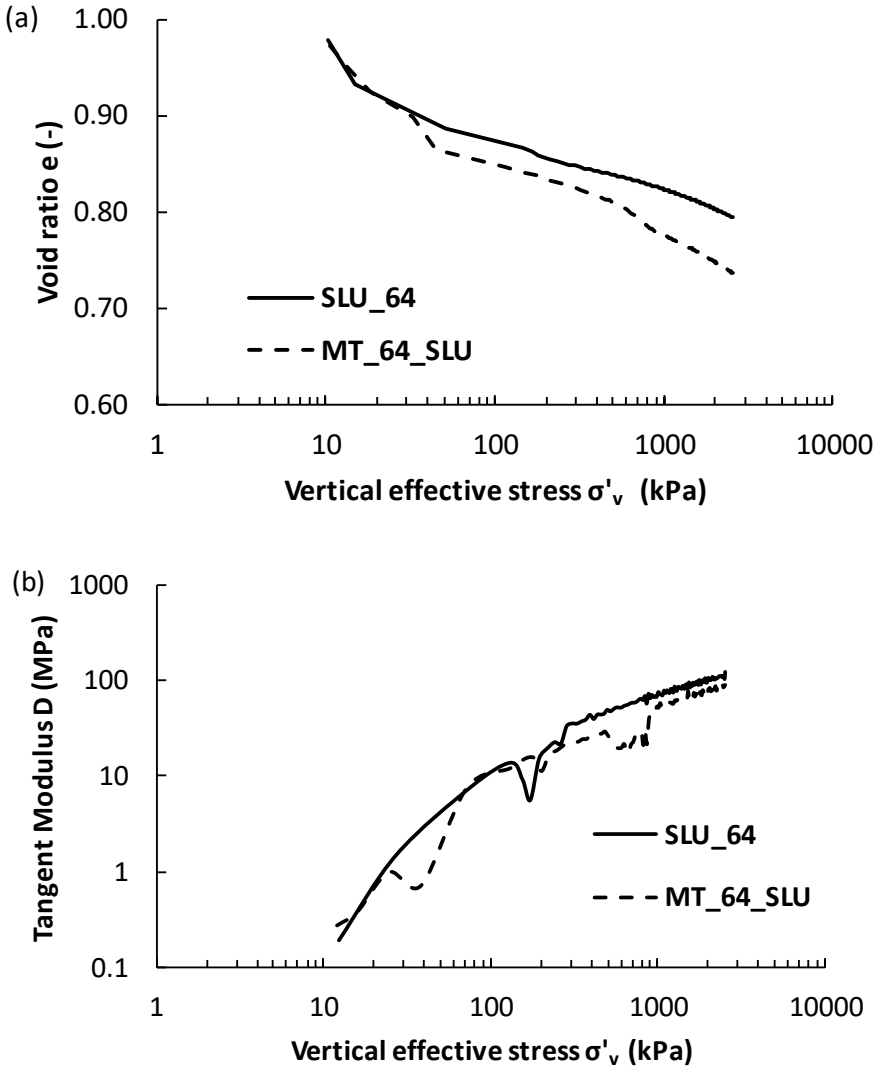

Figure 4-9: Effect of fabric from the constant rate of loading test a) compression curves and b) tangent constrained modulus.

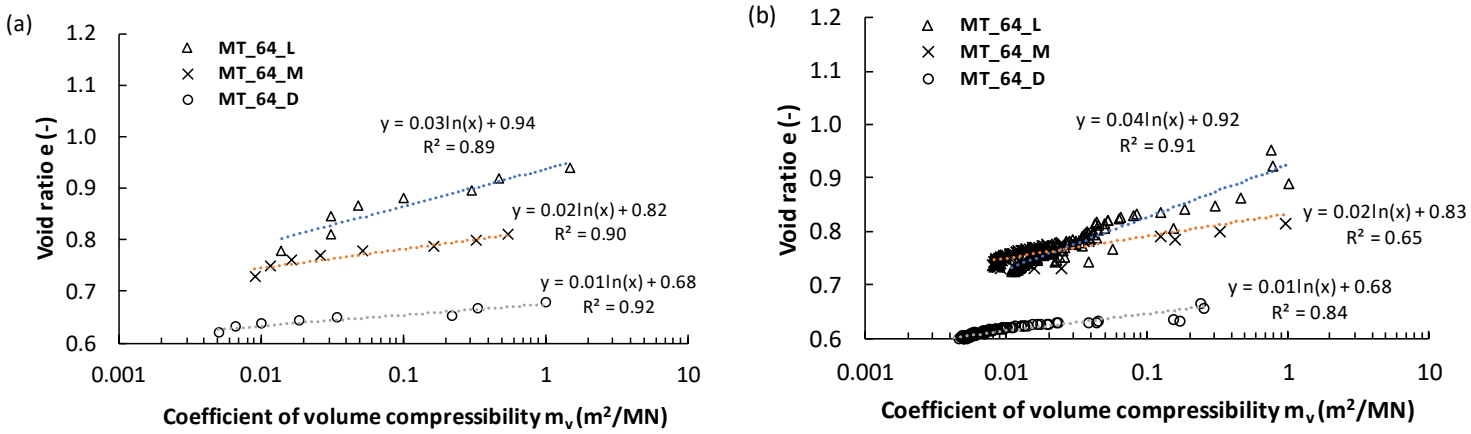

Figure 4-10: Coefficient of volume compressibility for the 64/61 loose, medium and dense specimens a) stepped loading test b) constant rate of loading test.

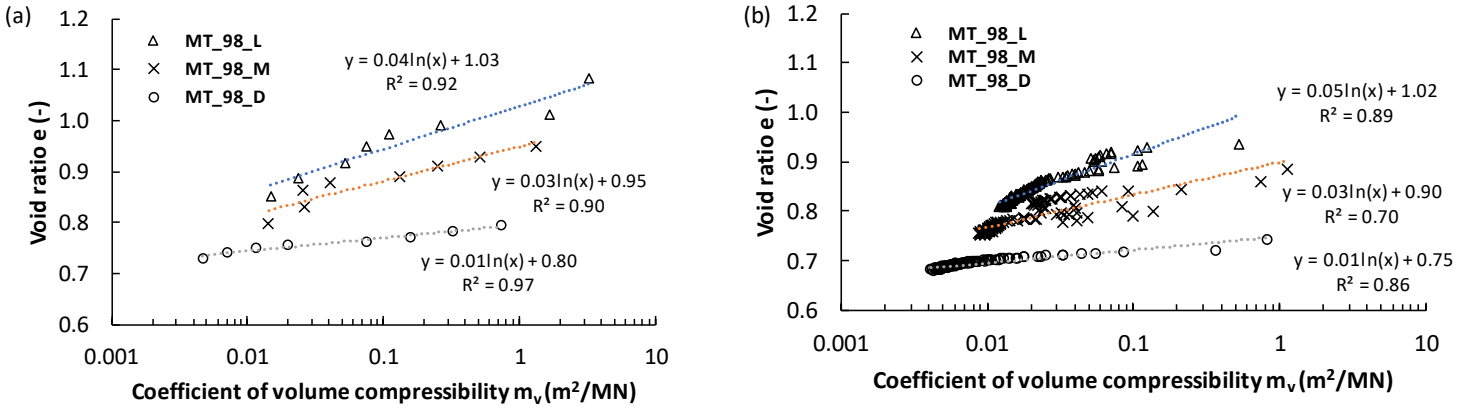

Figure 4-11: Coefficient of volume compressibility for the 98/68 loose, medium and dense specimens a) stepped loading test b) constant rate of loading test

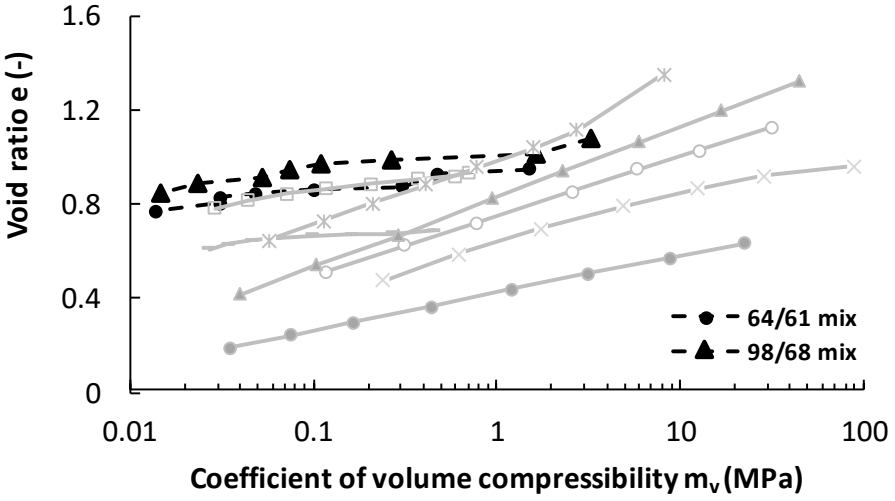

Figure 4-12: Coefficient of volume compressibility of the 64/61 and 98/68 mixes. Note: grey plots are m_v values of tailings reported in Table 2-1 and Table 2-2.

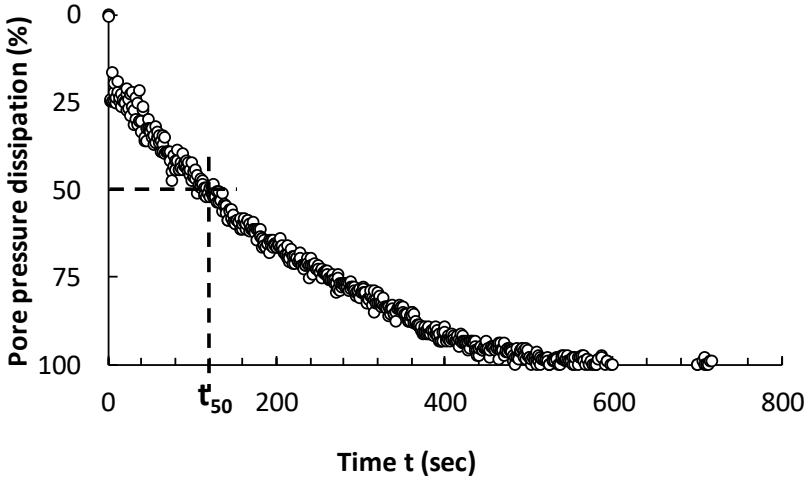

Figure 4-13: Pore pressure dissipation curve.

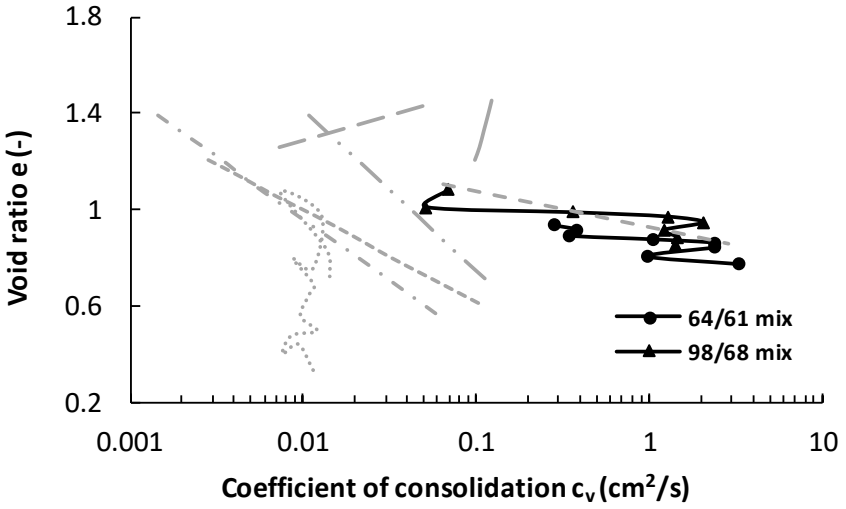

Figure 4-14: Coefficient of consolidation plots of the 64/61 and 98/68 mix. Grey lines are plots from previous studies presented in Table 2-1 and Table 2-2.

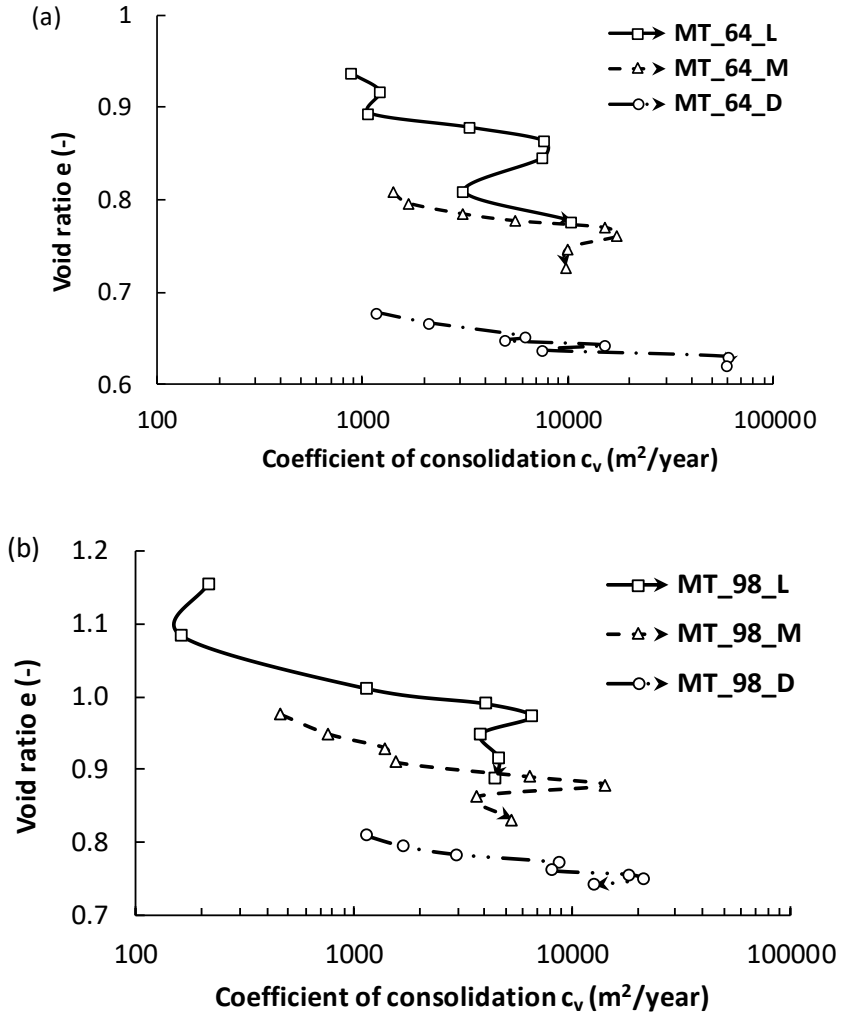

Figure 4-15: Coefficient of consolidation plot of a) 64/61 and b) 98/68.

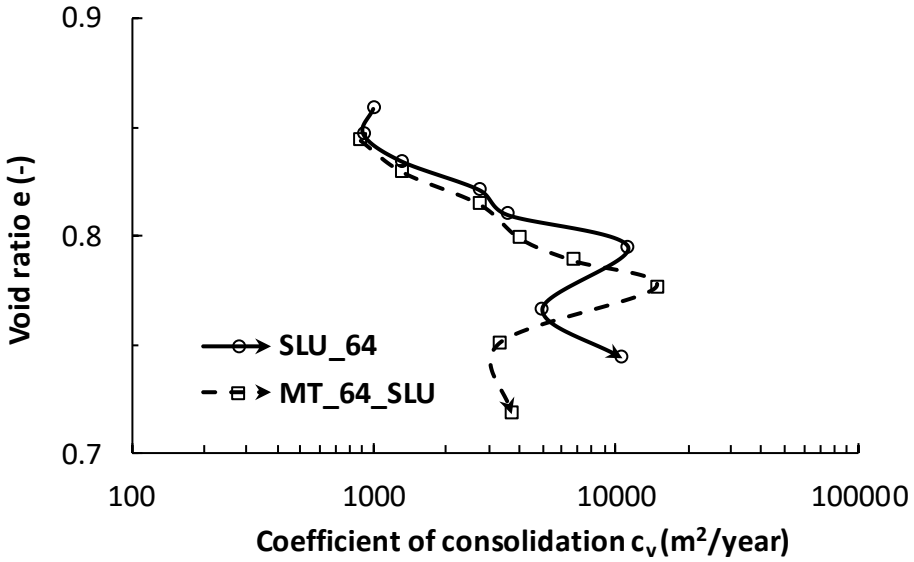

Figure 4-16: Effect of fabric on the coefficient of consolidation.

5 Model fitting

5.1 Introduction

Chapter 5 explores the compressibility models proposed by Chong and Santamarina (2016a) to represent the behaviour of the tailings tested herein and previously reported in the literature. The compression curves, tangent moduli, R^2 values and residual plots are used to validate the suitability of the models for non-plastic tailings compression curves.

5.2 Non-plastic tailings

Chapter 4 highlighted the limitations in defining the compression curves of non-plastic tailings using a linear model. Therefore to accurately capture soil behaviour, more complex models may be required. Chong and Santamarina (2016a) proposed five four-parameter models that were applied on plastic soils and were found to accurately define the compression curves. This chapter explores the suitability of these five models for non-plastic tailings. Their formulation as proposed by Chong and Santamarina (2016a) were discussed in Chapter 2. Both stepped loading and constant rate of loading data were fitted with the five models and the suitability of the models was assessed based on how well they fitted, compression and tangent constrained modulus curves.

Each stepped loading test specimen was fitted with the five models. According to the R^2 values in Table 5-1 and Table 5-2, the power, hyperbolic, exponential and arctangent models generally predict the compression curves fairly well with R^2 values ranging between 0.93-0.98 for both gradations. Much lower R^2 values were presented by the modified Terzaghi model having the lowest R^2 value of 0.73 (Table 5-2). Figure 5-1 to Figure 5-4 displays the stepped loading compression curves of the 64/61 and 98/68 mixes. The models capture the general trend of the compression curves more precisely than the linear Terzaghi model. However, variations in the stiffness of the soil are observed between the experimental data and all mathematical models. These differences are more significant for the loose (Figure 5-3b) and slurry (Figure 5-4d) 98/68 specimens.

The models were also fitted to the continuous compression curves attained from the constant rate of loading tests (Figure 5-5 to Figure 5-8). All models yielded good R^2 values (see Table 5-1 and Table 5-2). Unlike the fit from the SL results, the CRL tests fit, significantly underestimate the void ratio at low stresses but accurately model the compression behaviour at higher stresses. This results in the models overestimating the tangent constrained modulus (D) at low stresses. The behaviour is more pronounced in the 98/68 specimens (see Figure 5-7 and Figure 5-8). According to Chong and Santamarina (2016a), the models

inability to capture the small strain stiffness is derived from its fundamental differences to the tangent constrained modulus measured during a test. The models reveal the instantaneous rate of fabric change in large tests while small strain test measurement reveals the constant fabric measurement determined from contact deformation.

Cubrinovski and Ishihara, (2002) showed a correlation between volumetric strain and the limiting void ratio range (e_{max}-e_{min}) where they suggested that the limiting void ratio range correlates directly to the compressibility of cohesionless soils. This is because soils with high void ratio ranges tend to be uniformly graded, and highly angular. Both of these characteristics increase compressibility (Biarez and Hicher, 1994; Mitchell and Soga, 2005). Similarly, the difference between the limiting void ratios defined by the models (e_L-e_H) was correlated to the initial void ratio of the tests. Only data from the power model exhibited a significant correlation with $R^2 \geq 0.8$ for both gradations (Figure 5-9). An increase in the initial void ratio increases the difference between the limiting void ratios defined by the model. The correlation may be useful to make initial estimates of model fitting parameters.

5.3 Published compression curves

The four-parameter models present an alternative to defining the compression curves of non-plastic tailings. To further assess their validity, the models were fitted to numerous published compression curves of tailings. The tailings were observed to vary in mineralogy, plasticity and gradation as presented in Table 2-1 and Figure 2-5 respectively. Each compression curve was fitted with the five models but only a single model is presented herein to observe the goodness of fit.

Oil sand tailings and Aluminium Bauxite with plasticity index ranging from 9-29 % have been presented in Figure 5-10 and Figure 5-11 with their respective compression curves. The power model was fitted to Oil sand tailings while the arctangent model was fitted to the Aluminium bauxite data. The models capture the compression curves very well, with $R^2 \geq 0.99$ for all the specimens. The stiffness of the tailings is modelled more adequately for the Aluminium bauxite than it is for the high void ratio Oil sand specimen. The tangent modulus shows poor agreement at low stresses which increases with increasing stress (Figure 5-10b and Figure 5-11b). Iron tailings were fitted with the hyperbolic model in Figure 5-12 and the R^2 values are greater than 0.99 for all the different specimens. The stiffness behaviour of the tailings is better predicted in comparison to the Oil sand tailings.

Figure 5-13 shows the compression curves of Gold tailings fitted with the modified Terzaghi model. The model accurately captures the compression curves of the tailings with R^2 values of 0.99, with the exception of the ID 2 specimen which shows R^2 value of 0.93. Although the model gives R^2 values of 0.99 for the

compression curves, the stiffness behaviour of the tailings is underestimated at low stresses. This is also apparent in Figure 5-14 and Figure 5-15 in which the exponential model and arctangent models are fitted to tailings of different mineralogy. All five models consistently fail to capture the stiffness behaviour of tailings both for the reported tailings and tailings in this study.

Residual plots were created from the dataset plotted in Figure 5-15a to confirm the validity of each model. Figure 5-16 shows that the residual void ratio falls within the ± 0.08 range and are lower for the power and arctangent models. A non-linear pattern is observed in all the plots as we move along the x-axis highlighting the limitation of the models. Although the R^2 values (see Figure 5-15a) show that the models give a good general sense of the relationship between void ratio and effective stress, the prediction is not perfect.

5.4 Summary

This chapter presents the model fittings of the four-parameter models on compression curves of non-plastic platinum tailings and compression curves of documented tailings. The models captured the compression curve accurately, however they failed to capture the stiffness behaviour of the tailings. The discrepancies are highlighted by residual plots and were more noticeable for the low density specimens.

Table 5-1: R^2 values of the 64/61 mix

	Stepped loading test			Constant rate of loading test		
Model	**Minimum R^2**	**Maximum R^2**	**Average R^2**	**Minimum R^2**	**Maximum R^2**	**Average R^2**
Power model	0.976	0.988	0.981	0.963	0.992	0.980
Hyperbolic model	0.967	0.996	0.982	0.965	0.993	0.981
Modified Terzaghi model	0.967	0.989	0.981	0.966	0.992	0.982
Exponential	0.965	0.996	0.985	0.967	0.992	0.982
Arctangent	0.964	0.996	0.985	0.974	0.991	0.982

Table 5-2: R^2 values of the 98/68 mix.

	Stepped loading test			Constant rate of loading test		
Model	**Minimum R^2**	**Maximum R^2**	**Average R^2**	**Minimum R^2**	**Maximum R^2**	**Average R^2**
Power model	0.934	0.996	0.974	0.949	0.990	0.964
Hyperbolic model	0.934	0.996	0.973	0.953	0.990	0.966
Modified Terzaghi model	0.735	0.986	0.909	0.950	0.986	0.967
Exponential	0.923	0.996	0.969	0.936	0.986	0.965
Arctangent	0.934	0.988	0.972	0.950	0.986	0.972

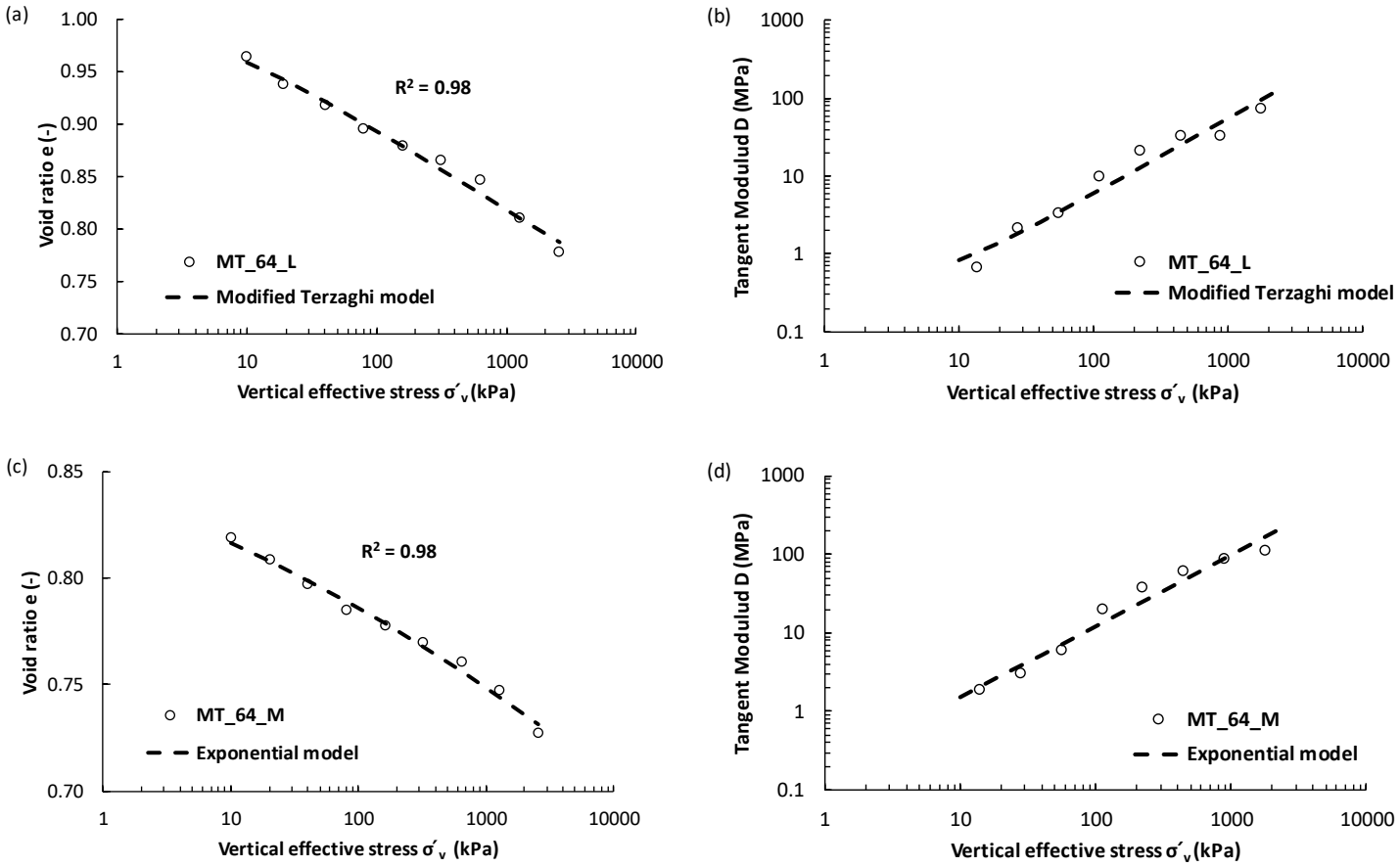

Figure 5-1: 64/61 Stepped loaded compression curves (a and c) and tangent modulus of (b and d) of the loose and medium density specimen.

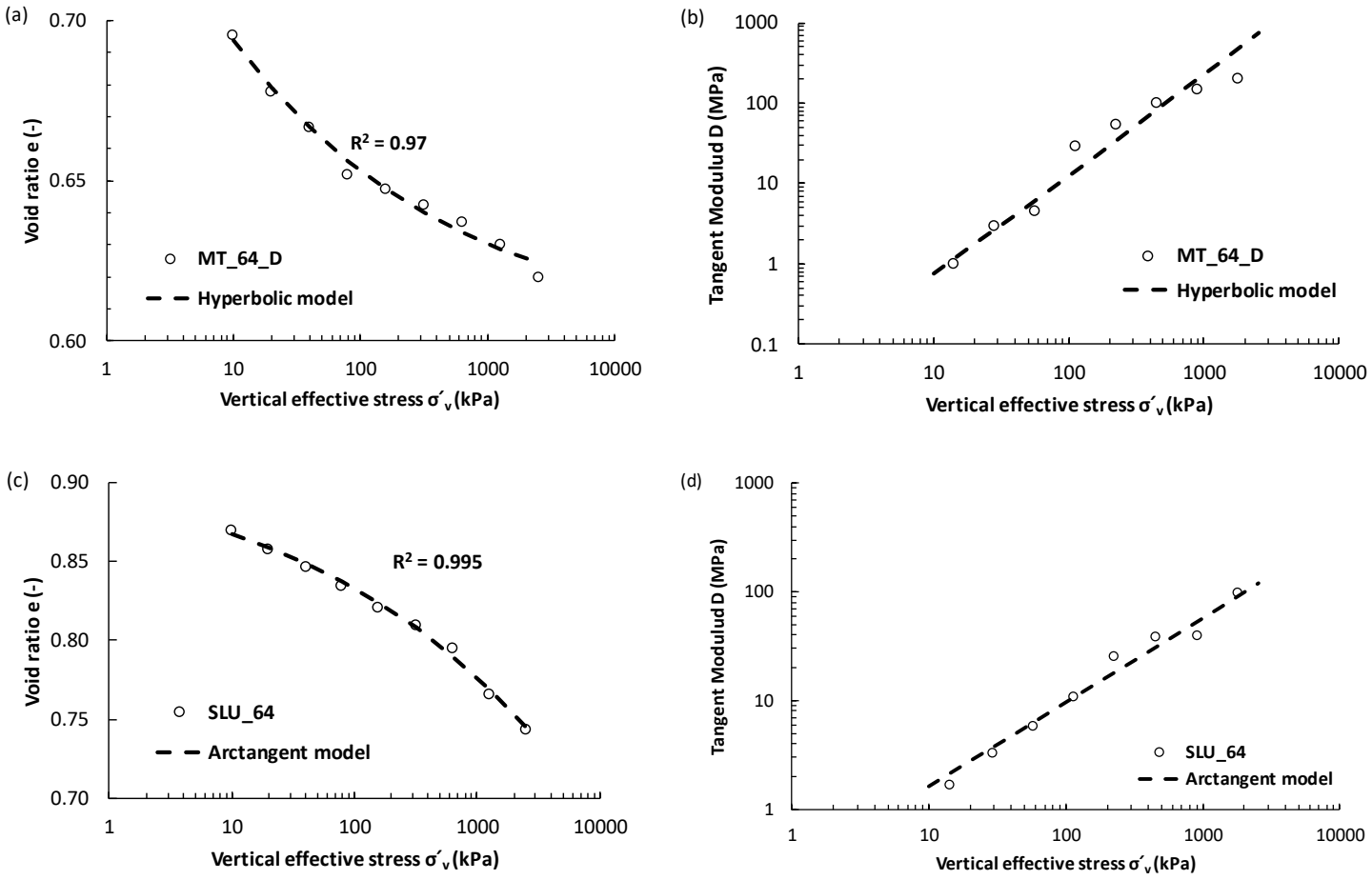

Figure 5-2: 64/61 Stepped loaded compression curves (a and c) and tangent modulus (b and d) of the dense and slurry specimen.

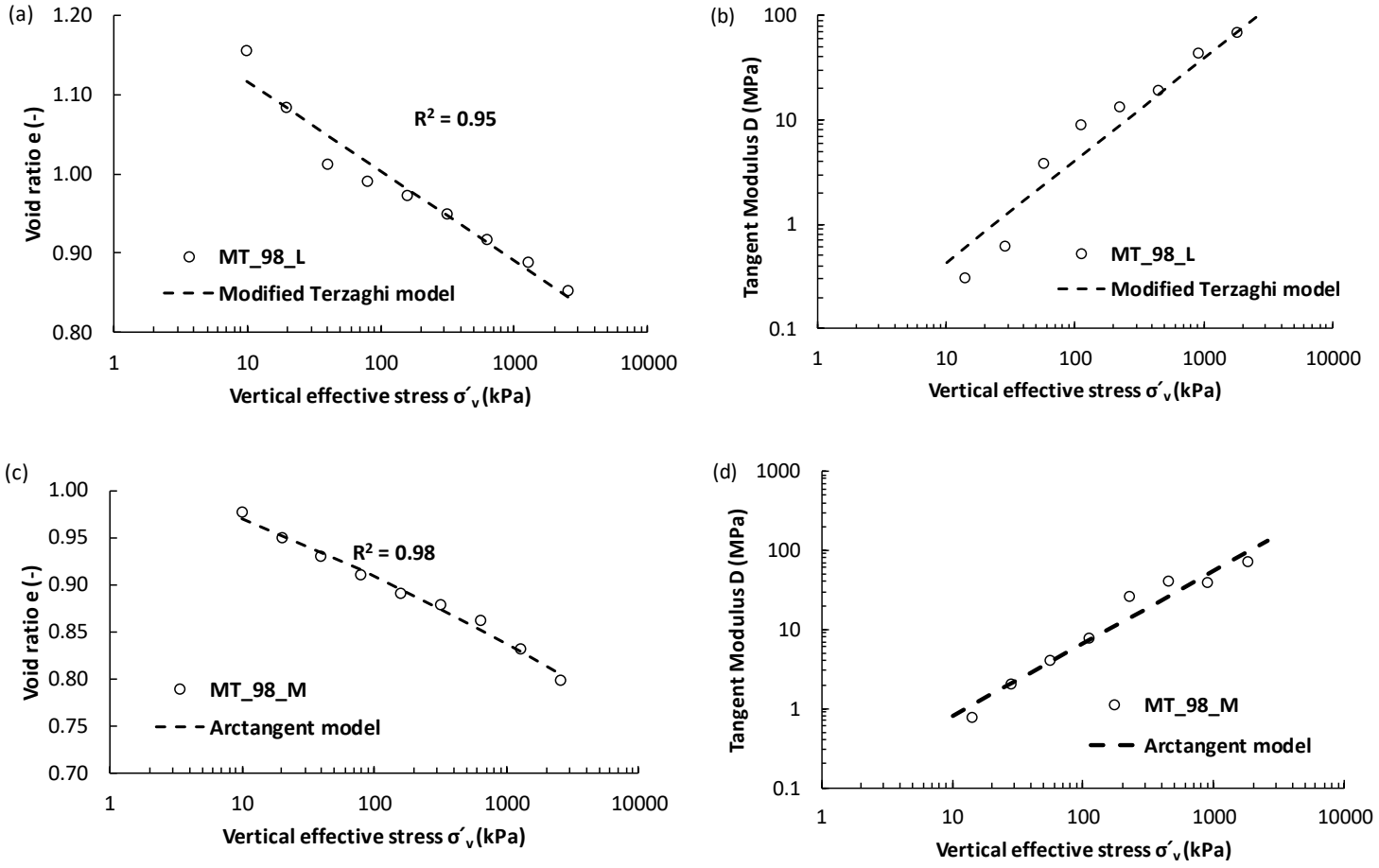

Figure 5-3: 98/68 Stepped loaded compression curves (a and c) and tangent modulus (b and d) of the loose and medium density specimen.

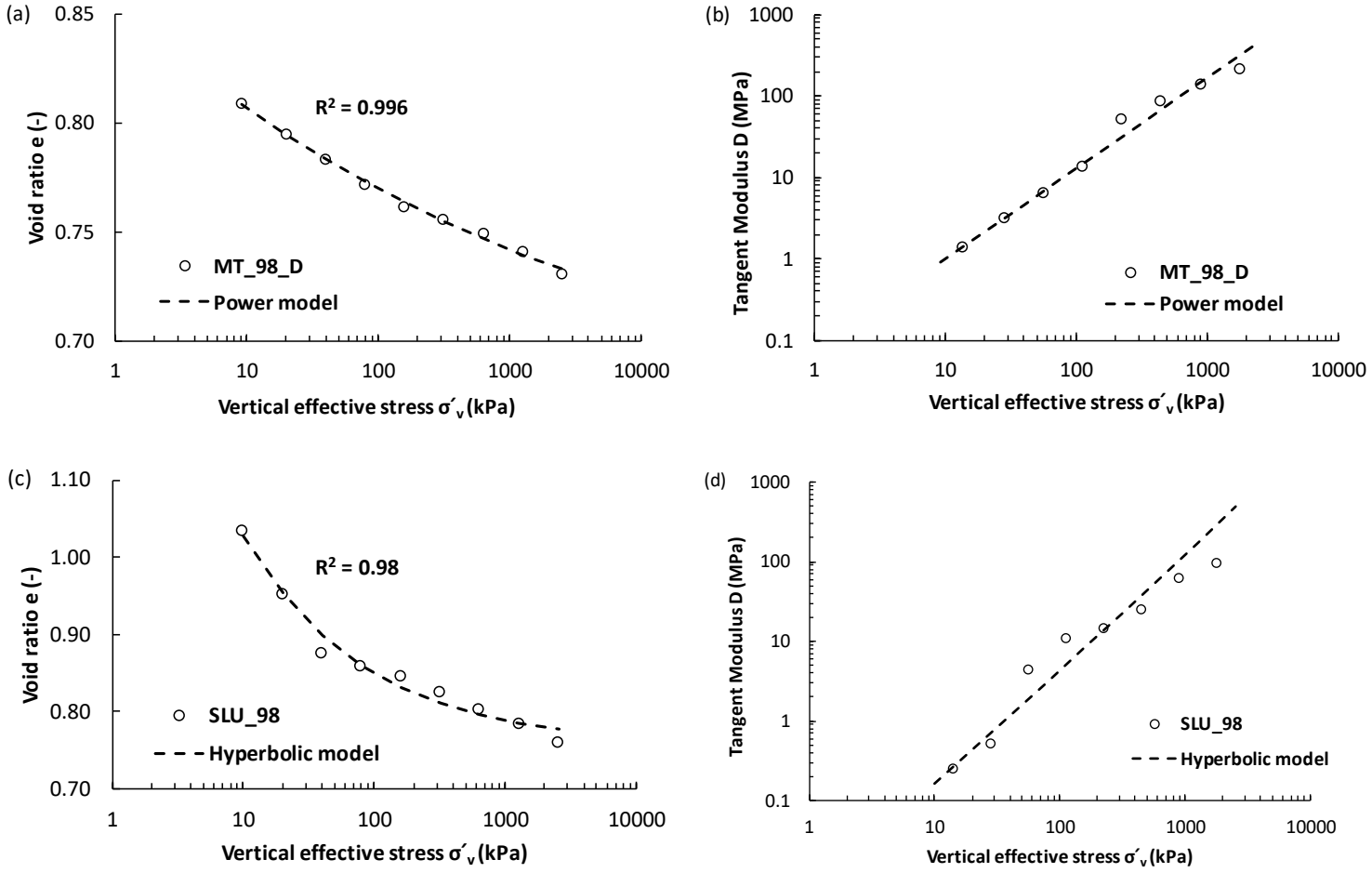

Figure 5-4: 98/68 Stepped loaded compression curves (a and b) and tangent modulus (c and d) of the dense and slurry specimen.

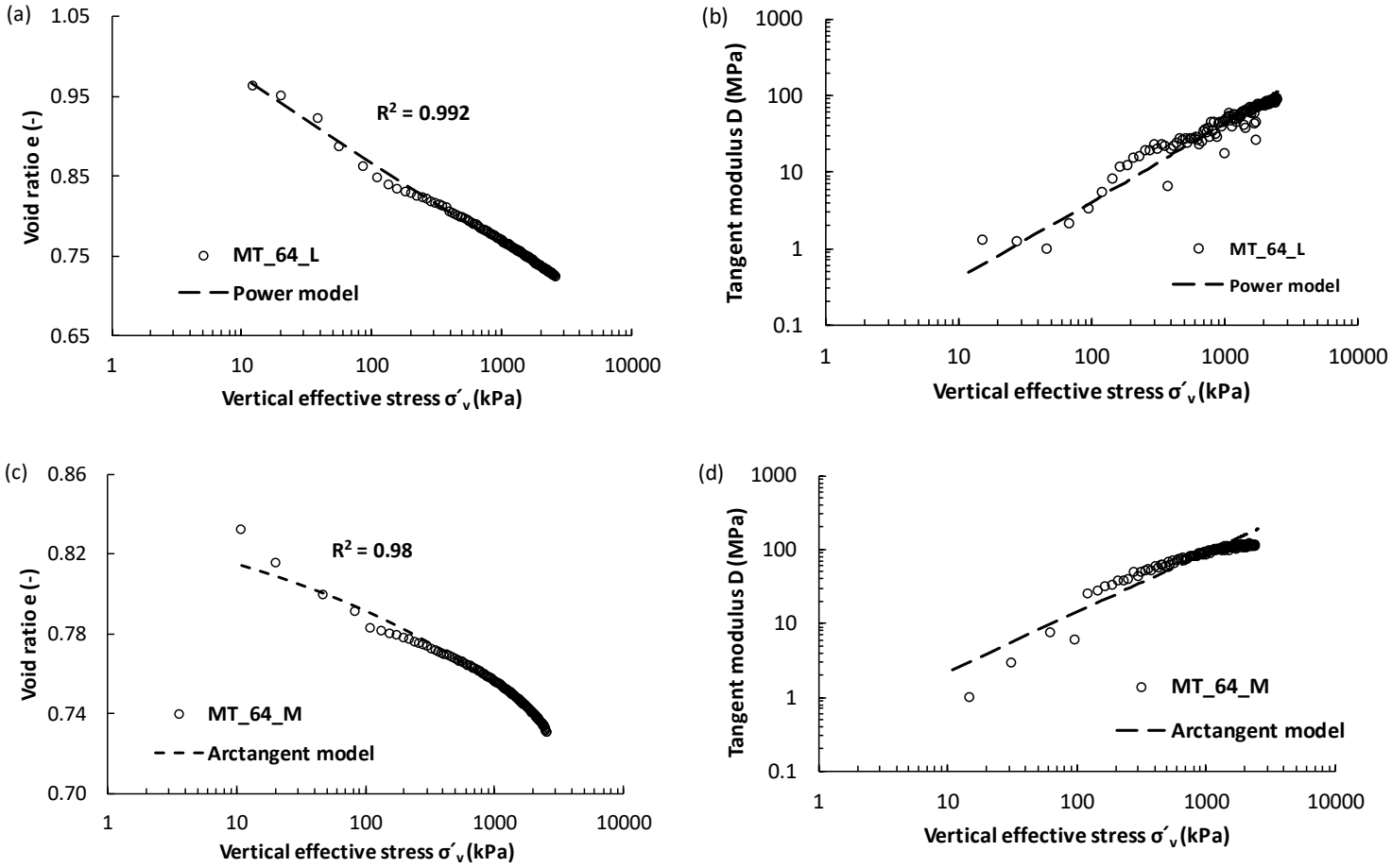

Figure 5-5: 64/61 CRL compression curves (a and c) and tangent modulus (b and d) of the loose and medium density specimen.

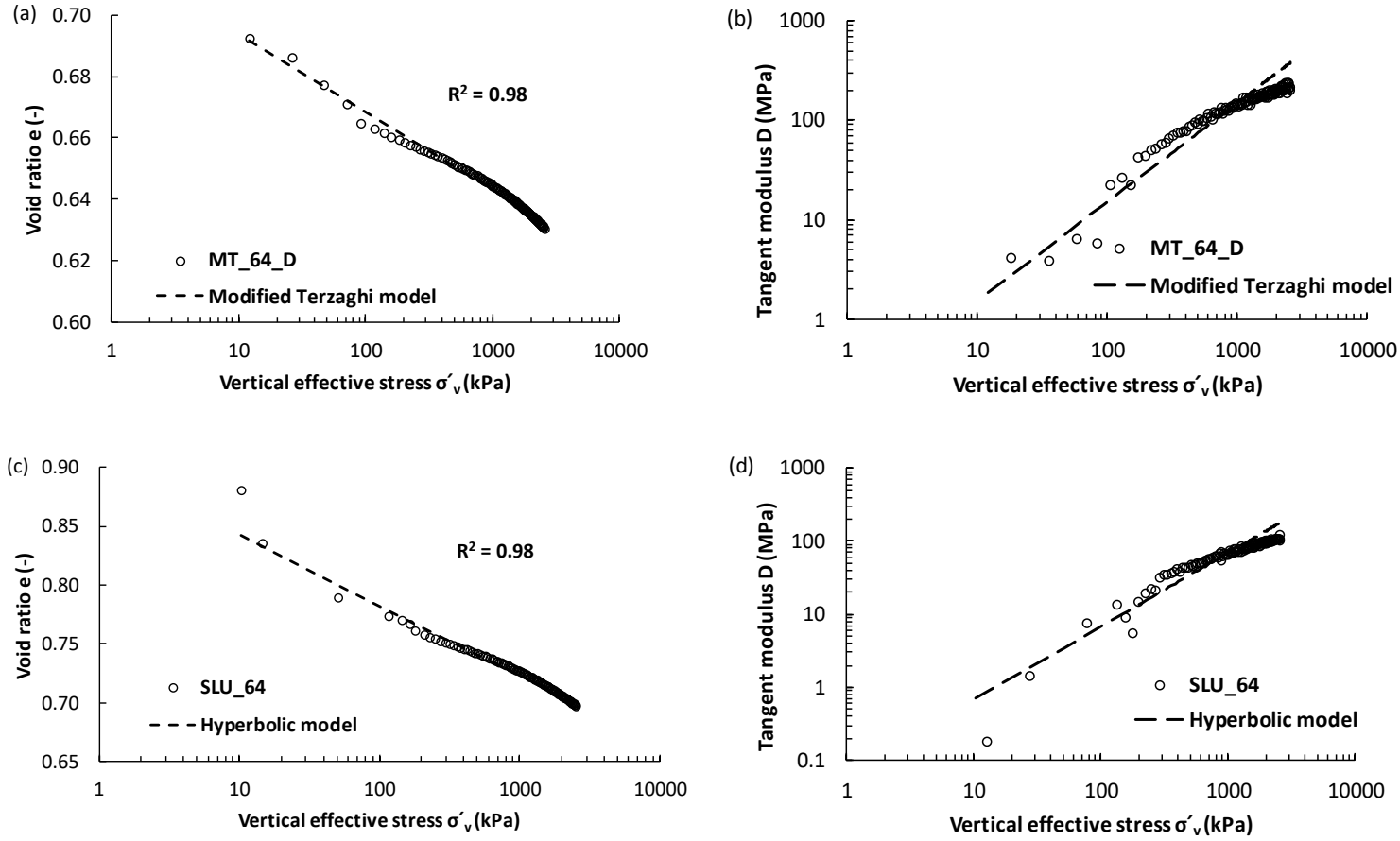

Figure 5-6: 64/61 CRL compression curves (a and c) and tangent modulus (b and d) of the dense and slurry specimen.

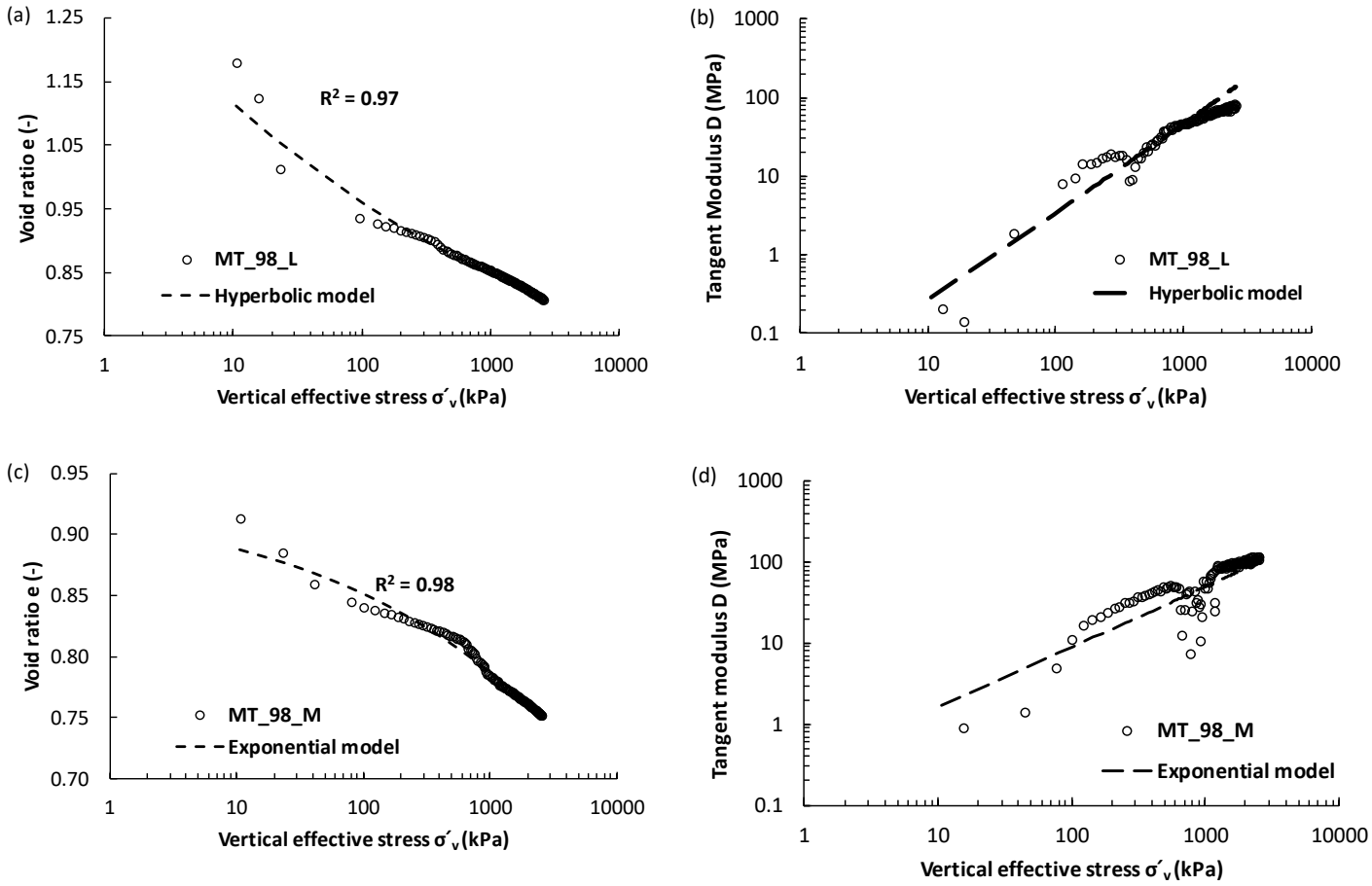

Figure 5-7: 98/68 CRL compression curves (a and c) and tangent modulus (b and d) of the loose and medium density specimen.

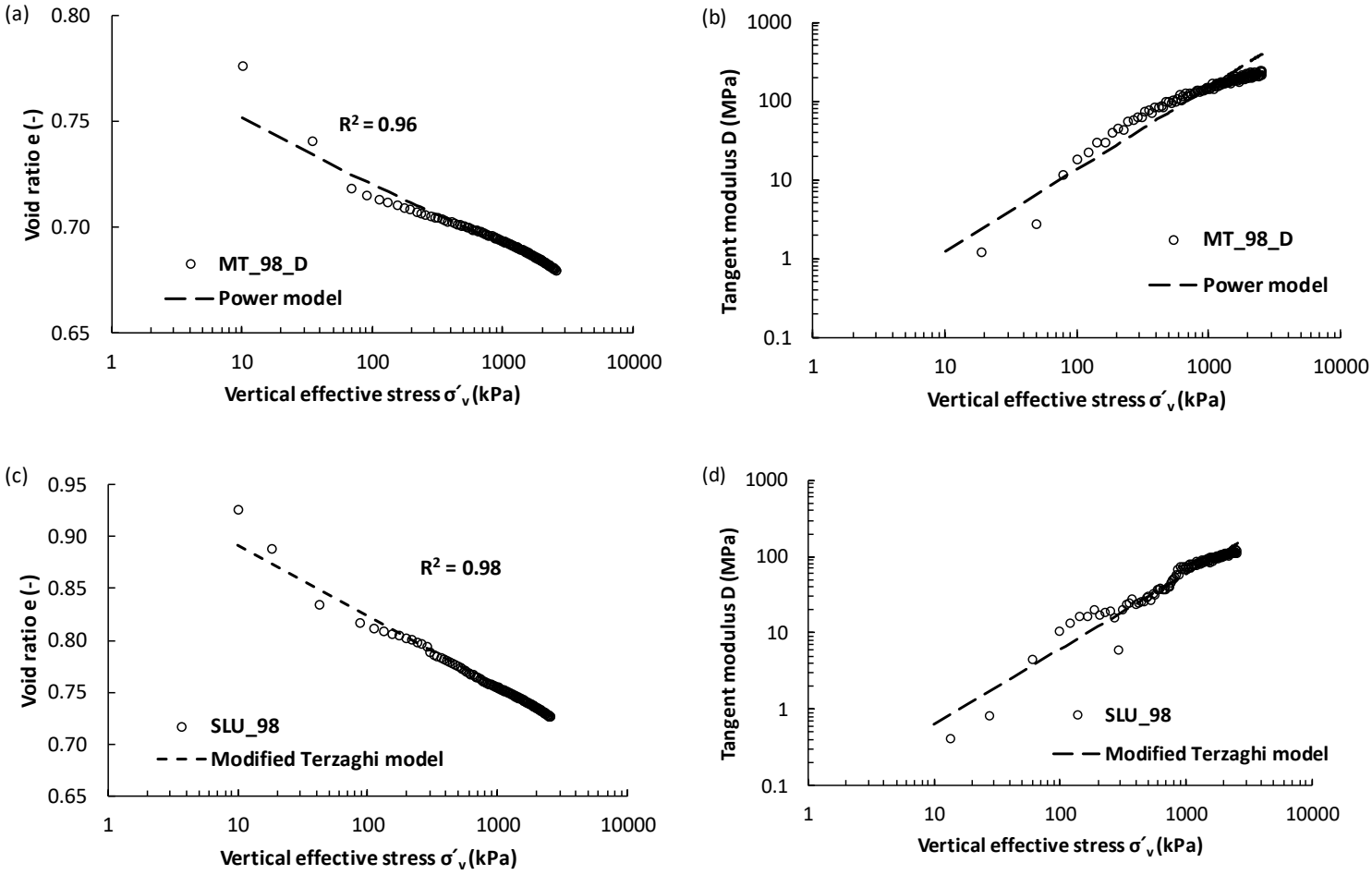

Figure 5-8: 98/68 CRL compression curves (a and c) and tangent modulus (b and d) of the dense and slurry specimen.

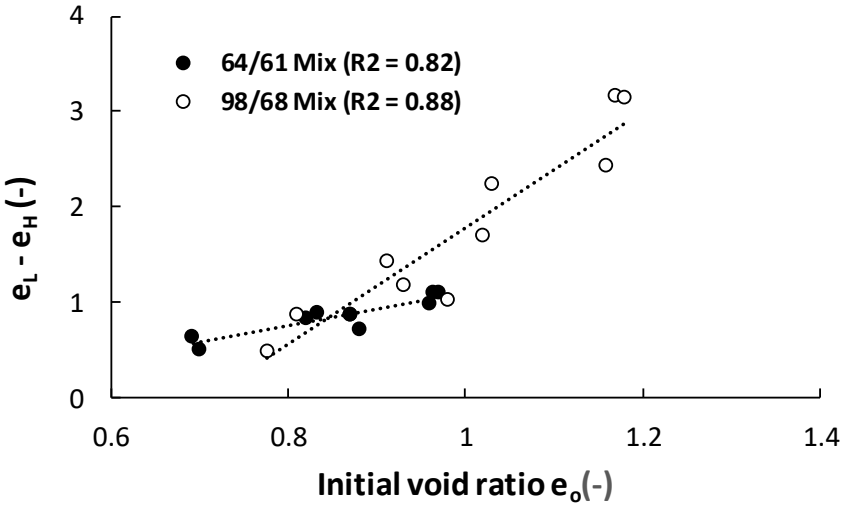

Figure 5-9: Power model correlation of the void ratio range with the initial void ratio of the 64/61 and 98/68 mix (where e_L is the limiting void ratio at low stress, e_H is the limiting void ratio at high stress and e_0 is the void ratio at 10 kPa).

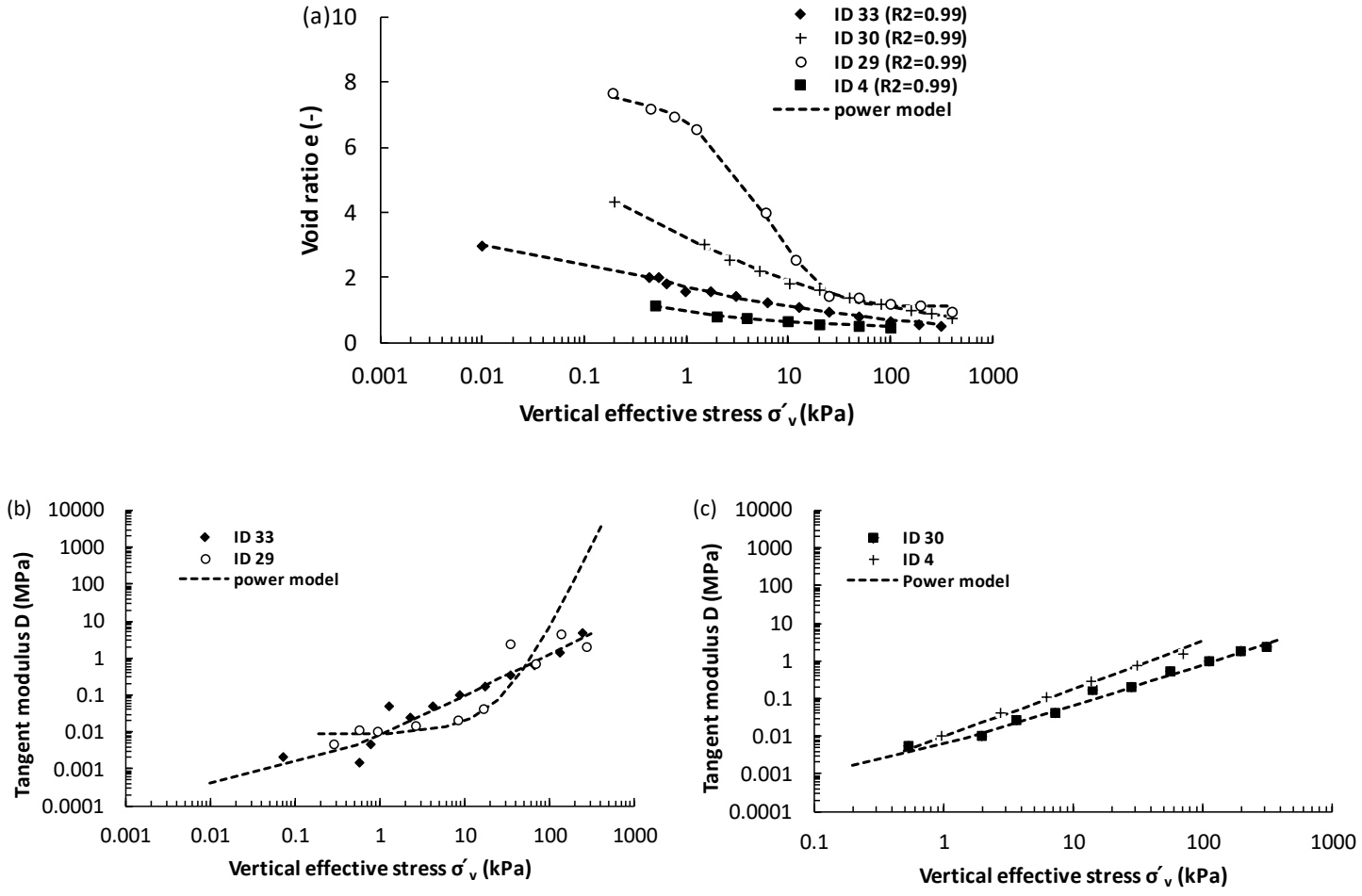

Figure 5-10: Compression curves (a) and tangent modulus (b and c) of Oil sand tailings fitted with the power model.

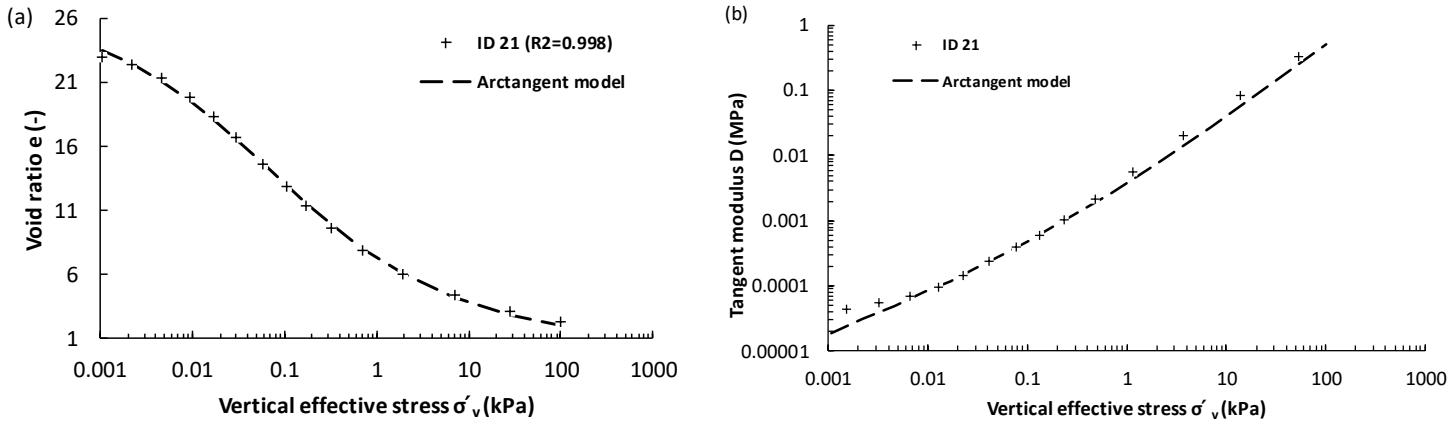

Figure 5-11: Compression curves (a) and tangent modulus (b) of Aluminium Bauxite fitted with the arctangent model.

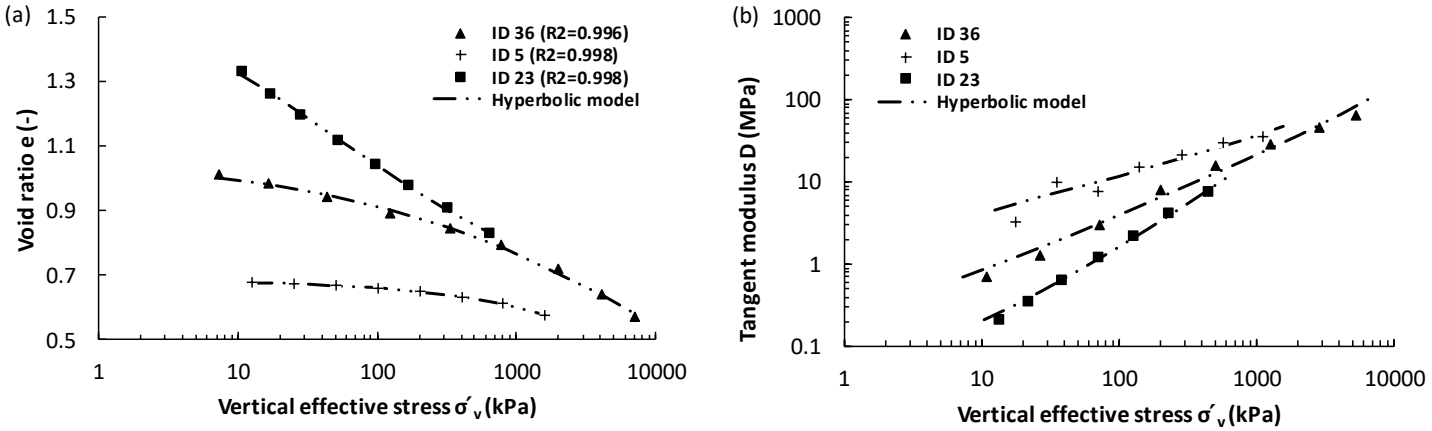

Figure 5-12: Compression curves (a) and tangent modulus (b and c) of Iron tailings fitted with the hyperbolic model.

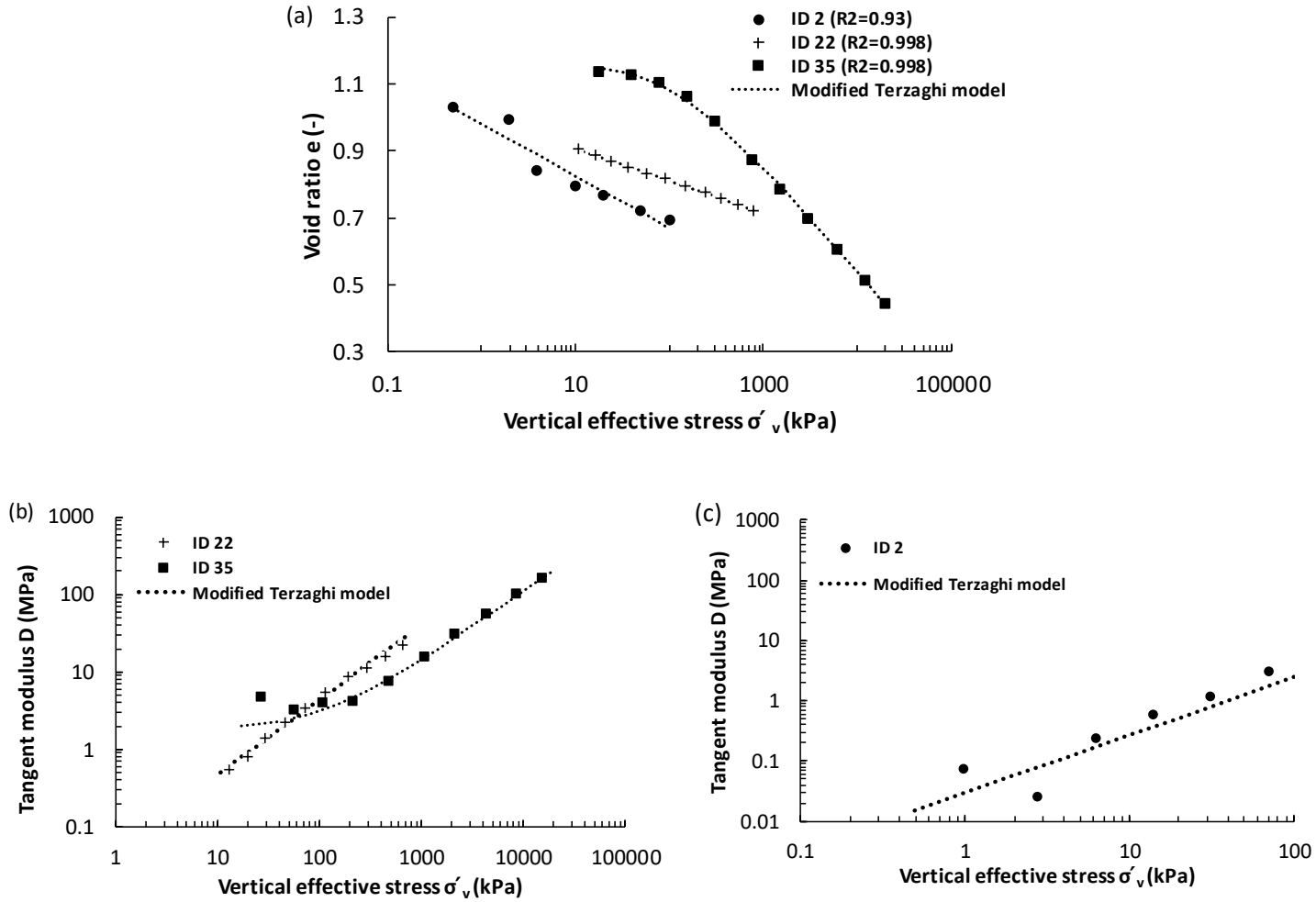

Figure 5-13: Compression curves (a) and tangent modulus (b and c) of Gold tailings fitted with the modified Terzaghi model.

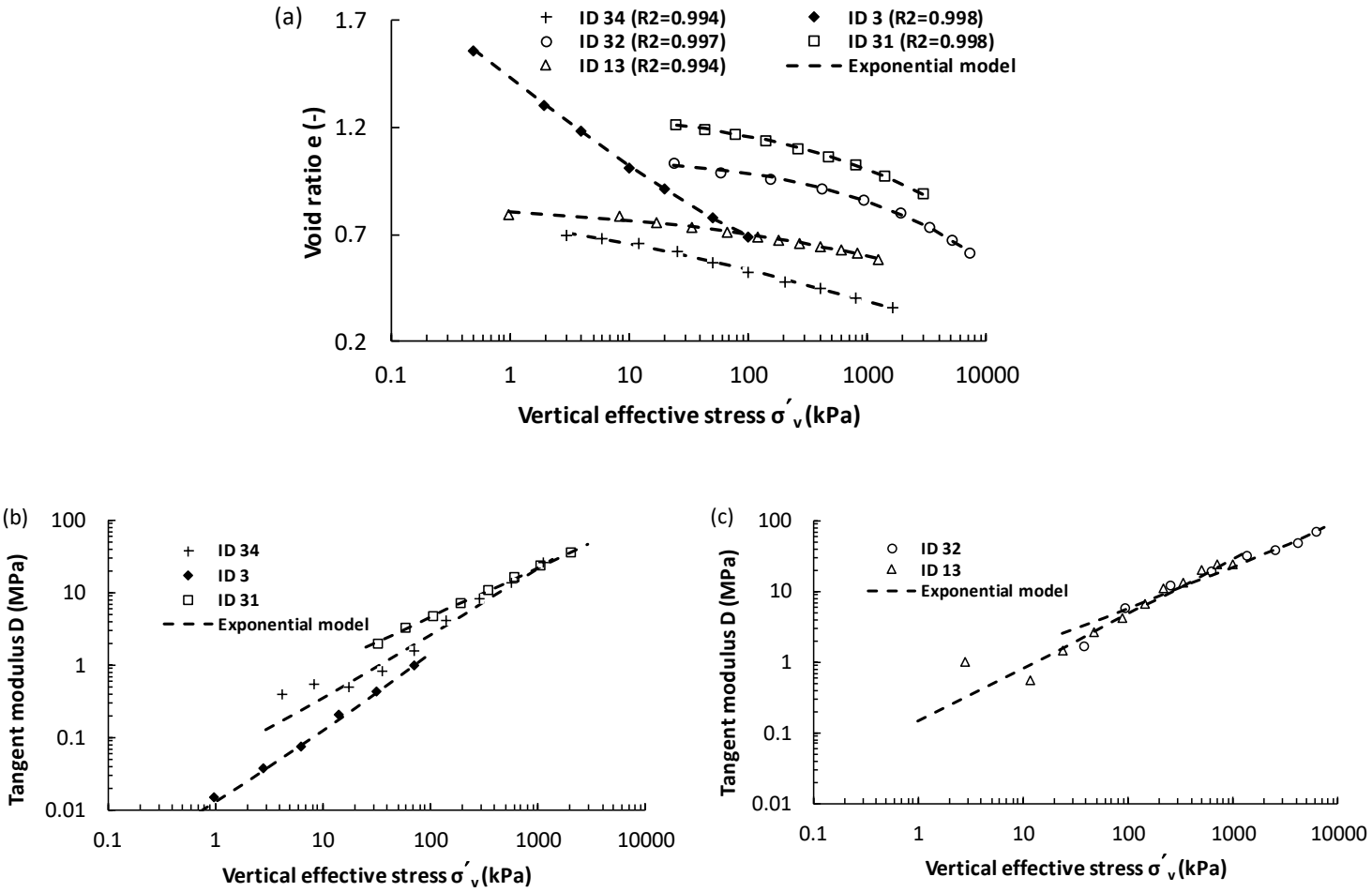

Figure 5-14: Compression curves (a) and tangent modulus (b and c) for tailings fitted with the exponential model.

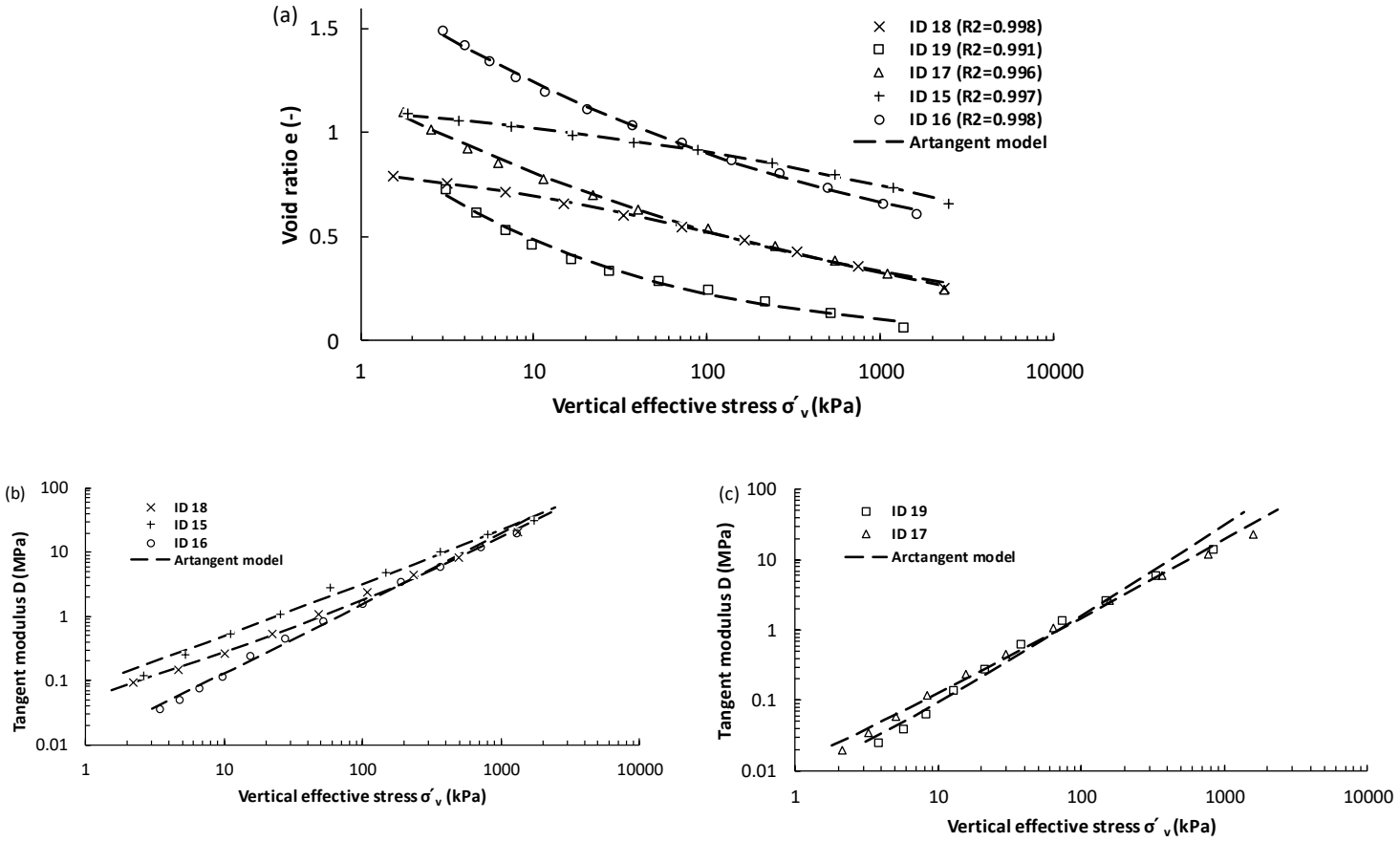

Figure 5-15: Compression curves (a) and tangent modulus (b and c) for tailings reported by (Mittal and Morgenstern, 1976) fitted with the arctangent model.

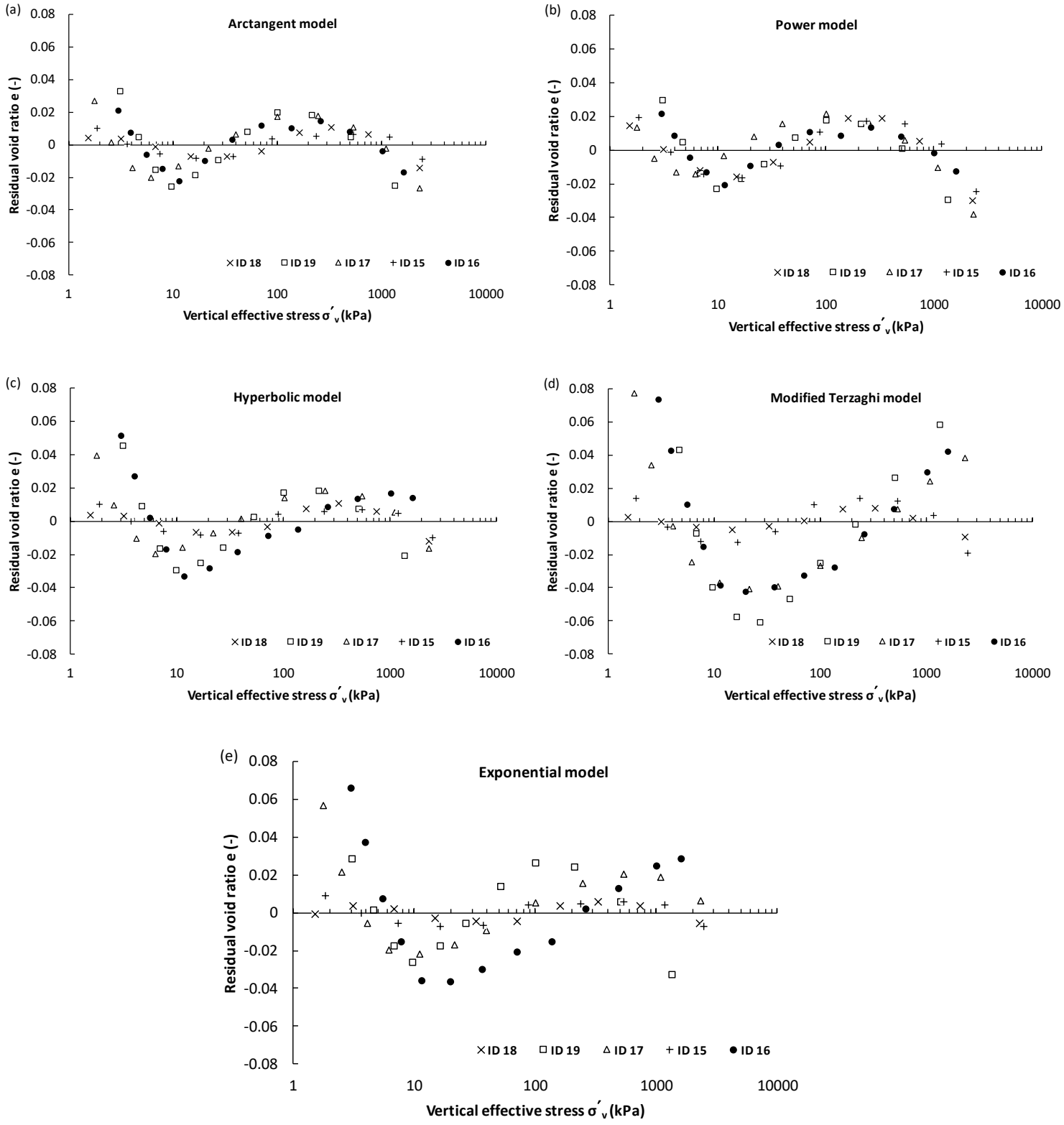

Figure 5-16: Residual plot of each model

6 Conclusion

- The non-plastic Platinum tailings tested did not exhibit a linear behaviour in the void ratio versus the logarithm of effective stress space. Instead, the compression indices varied with increasing stress. The 98/68 mix was found to be more compressible and therefore displayed the highest C_c values. The compression indices decreased with decreasing initial void ratio and were similar to reported indices of non-plastic tailings.
- The coefficient of volume compressibility was correlated to the void ratio of the specimens. Its values were dependent on the initial void ratio and were higher for low density specimens. The coefficient of volume compressibility values were also similar to documented tailings.
- The effect of the loading method (continuous vs stepped loading) was dependent on the initial void ratio of the specimens. In particular, the effects were more noticeable on loose specimens than in the dense ones.
- The coefficient of consolidation increased with decreasing void ratio. It was dependent on the initial void ratio and did not vary significantly for the two particle size distributions considered in this study. The values of the coefficient of consolidation were in the same range as other tailings.
- There was a minor fabric effect on the mechanical behaviour of non-plastic platinum tailings. Both the coefficient of consolidation and compressibility showed a minimal effect of fabric. The tangent constrained modulus of the slurried and moist tamped specimens showed good agreement and therefore the discrepancies observed in the compression curves were accounted to the difference in the initial void ratio. No effect of fabric was observed on the consolidation behaviour of the tailings.
- The four-parameter models captured the general trend of the compression curves more precisely in comparison to the linear Terzaghi model. However, the stiffness behaviour showed discrepancies, especially in the low density specimens. Of the five models, the power, exponential, hyperbolic and arctangent models showed good agreements consistently and the modified Terzaghi model gave the lowest R^2 values. Although the models exhibited high R^2 values, the residual plots revealed limitations in their ability to capture all aspects of the compressive behaviour of non-plastic tailings.

7 Recommendations

Recommendations are made based on the finding of this dissertation:

- The repeatability of the compressive curves attained from the Rowe-Barden consolidation test has to be evaluated. The finding will eliminate or confirm whether variations in the behaviour of tailings measured at the same initial void ratio are due to the testing method or material inherent variations.

- With repeatability confirmed, more tests are required to assess the effect of fabric on the compressibility and consolidation properties of tailings. Research may be required to quantify the effect of fabric.

- This research calculated hydraulic conductivity from the Kozeny-Carman equation. Permeability test may be conducted to confirm the hydraulic conductivity and further used to evaluate the relationship that permeability has with compressibility.

Acknowledgement

The experimental work was conducted at the University of the Witwatersrand's Geoffrey Blight Geotechnical laboratory. The scanning electron microscope (SEM) images in Figure 3-1 were captured at the King Abdullah University of Science and Technology.

8 References

Adajar, M.A.Q. and Cutora, M.D.L. (2018), "The effect of void ratio , moisture content and vertical pressure on the hydrocompression settlement of copper mine tailing", *International Journal of GEOMATE*, Vol. 14 No. 44, pp. 82–89.

Ahmed, S.I. and Siddiqua, S. (2014), "A review on consolidation behavior of tailings", *International Journal of Geotechnical Engineering*, Vol. 8 No. 1, pp. 102–111.

Aubertin, M., Bussiere, B. and Chapuis, R. (1996), "Hydraulic conductivity of homogenized tailings from hard rock mines", *Canadian Geotechnical Journal*, Vol. 33 No. 3, pp. 470–482.

Beuselinck, L., Govers, G., Poesen, J., Degraer, G. and Froyen, L. (1998), "Grain-size analysis by laser diffractometry: Comparison with the sieve-pipette method", *Catena*, Vol. 32 No. 3–4, pp. 193–208.

Biarez, J. and Hicher, P.Y. (1994), *Elemental Mechanics of Soil Behaviour: Saturated Remolded Soils*, AA Balkema.

Blight, G. (2010), *Geotechnical Engineering for Mine Waste Storage Facilities*, CRC Press/Balkema, Netherlands.

Blight, G.E. (1979), "Properties of pumped tailings fill", *Journal of the South African Institute of Mining and Metallurgy*, Vol. 79 No. 15, pp. 446–454.

Blight, G.E. and Bentel, G.M. (1983), "The behaviour of mine tailings during hydraulic deposition", *Journal of the South African Institute of Mining and Metallurgy*, Vol. 83 No. 4, pp. 73–86.

Blight, G.E. and Steffen, O.K.H. (1979), "Geotechnics of gold mining waste disposal", *Current Geotechnical Practice in Mine Waste Disposal*, ASCE, New York, pp. 1–52.

Blott, S.J. and Pye, K. (2006), "Particle size distribution analysis of sand-sized particles by laser diffraction: An experimental investigation of instrument sensitivity and the effects of particle shape", *Sedimentology*, Vol. 53 No. 3, pp. 671–685.

BS 1377-6. (1990), *Methods of Test for Soils for Civil Engineering Purposes- Part 6: Consolidation and Permeability Tests in Hydraulic Cells and with Pore Pressure Measurement, British Standards Institution.*, London.

Butterfield, R. (1979), "A natural compression law for soils (an advance on e-log p')", *Geotechnique*, Vol. 29 No. 4, pp. 469–480.

Chaney, R., Stevens, E. and Sheth, N. (1979), "Suggested Test Method for Determination of Degree of Saturation of Soil Samples by B Value Measurement", *Geotechnical Testing Journal*, Vol. 2 No. 3, pp. 158–162.

Chang, N. (2009), *The Effect of Fabric on the Behaviour of Gold Tailings*, University of Pretoria.

Chong, S. and Santamarina, J.C. (2016a), "Soil Compressibility Models for a Wide Stress Range", *Journal of Geotechnical and Geoenvironmental Engineering*, Vol. 142 No. 6, pp. 1–7.

Craig, R.F. (2004), *Craig's Soil Mechanics*, 7th ed., Spon Press, London.

Cubrinovski, M. and Ishihara, K. (2002), "Maximum and minimum void ratio characteristics of sands", *Soils and Foundations*, Vol. 42 No. 6, pp. 65–78.

Dacosta, M.A. (2017), *Mineralogical Characterization of South African Mine Tailings with Aim of Evaluating Their Potential for the Purposes of Mineral Carbonation*, University of Cape Town.

Gregory, A.S., Whalley, W.R., Watts, C.W., Bird, N.R.A., Hallett, P.D. and Whitmore, A.P. (2006), "Calculation of the compression index and precompression stress from soil compression test data", *Soil and Tillage Research*, Vol. 89 No. 1, pp. 45–57.

Head, K.H. (1986), *Manual of Soil Laboratory Testing.*, 3rd edition., Pentech Press Limited, London.

Head, K.H. (1994), *Manual of Soil Laboratory Testing*, Vol. 3, John Wiley and Sons, Chichester.

Hu, L., Wu, H., Zhang, L., Zhang, P. and Wen, Q. (2017), "Geotechnical Properties of Mine Tailings", *Journal of Materials in Civil Engineering*, Vol. 29 No. 2, pp. 04016220-1–10.

Ito, M. and Azam, S. (2013), "Large-strain consolidation modelling of mine waste tailings", *Environmental Systems Research*, Vol. 2 No. 7, pp. 2–12.

Juarez-Badillo, E. (1981), "General compressibility equation for soils.", *Soil Mechanics and Foundation Engineering. Proc. 10th International Conference, Stockholm, June 1981. Vol. 1, (A.A.Balkema)*, No. 2, pp. 171–178.

Kianfar, K. (2013), *Implications of PVD and Vacuum Preloading on Viscoplastic Behaviour of Soft Soils*,

Implications of PVD and Vacuum Preloading on Viscoplastic Behaviour of Soft Soils, University of Wollongong.

Knappett, J.A. and Craig, R.F. (2012), *Craig's Soil Mechanics*, 8th ed., Spon Press, London.

Konert, M. and Vandenberghe, J. (1997), "Comparison of laser grain size analysis with pipette and sieve analysis: A solution for the underestimation of the clay fraction", *Sedimentology*, Vol. 44 No. 3, pp. 523–535.

Lambe, T.W. and Whitman, R. V. (1969), *Soil Mechanics*, John Wiley and Sons, Chichester.

Li, W. (2017), *The Mechanical Behaviour of Tailings*, City University of Hong Kong.

Mitchell, J.K. and Soga, K. (2005), *Fundamentals of Soil Behaviour*, 3rd Editio., John Wiley and Sons, New Jersey.

Mittal, H.K. and Morgenstern, N.. (1975), "Parameters for the design of tailings dams", *Canadian Geotechnical Journal*, Vol. 12 No. 2, pp. 235–261.

Mittal, H.K. and Morgenstern, N.R. (1976), "Seepage control in tailings dams", *Canadian Geotechnical Journal*, Vol. 13 No. 3, pp. 277–293.

Oberie, B., Brereton, D. and Mihaylova, A. (2020), *Towards Zero Harm-A Compendium of Papers Prepared for the Global Tailings Review*, Switzerland.

Pestana, J.M. and Whittle, A.J. (1995), "Compression model for cohesionless soils", *Geotechnique*, Vol. 45 No. 4, pp. 611–631.

Qiu, Y.J. and Sego, D.C. (2001), "Laboratory properties of mine tailings", *Canadian Geotechnical Journal*, Vol. 38 No. 1, pp. 183–190.

Reid, D. and Fourie, A.B. (2015), "The influence of slurry density on in situ density", *Proceedings of the 18th International Seminar on Paste and Thickened Tailings*, Australian Centre for Geomechanics, Perth, pp. 95–106.

Rowe, P.W. and Barden, L. (1966), "A New Consolidation Cell", *Géotechnique*, Vol. 16 No. 2, pp. 162–170.

Santamarina, J.C., Torres-Cruz, L.A. and Bachus, R.C. (2019), "Why coal ash and tailings dam disasters

occur", *Science*, Vol. 364 No. 6440, pp. 526–528.

Sengupta, S. (2018), "Effect of loading behaviour on compressional property of needle-punched nonwoven fabric", *Indian Journal of Fibre and Textile Research*, Vol. 43, pp. 194–202.

Shamsai, A., Pak, A., Bateni, S.M. and Ayatollahi, S.A.H. (2007), "Geotechnical characteristics of copper mine tailings: A case study", *Geotechnical and Geological Engineering*, Vol. 25 No. 5, pp. 591–602.

Shokouhi, A. and Williams, D.J. (2015), "Settling and consolidation behaviour of coal tailings slurry under continuous loading", *Proceedings Tailings and Mine Waste 2015*, Vancouver.

Shukla, S., Sivakugan, N. and Das, B. (2009), "Methods for determination of the coefficient of consolidation and field observations of time rate of settlement — an overview", *International Journal of Geotechnical Engineering*, Vol. 3 No. 1, pp. 89–108.

Soumaya, B. and Kempfert, H. (2010), "Deformation behavior of soft floors in the voltage controlled compression attempt", *Bautechnik*, Vol. 87, pp. 73–80.

Sridharan, A. and Gurtug, Y. (2005), "Compressibility characteristics of soils", *Geotechnical and Geological Engineering*, Vol. 23 No. 5, pp. 615–634.

Sridharan, A. and Nagaraj, H.B. (2011), "Compressibility behaviour of remoulded, fine-grained soils and correlation with index properties", *Canadian Geotechnical Journal*, Vol. 37 No. 3, pp. 712–722.

Taylor, D.W. (1948), *Fundamentals of Soil Mechanics*, John Wiley and Sons, London.

Terzaghi, K. (1943), *Theoretical Soil Mechanics*, John Wiley and Sons, London.

Torres-Cruz, L.A. (2016), *Use of the Cone Penetration Test to Assess the Liquefaction Potential of Tailings Storage Facilities*, University of the Witwatersrand.

Torres-Cruz, L.A. and Santamarina, J.C. (2020), "The critical state line of nonplastic tailings", *Canadian Geotechnical Journal*, Vol. 57 No. 10, pp. 1508–1517.

Verdugo, R. and Ishihara, K. (1996), "The steady state of sandy soils", *Soils and Foundations*, Vol. 36 No. 2, pp. 81–91.

Vick, S.G. (1990), *Planning, Design, and Analysis of Tailings Dams*, Wiley and Sons, London.

von Fay, K.F. and Cotton, C.E. (1986), “Constant rate of loading (CRL) consolidation test”, *Consolidation of Soils: Testing and Evalution, ASTM STP 892*, ASTM, Philadelphia, pp. 236–256.

Appendices

Appendix A Tangent Modulus equations of the four-parameter models.

Table A 1: Tangent modulus equation of the four-parameter models. Source: Chong and Santamarina (2016a).

Model	**Tangent Stiffness (M)**
Modified Terzaghi model	$M = 2.3\frac{(1+e)}{C_c}\cdot(\sigma' + \sigma'_L)\cdot\left(1+\frac{\sigma' + \sigma'_L}{\sigma'_H}\right)$
Power model	$M = \left(\frac{1+e}{e-e_H}\right)\cdot\frac{\sigma' + \sigma'_c}{\beta}$
Exponential model	$M = \left(\frac{1+e}{e-e_H}\right)\cdot\frac{\sigma'}{\beta}\cdot\left(\frac{\sigma'}{\sigma'_c}\right)^{\beta}$
Hyperbolic model	$M = \left(\frac{1+e}{e_L-e}\right)\cdot\frac{\sigma'}{\beta}\cdot\left[1+\left(\frac{\sigma'_c}{\sigma'}\right)^{-\beta}\right]$
Arctangent model	$M = \frac{\pi}{2}\cdot\left(\frac{1+e}{e_L-e_H}\right)\cdot\frac{\sigma'}{\beta}\cdot\left[\left(\frac{\sigma'}{\sigma'_c}\right)^{\beta}+\left(\frac{\sigma'}{\sigma'_c}\right)^{-\beta}\right]$

Appendix B Calculation of the forces acting on the spindle

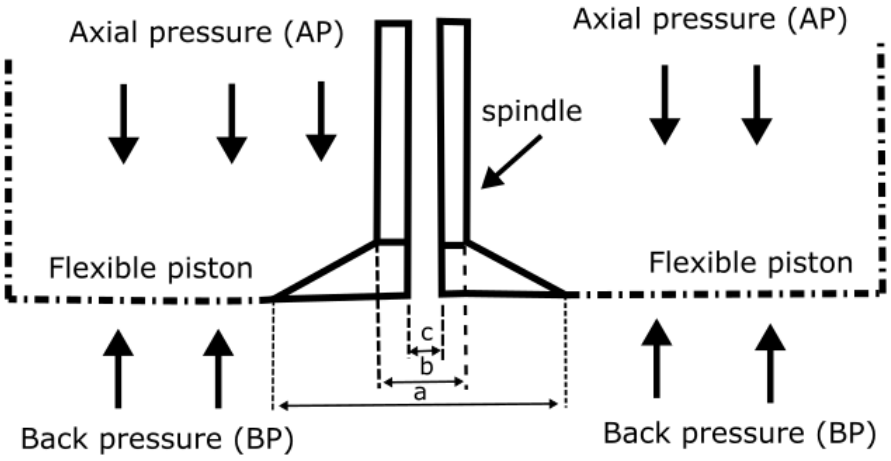

Figure B 1: Schematic of the pressure acting on the spindle.

The force applied by the back pressure (BP) transducer on the spindle can be written as:

$$F_{BP} = BP(Area\ a - Area\ c) = BP(\pi r_a^2 - \pi r_c^2)$$

The force applied by the axial pressure (AP) transducer on the spindle can be written as:

$$F_{AP} = AP(Area\ a - Area\ b) = AP\left(\pi r_a^2 - \pi r_b^2\right)$$

To avoid the shooting of the spindle, the axial force must be more or equal to the back force,

$$F_{BP} \leq F_{AP}$$

Therefore

$$BP(\pi r_a^2 - \pi r_c^2) \leq AP\ (\pi r_a^2 - \pi r_b^2)$$

The expression can be simplified as

$$BP \leq AP\frac{\left(\pi r_a^2 - \pi r_b^2\right)}{(\pi r_a^2 - \pi r_c^2)}$$

$$BP \leq AP\frac{\left(r_a^2 - r_b^2\right)}{(r_a^2 - r_c^2)}$$

$$\frac{BP}{AP} \leq \frac{\left(r_a^2 - r_b^2\right)}{(r_a^2 - r_c^2)}$$

The measured radius of a = 8.9, b = 3 and c = 0.75. Therefore, the expression can be written as:

$$\frac{BP}{AP} \leq \frac{(8.9^2 - 3^2)}{(8.9^2 - 0.75^2)}$$

$$\frac{BP}{AP} \leq 0.89$$

To circumvent the spindle from shooting out, the back pressure (BP) must never be more than 0.89 times the axial pressure.

Appendix C Void ratio calculations

Firstly, the volume of solids was calculated as

$$V_s = \left(\frac{\rho_s}{m_{dry}}\right) \cdot 1000$$

Where ρ_s is the particle density and m_{dry} is the mass of the total solids.

The void ratio changes during the test were measured by the back pressure transducer which measures volume (V) changes and the displacement transducer which measures height (H) changes. Using the dataset measured by the transducers, the void ratio (Δe) changes were calculated as follows:

1. The volume changes (ΔV) measured during drainage by the back pressure (BP) transducer as:

$$\Delta V = V_{i-1} - V_i$$

Therefore, the void ratio change was calculated as

$$\Delta e_v = \frac{\Delta V}{V_s}$$

2. The height changes (ΔH) measured from the displacement transducer as:

$$\Delta H = H_{i-1} - H_i$$

Height changes in terms of volume can be written as

$$\Delta V_H = \pi(r^2) \cdot \Delta H$$

Therefore, the void ratio change was calculated as

$$\Delta e_H = \frac{\Delta V_H}{V_s}$$

The void ratio at a specific point during the test was determined at maximum stress (max σ) and at the end of the test (EOT) as follows:

1. Measurement at maximum stress

Firstly, the following information had to be acquired,

Height of spindle for specimen height of 32 mm (undeformed specimen) = 37.8 mm

Height of spindle during the test at maximum stress = *x*

The height of the specimen at maximum stress (max σ) was calculated as follows

$$H_{max} = 32 - (37.8 - x)$$

The volume of the specimen at max stress was calculated as

$$V_{max} = \pi(r^2) \cdot H_{max}$$

The volume of voids is equal to:

$$V_v = \frac{V_{max}}{V_s}$$

The void ratio at maximum stress is

$$e_{max} = \frac{V_v}{V_s}$$

2. Measurement at end of test

At the end of the testing programme, the wet weight of the specimen was measured. Thereafter, the specimen was placed in an oven to dry.

The mass of water in the specimen was calculated as follows:

$$m_{water} = m_{wet} - m_{dry}$$

The water content was calculated as,

$$w_{\%} = \frac{m_{water}}{m_{dry}} \cdot 100$$

The void ratio at the end of the test is

$$e_{EOT} = \frac{w_{\%} \cdot \rho_s}{100}$$

From the above data, four methods of calculating void ratio are observed:

1. The void ratio calculated starting from the end of test void ratio (EOT) while considering the changes measured by the back pressure transducer,

$$e_{(\Delta v_EOT)} = e_{EOT} - \Delta e_v$$

2. The void ratio calculated starting from the end of test void ratio (EOT) while considering the changes measured by the displacement transducer,

$$e_{(\Delta H_EOT)} = e_{EOT} - \Delta e_H$$

3. The void ratio calculated starting from the maximum stress void ratio (max σ) while considering the changes measured by the back pressure transducer,

$$e_{(\Delta v_max)} = e_{max} - \Delta e_v$$

4. The void ratio calculated starting from the maximum stress void ratio (max σ) while considering the changes measured by the displacement transducer,

$$e_{(\Delta H_max)} = e_{max} - \Delta e_H$$